

TIN MINERALIZATION WITHIN RHYOLITE  
FLOW-DOMES, BLACK RANGE, NEW MEXICO

A DISSERTATION  
SUBMITTED TO THE DEPARTMENT OF GEOLOGY  
AND THE COMMITTEE ON THE GRADUATE DIVISION  
OF STANFORD UNIVERSITY  
IN PARTIAL FULFILLMENT OF THE REQUIREMENTS  
FOR THE DEGREE OF  
DOCTOR OF PHILOSOPHY

By

John Laidley Lufkin

June 1972

I certify that I have read this thesis and that in my opinion it is fully adequate, in scope and quality, as a dissertation for the degree of Doctor of Philosophy.

Richard H. Jahne

I certify that I have read this thesis and that in my opinion it is fully adequate, in scope and quality, as a dissertation for the degree of Doctor of Philosophy.

Charles E. Tuck

I certify that I have read this thesis and that in my opinion it is fully adequate, in scope and quality, as a dissertation for the degree of Doctor of Philosophy.

Robert R. Coonster

I certify that I have read this thesis and that in my opinion it is fully adequate, in scope and quality, as a dissertation for the degree of Doctor of Philosophy.

K. E. D. Allen

Approved for the University Committee  
on the Graduate Division:

Lincoln E. Moses

Dean of the Graduate Division



## ACKNOWLEDGMENTS

Several faculty and students at Stanford University generously offered ideas and useful comments during the course of this investigation. In particular, I would like to thank Dr. Richard H. Jahns, principal thesis adviser, who first introduced me to New Mexico and the general area of the tin-bearing rhyolites, and who provided helpful suggestions and constructive criticism, as well as a sense of humor necessary to the development and completion of this study; Dr. Kenneth L. Williams and Dr. Charles M. Taylor for their help in obtaining microprobe analyses; Dr. Arvid M. Johnson for his suggestions on certain aspects of structural interpretation; and the late Dr. C. Osborne Hutton for his help in mineral identification. Professors Charles F. Park, Richard H. Jahns, Robert R. Compton, and Kenneth L. Williams read the manuscript and made helpful suggestions for its improvement. The help and ideas of my colleagues, including Rodney J. Holcombe, Phillip M. Fenn, Frederick R. Dowsett, Randolph A. Koski, and Robert F. Martin, now at McGill University, are also gratefully acknowledged.

The investigation was supported financially by the New Mexico Bureau of Mines and Mineral Resources, the Geological Society of America (Research Grant 1325-69), and Stanford University (Shell-Esso Research Fund). For many kinds of advice and assistance, I am particularly grateful to staff members of the New Mexico Bureau of Mines and Mineral Resources, including Don H. Baker, Jr., Director,

geologists Max E. Willard and Frank E. Kottowski, and Mrs. Lynn Brandvold, chemist, who performed the bulk of the necessary chemical analyses. Oxide minerals used as standards for microprobe analyses were generously provided by C. L. Sainsbury and G. A. Desborough of the U. S. Geological Survey, Brian Mason of the Smithsonian Institution, and C. O. Hutton of Stanford University.

Field work was greatly facilitated by the kindnesses of Dr. and Mrs. Bruce H. Sage, Poverty Creek Ranch, and Mr. and Mrs. H. Roland Johnson, Williamsburg, New Mexico, who provided housing accommodations during the field seasons.

Finally, I wish to thank my wife, Sue, who typed copies of the thesis draft and matched my endurance and desire to see this project completed.

## ABSTRACT

The tin-bearing Taylor Creek Rhyolite forms several flow-domes in the Tertiary volcanic section of the Black Range in southwestern New Mexico. Two of the rhyolite domes are well exposed along Taylor Creek, a prominent intermittent stream draining country on the west side of the Continental Divide.

The flow-layered, porphyritic rhyolite is pale red to gray, with phenocrysts of microperthitic sanidine, quartz, and minor plagioclase and biotite enclosed in a devitrified groundmass of alkali feldspar and quartz. Accessory igneous minerals include titaniferous magnetite, sphene, fayalite (?), and zircon.

X-ray study of the alkali feldspars indicates that the phenocrysts are low-sanidine, and that post-emplacement processes, including devitrification of glass and argillization in the groundmass, appear to have had little effect on these phases. Groundmass alkali feldspar appears to be of similar structural state and slightly more potassic than phenocryst compositions. Sanidines separated from one tin-bearing hematite veinlet were found to be the most potassic of all feldspars studied.

A variety of textures and colors has provided a basis for subdividing the rhyolite into several facies. These range from miarolitic, lithophysal types near the tops of the exposed domes to more dense, spherulitic types that compose the bulk of the rhyolite

masses. Pyroclastic rocks are interbedded with and marginal to the rhyolite domes.

Flow-layering in the dome interiors is gentle to moderately inclined, but near some of the dome margins it is steeply inclined and locally expresses recumbent flow-folds. The association of rhyolite with interbedded pyroclastic rocks, and the occurrence of vitrophyric and flow-breccia facies within the volcanic pile indicate that the emplacement of the rhyolite domes was not one uninterrupted event, but was broken by periods of explosive activity, followed by renewed lava outpouring in different directions from different sources.

Tin mineralization appears to be cogenetic with the rhyolite. The lode tin occurs as cassiterite, both inmiarolitic cavities and in hematite-rich veinlets; it also appears as finely crystalline "wood-tin" in local placer accumulations. The cassiterite is commonly associated with hematite and quartz, and locally with bixbyite, pseudobrookite, alkali feldspar, topaz, and monazite. Its most widespread occurrence is in the hematite-bearing veinlets, which are restricted to the argillized, bleached rhyolite. These veinlets are discontinuous, and cannot be traced more than a few feet in any one outcrop. Rarely do they exceed 8 mm in thickness. Analysis of structural features, including rhyolite flow-layering, shear fractures, and tin-bearing fractures concentrated near one of the dome margins at Taylor Creek, reveals that the tin-bearing veinlets reflect tensional features developed after flowage ceased, probably as a result of contraction of nearly solid rhyolite.

The association of cassiterite with bixbyite and pseudobrookite, minerals that occur primarily in cavities within a microlitic, lithophysal rhyolite facies and for which thermal stabilities have been determined, suggests that tin was deposited, at temperatures of 600°C or higher, from a gas phase derived from the cooling rhyolite under oxidizing conditions. A similar environment of deposition probably applies to the veinlets as well.

Rhyolite alteration includes widespread bleaching and disseminated weak argillization, which leave the rock white and porous. Sericitization and topaz replacement of K-feldspar are recognizable locally, but are not intense adjacent to the walls of the tin-bearing veinlets. Composition of veinlet feldspar and whole-rock analyses indicate that the alteration is characterized primarily by enrichment in alkalis, chiefly potash.

A comparison of bulk compositions of some "tin-rhyolites" with those of unmineralized rhyolites suggests that the "tin-rhyolites" are not uniquely characterized by major element content, but range in composition from the siliceous-alkaline type of the Black Range variety to the more alumina-rich type found in parts of Mexico.

# TABLE OF CONTENTS

	Page
ACKNOWLEDGMENTS . . . . .	iii
ABSTRACT . . . . .	v
LIST OF TABLES . . . . .	x
LIST OF ILLUSTRATIONS . . . . .	xi
INTRODUCTION . . . . .	1
Location and Accessibility . . . . .	1
Previous Work . . . . .	2
Brief History and Production of District . . . . .	4
Geologic Setting . . . . .	6
Field Work . . . . .	8
Laboratory Studies . . . . .	9
PARAMOUNT CANYON-TAYLOR PEAK AREA . . . . .	10
Location . . . . .	10
General Features . . . . .	11
Datil Formation, Taylor Creek Rhyolite . . . . .	13
Petrology . . . . .	14
Bleached Facies . . . . .	23
Porphyritic Vitrophyre . . . . .	26
Flow-Breccia . . . . .	30
Microclitic Rhyolite . . . . .	32
Minerals within the microclites and lithophysae . . . . .	33
Temperature of formation of oxide minerals . . . . .	41
Discussion . . . . .	47
Pyroclastic rocks . . . . .	49
Gila Conglomerate . . . . .	50
Holocene Deposits . . . . .	52
RHYOLITE STRUCTURE AND MODE OF EMPLACEMENT . . . . .	53
TAYLOR CREEK PROSPECTS . . . . .	61
Introduction . . . . .	61
General Features . . . . .	61
Taylor Creek Rhyolite . . . . .	64
Alteration . . . . .	67
Tin-Bearing Veinlets . . . . .	67

	Page
Rhyolite Chemistry . . . . .	71
Rhyolite Structure and Localization of Veinlets . . . . .	72
Source of Tin and Mineralizing Fluids . . . . .	82
SOUTH KEMP MESA-BEAVER CREEK AREA . . . . .	87
General Features . . . . .	87
Taylor Creek Rhyolite . . . . .	88
Tin-Bearing Veinlets . . . . .	91
Andesite . . . . .	92
Holocene Deposits . . . . .	93
Summary . . . . .	93
ALKALI FELDSPARS . . . . .	94
Introductory Statement . . . . .	94
Phenocrysts . . . . .	96
Structural State . . . . .	99
Composition . . . . .	103
Discussion . . . . .	104
CHEMISTRY OF VOLCANIC ROCKS . . . . .	107
General Statement . . . . .	107
Major Elements . . . . .	113
Trace Elements . . . . .	121
APPENDIX: TIN-BEARING NUGGETS . . . . .	128
Introduction . . . . .	128
Mineralogy and Texture . . . . .	129
Composition . . . . .	133
Specific Gravity . . . . .	135
Speculations on Mode of Origin . . . . .	138
REFERENCES . . . . .	141

# LIST OF TABLES

Table		Page
I	Unit-cell dimensions and optic axial angles of some natural topaz crystals . . . . .	35
II	Tin content of hematite, Paramount Canyon . . . . .	36
III	Composition of bixbyite, Paramount Canyon . . . . .	39
IV	Composition of pseudobrookite . . . . .	40
V	Unit-cell dimensions of alkali feldspar from the Taylor Creek Rhyolite, Black Range, New Mexico . .	100
VI	Chemical, normative, and trace-element analyses of volcanic rocks, Taylor Creek and Beaver Creek areas . . . . .	108
VII	Spectrographic analyses for F and Sn in Cenozoic hypohyaline silicic volcanic rocks from the southwestern United States . . . . .	125
VIII	Tin analyses and specific gravities of selected tin-bearing nuggets from the Black Range, New Mexico . . . . .	134



# LIST OF ILLUSTRATIONS

Plate		Page
1.	Regional geologic map of the Black Range tin district . . . . .	in pocket
2.	Geologic map of the Paramount Canyon-Taylor Peak area . . . . .	"
3.	Map showing inferred flow directions of the Taylor Creek Rhyolite, Paramount Canyon-Taylor Peak area . . . . .	"
4.	Geologic map of the Taylor Creek prospects area . . . . .	"
5.	Tin assay data for the Taylor Creek prospects area . . . . .	"
6.	Geologic map of the South Kemp Mesa-Beaver Creek area . . . . .	"

Figure		
1.	Index map of study area . . . . .	3
2.	Broad erosional surface developed on the Taylor Creek Rhyolite . . . . .	12
3.	Modal analyses of rhyolite, from point-counts on stained slabs . . . . .	15
4.	Ratios of sanidine and quartz phenocrysts in rhyolite . . . . .	16
5a.	Photomicrograph of the Taylor Creek Rhyolite, Taylor Peak area . . . . .	17
5b.	Same photomicrograph, crossed nicols . . . . .	17
6a.	Spherulitic growth of alkali feldspar and silica . . . . .	20
6b.	Spherulite rosette of micropoikilitic quartz and alkali feldspar . . . . .	20

Figure		Page
6c.	Interlocking crystals of quartz and K-feldspar . . . .	21
6d.	Granophyric intergrowths of quartz and alkali feldspar . . . . .	21
7.	Basal portion of porphyritic vitrophyre exposed in Paramount Canyon . . . . .	28
8.	Detailed view of vitrophyre, showing lensoid black color mottling . . . . .	28
9.	Prominent ledge of flow-breccia as exposed in the south wall of Taylor Creek canyon . . . . .	31
10.	Detailed view of flow-breccia . . . . .	31
11.	Miarolitic, lithophysal rhyolite exposed on north rim of Paramount Canyon . . . . .	34
12.	Hand specimen of miarolitic rhyolite, fea- turing lithophysal structures and a cube of bixbyite . . . . .	34
13.	Photomicrograph of growth zoning in bixbyite . . . .	38
14.	Hematite blebs in pseudobrookite . . . . .	38
15.	Twinned crystal of cassiterite with enclosed blade of hematite . . . . .	42
16.	Phase relations in the system iron oxide- manganese oxide in air . . . . .	44
17.	Phase relations involving the ferropseudo- brookite-pseudobrookite series . . . . .	44
18.	Basal part of pyroclastic section in Paramount Canyon . . . . .	51
19.	Panoramic view of the Boiler Peak flow-dome . . . . .	55
20.	Diagrammatic sketch of the Peleán-type dome . . . . .	60
21.	Sketch of fan-structure in a volcanic dome . . . . .	60
22.	Experimental dome formed by squeezing viscous material through a narrow aperture . . . . .	60
23a.	A prominent recumbent flow-fold developed near the margin of a rhyolite dome in the Taylor Creek prospects area . . . . .	63

Figure		Page
23b.	Delineation of structural details in recumbent flow-fold . . . . .	63
24.	Representative samples of Taylor Creek Rhyolite exposed in the Taylor Creek prospects area . . . . .	65
25.	Sanidine phenocryst mantling plagioclase . . . . .	65
26.	Typical cassiterite-hematite veinlet exposed in the Taylor Creek prospects area . . . . .	69
27a.	Photomicrograph of sharp contact between rhyolite groundmass and tin-bearing veinlet . . . . .	70
27b.	Sericitization embayment of a sanidine phenocryst . . . . .	70
28.	Pole projections of structural features in rhyolite, Taylor Creek prospects area . . . . .	73
29.	Well-defined flow-layering in argillized facies of Taylor Creek Rhyolite in the Taylor Creek prospects area . . . . .	75
30.	Slickensided shear surface in rhyolite . . . . .	75
31.	Slip-line pattern beneath stress-free surface of a theoretical dome of large diameter . . . . .	79
32.	Details of slip-line pattern beneath stress-free surface in snout region of a theoretical dome . . . . .	80
33.	View looking northeast across Beaver Creek at the Taylor Creek Rhyolite . . . . .	89
34.	Typical cassiterite-hematite veinlet exposed in the vicinity of Beaver Creek . . . . .	89
35.	Photomicrograph of sanidine phenocryst, showing albite exsolution lamellae parallel to (001) . . . . .	97
36.	Optic angles of sanidine phenocrysts, Taylor Creek Rhyolite . . . . .	98
37.	b-c plot of alkali feldspars, Taylor Creek Rhyolite . . . . .	101

## Figure

## Page

38.	Normative Ab-Or-Q plot of bulk compositions of the Taylor Creek volcanic rocks . . . . .	114
39.	Normative Q-Ab+An-Or plot of rhyolite analyses . . .	117
40.	Normative Al-Alk-CFM plot of rhyolite analyses . . .	118
41.	FeO/FeO+Fe <sub>2</sub> O <sub>3</sub> ratios in some rhyolites . . . . .	120
42.	Volcanic provinces of the western United States . . .	124
43.	Plot of Sn versus F for Cenozoic hypohyaline silicic volcanic rocks, Nacimiento Subprovince . .	126
44.	Plot of Sn versus F for Cenozoic hypohyaline silicic volcanic rocks, Rio Grande Subprovince . .	126
45.	Plot of Sn versus F for Cenozoic hypohyaline silicic volcanic rocks, Mohave Subprovince . . . .	127
46a.	Representative specimens of tin-bearing nuggets collected in the Taylor Creek district . . . . .	130
46b.	Colloform texture in a typical tin nugget . . . . .	130
47.	Electron probe scanning images, showing distri- bution of several elements in wood-tin . . . . .	136
48.	Plot of specific gravity versus tin content for tin-bearing nuggets from the Black Range . . . . .	137

## INTRODUCTION

The tin deposits in the Black Range of southwestern New Mexico represent one of several cassiterite-rhyolite associations in North America. Among the world's tin deposits, the tin-rhyolite occurrences have received relatively little study, mainly because of their limited economic importance. Moreover, they generally are fine grained and difficult to interpret genetically. Association of tin with biotite granite has long been recognized, but in the tin-rhyolite occurrences biotite and other mafic constituents are scarce.

The Black Range tin occurs inmiarolitic cavities within porphyritic rhyolite, in cassiterite-specularite veinlets that traverse the rhyolite, and also in widespread placer accumulations. This study was undertaken to determine relationships between the rhyolite and associated tin deposits. It was addressed most specifically to the problem of whether the lode tin deposits are indigenous to the host rhyolite, or whether they were introduced and concentrated by late-stage hydrothermal fluids that issued from volcanic vents, as suggested by some earlier workers (e.g., Fries, 1940).

### Location and Accessibility

The Black Range tin district, occupying a rectangular area approximately 18 miles wide and 30 miles long, lies immediately west of the Continental Divide in Sierra and Catron Counties, New

Mexico (Fig. 1 and Plate 1). It includes no villages or towns, but a small population is scattered among several ranches. The U. S. Forest Service operates a Ranger Station near Beaverhead, site of a former hunting lodge in the west-central part of the area.

The area is accessible from the north via State Highway 78 or State Highway 52, both dirt and gravel roads. From Silver City, the area can be reached over State Highways 25 and 61, which are mainly unimproved dirt or gravel roads; this road is referred to locally as the "Outer Loop Drive." The most ready access is from the east via State Highways 52 and 59, which are paved from Truth or Consequences to the Beaverhead Ranger Station. Beaverhead is approximately 87 miles by road southwest of Magdalena, 75 miles west of Truth or Consequences (formerly Hot Springs), and 87 miles north of Silver City. Food and supplies can be obtained in Winston, a small community 43 miles east of Beaverhead.

#### Previous Work

The Black Range tin district and adjacent areas have been studied by several investigators since the initial discovery of stream tin by J. W. Welch in 1918. The first reconnaissance study was made by Hill (1921) in 1920. The regional geology was mapped later between coordinates  $33^{\circ}15' - 33^{\circ}30'$  N latitude and  $107^{\circ}45' - 108^{\circ}15'$  W longitude on a scale of 1:62,500 (Fries, 1940; Fries and Butler, 1943).

Between 1939 and 1943, the U. S. Bureau of Mines conducted an extensive sampling program throughout the district (Volin and others, 1947). In this investigation, 1188 samples were collected and analyzed.

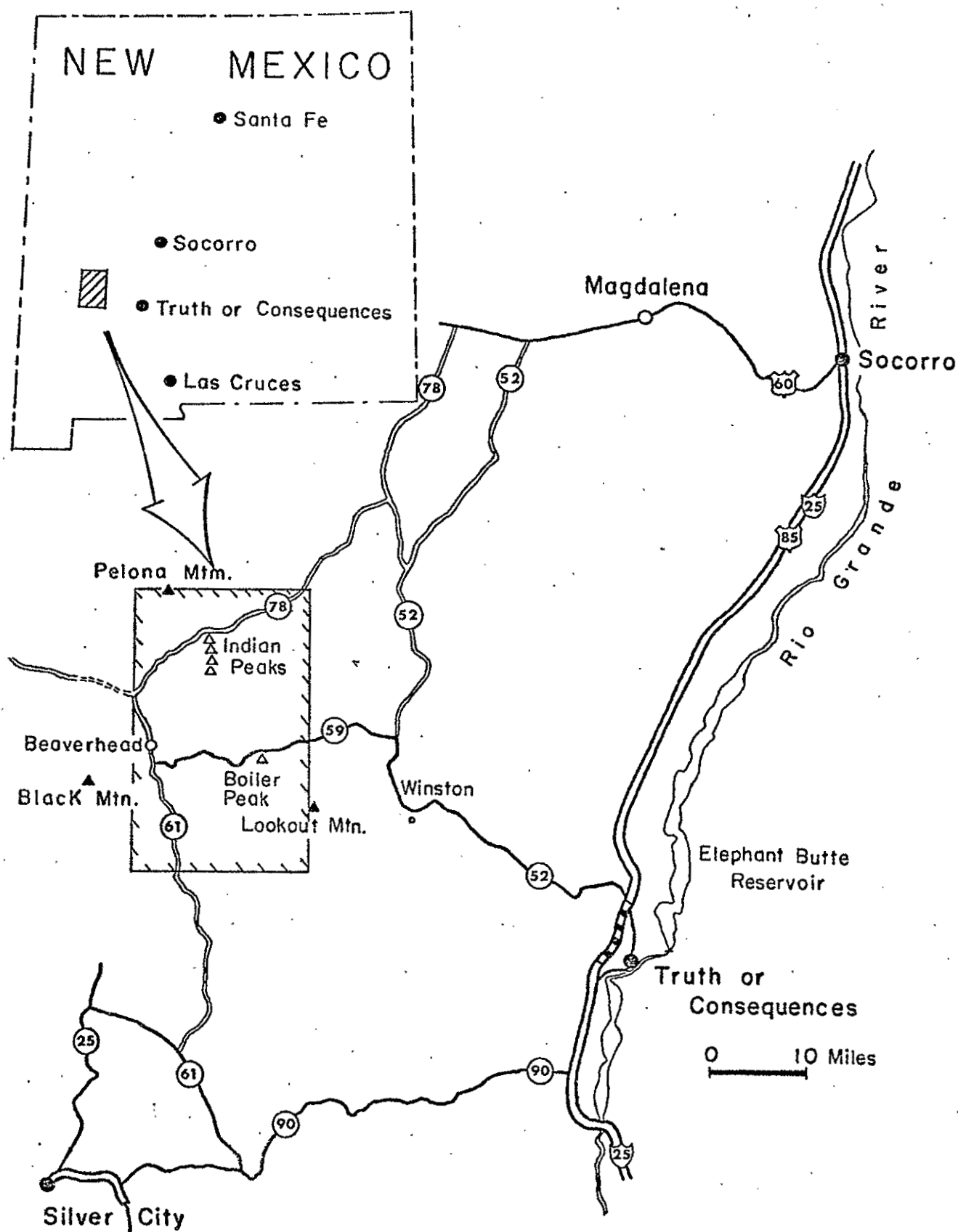


Fig. 1. Index map of study area.

Reconnaissance mapping by geologists of the New Mexico Bureau of Mines has extended over several years in quadrangles adjacent to, and including the tin district (Willard, 1957a, b; Willard and Givens, 1958; Weber and Willard, 1959a, b; and Stearns, 1962).

Elston and others (1968), who have studied the volcano-tectonic relationships of the Mogollon Plateau, have referred to the tin-bearing rhyolite as the Taylor Creek Rhyolite, after a prominent drainage in the area. This informal terminology is retained in this study.

Richard H. Jahns, Stanford University, has worked in the area intermittently since World War II, mapping and sampling for the U. S. Geological Survey and the New Mexico Bureau of Mines and Mineral Resources.

More recently, the Geological Survey (Erickson and others, 1970) has conducted a geochemical sampling and mapping program in the Black Range Primitive Area, which lies immediately south of the tin district.

#### Brief History and Production of District

Since the discovery of tin in the Black Range, mining activity has been sporadic, with no substantial or sustained production. At least seven companies showed interest in parts of the district during the late 1930's and early 1940's. They included the Beaver Creek Tin Mining Co., New Mexico Tin and Metals Co., Nevada Consolidated Copper Co., American Tin Mines Co., Colorado-New Mexico Tin Corp., LaCruz Development Co., and Sierra Metals Co. No extensive operations were developed.



Considerable effort by individual miners and small mining companies has been directed toward eluvial and alluvial placer deposits associated with intermittent streams, principally Hardcastle and Squaw Creeks north of Highway 59, and Sawmill Canyon and Taylor Creek to the south (Plate 1). The greatest production has come from Nugget Gulch near Hardcastle Creek (8000 lbs of concentrate during 1940-43), largely through the work of Mr. Paul Bellamy, a local resident who is now retired.

The best exposed concentrations of lode tin are near the mouth of Taylor Creek above Wall Lake and at Squaw Creek. The hematite-cassiterite veinlets have not proved economical to mine, owing to their low grade, small dimensions, and lack of persistency.

Total production from the district is unknown, but the U. S. Bureau of Mines (Volin and others, 1947) estimated that a total of 21,900 lbs of tin concentrate was produced between 1940 and 1943, more than one-third coming from Hardcastle Creek. Excluding minor lode production from Taylor Creek, output from the district for this interval was 9.85 tons of concentrate averaging 50 percent tin.

In 1969, Paul Bellamy leased some of his claims on Hardcastle Creek to Clarence L. Gitman, who constructed a small tin mill that included four sets of Pan American jigs. Since its construction, the mill has been plagued by water shortage and mechanical breakdowns. To date, there has been no production from this effort.

During the spring of 1970, R. C. Kur did assessment work on claims recently staked on Sawmill Canyon, south of Highway 59. According to reports, other claims recently have been staked at

Indian Peaks in an area also characterized by porphyritic rhyolite at the north end of the district.

### Geologic Setting

Fries and Butler (1943) first mapped the regional geology of the Black Range tin district (Plate 1), and a summary of their results is included here to provide a lithologic and chronologic framework for the tin-bearing rhyolite. They subdivided the pile of Tertiary to Quaternary volcanic rocks into six units that represent a range in composition from basalt to rhyolite. From oldest to youngest, these units include:-- a lower basic volcanic series (Tba), a felsitic volcanic series (Tfl), a rhyolitic volcanic series (Tt) that includes the tin-bearing rhyolite (Tr); an upper basic volcanic series (QTb), a thick clastic unit (QTc), and alluvium (Qal). Four of these units have now received formal names. The lower three units have been correlated with the Datil Formation, which has been mapped farther to the north and west (Willard, 1957a, b; Willard and Givens, 1958; Weber and Willard, 1959a, b). The upper clastic unit is designated the Gila Conglomerate on the New Mexico State map and is roughly equivalent to the Santa Fe Group exposed in the Rio Grande Valley (Dane and Bachman, 1965). Most of the units are separated from adjacent ones by erosional unconformities. Interfingering of units, particularly within the Datil Formation, also is common.

The lower, basic volcanic rocks, exposed only in the southern half of the district, are at least 1000 feet in thickness. The base of this section is not exposed. The rocks are dominantly basaltic and andesitic lavas with interlayered tuff, breccia, and clastic

sediments. This series presumably lies on upper Paleozoic (Pennsylvanian and Permian) sedimentary rocks, which are known to crop out east of the district.

The felsitic volcanic series is 50 to 200 feet thick and consists of felsite, latite, and andesite flows, with interlayered tuff and breccia.

The rhyolitic volcanic series includes rhyolitic tuff and breccia with interlayered flows of latite and porphyritic rhyolite. Minor sandstone and conglomerate are included. Within this series, the tin-bearing rhyolite, referred to in this study as the Taylor Creek Rhyolite, forms broad flow-domes and is dominant in the lower section. The upper rhyolitic section is mainly latite and rhyolite, with some breccia.

The upper basic flows, which are widespread in the western part of the district, were mapped by Fries and Butler as basalts. This series also includes andesites and probably basaltic andesites similar to other recent flows of the Mogollon Plateau (Elston, oral comm.). Its maximum thickness is 1500 feet or more at Pelona Mountain to the north, but in general the thickness is much less. A 300- to 400-foot section of andesite is well exposed along the walls of Beaver Creek near Kemp Mesa (Plate 6).

The clastic sequence (Gila Conglomerate) is the most widespread unit. It comprises tuffaceous sandstones and coarse gravels derived from the underlying volcanic rocks. Good exposures are found along upper Beaver Creek and its tributaries. Several hundred feet of predominantly brown, tuffaceous sandstone crops out north of Greer's Ranch (Plate 2).

Recent alluvium and terrace deposits are present in and along intermittent streams and their tributaries. Many of these occurrences have been prospected for tin in the past, and as recently as 1970, alluvial placers were being worked by C. L. Gitman near Hardcastle Creek.

### Field Work

Five months during the summer of 1969 and the spring of 1970 were spent in field mapping and sampling, principally in three areas covering a total of about 10 square miles within the tin district. These areas are outlined on the geologic map of Fries and Butler (Plate 1). From east to west, they include the Paramount Canyon-Taylor Peak area, the Taylor Creek Prospects area, and the south Kemp Mesa-Beaver Creek area. They were selected for study because they provide good exposures of the tin-bearing rhyolite, and because cassiterite-hematite veinlets can be observed in a few places.

Paramount Canyon and vicinity were mapped on the Lookout Mountain 15' quadrangle sheet, enlarged to a scale of approximately 1" = 1000' (Plate 2). Two weeks were spent in the Taylor Creek Prospects area chiefly for sampling and adding minor structural details to a large-scale geologic map compiled from the excellent work of Fries (1940) and Jahns (1957-62, unpubl.).

The small South Kemp Mesa-Beaver Creek area was mapped on a U. S. Forest Service aerial photograph, enlarged to a scale of approximately 1" = 900'. This map subsequently has been enlarged to 1" = 400' and is presented as Plate 6.

Laboratory Studies

More than one hundred samples were slabbed in preparation for thin-section and polished-section study. Of these, forty slabs were stained and point-counted to determine phenocryst ratios. Several of these were also point-counted in thin-section for comparison.

Mineral separations were prepared from ten samples. Individual, fist-sized samples were crushed and pulverized to a -80+120 mesh fraction. Alkali feldspar phenocrysts were concentrated by centrifuging in bromoform, with successive dilutions by acetone. A clean concentrate of feldspar phenocrysts generally was not obtained by this process, owing to similarities in specific gravity between these crystals and devitrified groundmass feldspar. Phenocrysts then were hand-picked under the binocular microscope. The Frantz magnetic separator was found to be unsatisfactory for the separation of feldspar from devitrified groundmass, but it was highly effective in the removal of the more magnetically susceptible glassy groundmass of a vitrophyric rhyolite facies. Feldspar phenocrysts, as well as some groundmass and veinlet phases, were then later X-rayed for determinations of composition and structural state.

Oxide minerals, including bixbyite, pseudobrookite, hematite, and cassiterite, were separated from a facies of microlitic rhyolite, and their compositions were determined by ARL electron microprobe, using appropriate natural oxides of similar composition as standards.

Fourteen samples were prepared for bulk chemical and trace-element analyses. Fist-sized material was broken in a chipmunk jaw-crusher to about -3 mesh, and was sieved through -11 mesh nylon

screen. The -11 mesh fraction was then split to give two 100-150 gram samples, which were reduced to -100+120 mesh in a micro-pulverisator equipped with 99.9 percent alumina plates. Two 20- to 30-gram splits of each sample were then obtained, one of which was submitted to the New Mexico Bureau of Mines and Mineral Resources for analysis. The other was retained as a duplicate.

#### PARAMOUNT CANYON-TAYLOR PEAK AREA

##### Location

The Paramount Canyon-Taylor Peak area (Plate 2) lies south of State Highway 59; the eastern border is approximately four miles west of the Continental Divide. From Truth or Consequences, the distance is approximately 60 miles via Winston on paved Highways 52 and 59. Geologic mapping done in this area covers the southeast corner of T 10 S, R 11 W, including most of sections 13, 14, 23, 24, 25, and 26 and the southwestern portion of T 10 S, R 10 W, sections 18, 19, and 30.

The north rim of Paramount Canyon is readily accessible immediately south of Highway 59. The canyon, occupied by an intermittent tributary of Taylor Creek, also can be reached via the Lookout Mt. road, which is graded dirt and branches southward from Highway 59 about one mile east of Boiler Peak. From this road, a jeep trail extends for several miles down Taylor Creek, well past the junction with Paramount Canyon.

Taylor Peak, a prominent landmark at 8288 ft, is two miles southeast of Paramount Canyon. It also can be reached via the Lookout Mt. road.

### General Features

An area of approximately 9 square miles was mapped geologically in order to determine relationships throughout the interior of a rhyolite flow-dome approximately 7 miles long and 4 miles wide. This rhyolite mass is here referred to as the Boiler Peak dome.

Three rock units, with associated distinguished facies, have been recognized. They include, from oldest to youngest, the Datil Formation, Gila Conglomerate, and Quaternary deposits. They range in age from Oligocene to Holocene.

Within this area, rhyolite of the Datil Formation has been eroded in Quaternary time to a broad pediment surface that slopes gently westward at a grade of approximately 70 feet per mile ( $1^{\circ}$ ). This surface (Fig. 2), probably of Pleistocene age, is youthfully dissected, with Boiler Peak (8648 ft) and Taylor Peak (8288 ft) standing as conspicuous landmark remnants a few hundred feet above the surrounding country. Taylor Creek, in one of the prominent drainage courses in the Black Range, flows intermittently westward through the southern part of the area, where the average local relief is 400 to 500 feet. The creek in Paramount Canyon is an intermittent tributary of Taylor Creek.

The area lies within the Gila National Forest, and features extensive stands of small but abundant ponderosa pine. The climate is dry throughout most of the year, with the exception of snow during the winter months and scattered thunder showers occurring principally during the summer months of July and August.

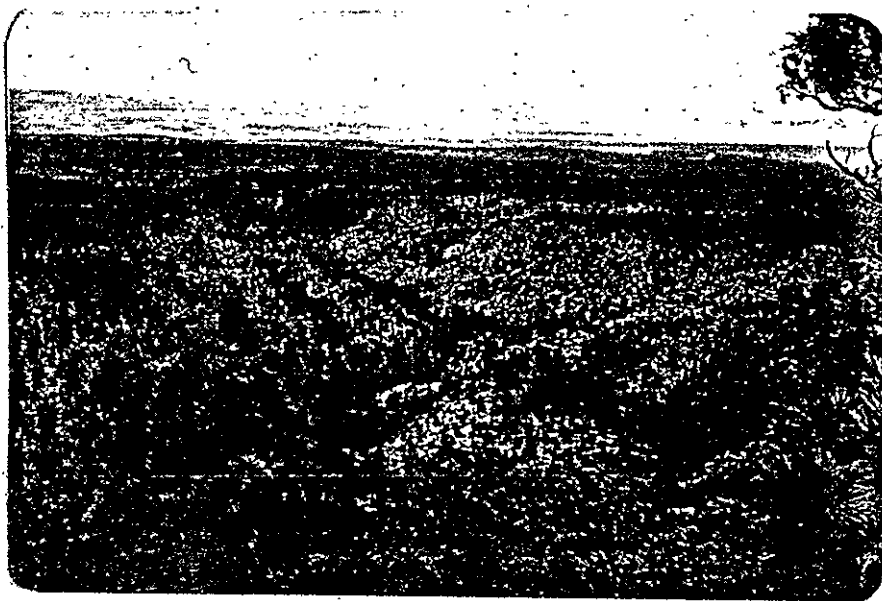


Fig. 2. View from Taylor Peak looking westward down Taylor Creek canyon, showing a broad erosional surface developed on top of the Taylor Creek Rhyolite. Black Mountain is in right background.



Datil Formation, Taylor Creek Rhyolite

The Boiler Peak dome consists mainly of pale red to gray, flow-layered, porphyritic rhyolite. Sanidine and quartz are pre-dominant among the phenocrysts. Five intergradational facies of porphyritic rhyolite have been differentiated on the basis of texture and color. Except for a microlitic facies, these rocks are mineralogically similar to one another. These facies formerly were not differentiated, due largely to smaller map scales, but were described as one unit, the "tin-bearing rhyolite" (Tr of Fries, 1940; Fries and Butler, 1943; Tdrs of Bricksen and others, 1970). Elston and others (1968) referred to this unit informally as the Taylor Creek Rhyolite, and this designation is adopted here. The Taylor Creek Rhyolite (Tdto) belongs to the second of three calc-alkaline volcanic cycles represented in the Datil Formation of the Mogollon Plateau (Elston and others, 1968).

The most conspicuous feature of the rhyolite is flow-layering, which is characterized by reddish spherulitic patches and lenses enclosed in a lavender to gray, aphanitic matrix. Well-defined parting surfaces, spaced less than one to two feet apart, are commonly developed parallel to the flow-layering.

The rhyolite unit is well exposed along Taylor Creek and its tributaries, as well as on Taylor Peak and Boiler Peak. Weathering features are variable. On the upland surfaces, the rock generally weathers to lavender-colored, boulder-like forms. Along the upper walls of Taylor Creek, weathering is controlled by intersecting sets of vertical joints that produce prismatic columns twenty feet or

more high. In other places, the rhyolite weathers into thin slabs controlled by parting planes parallel to the flow-layering. Rarely, weathering produces a natural arch, which was observed in only one locality in the south wall of Taylor Creek Canyon.

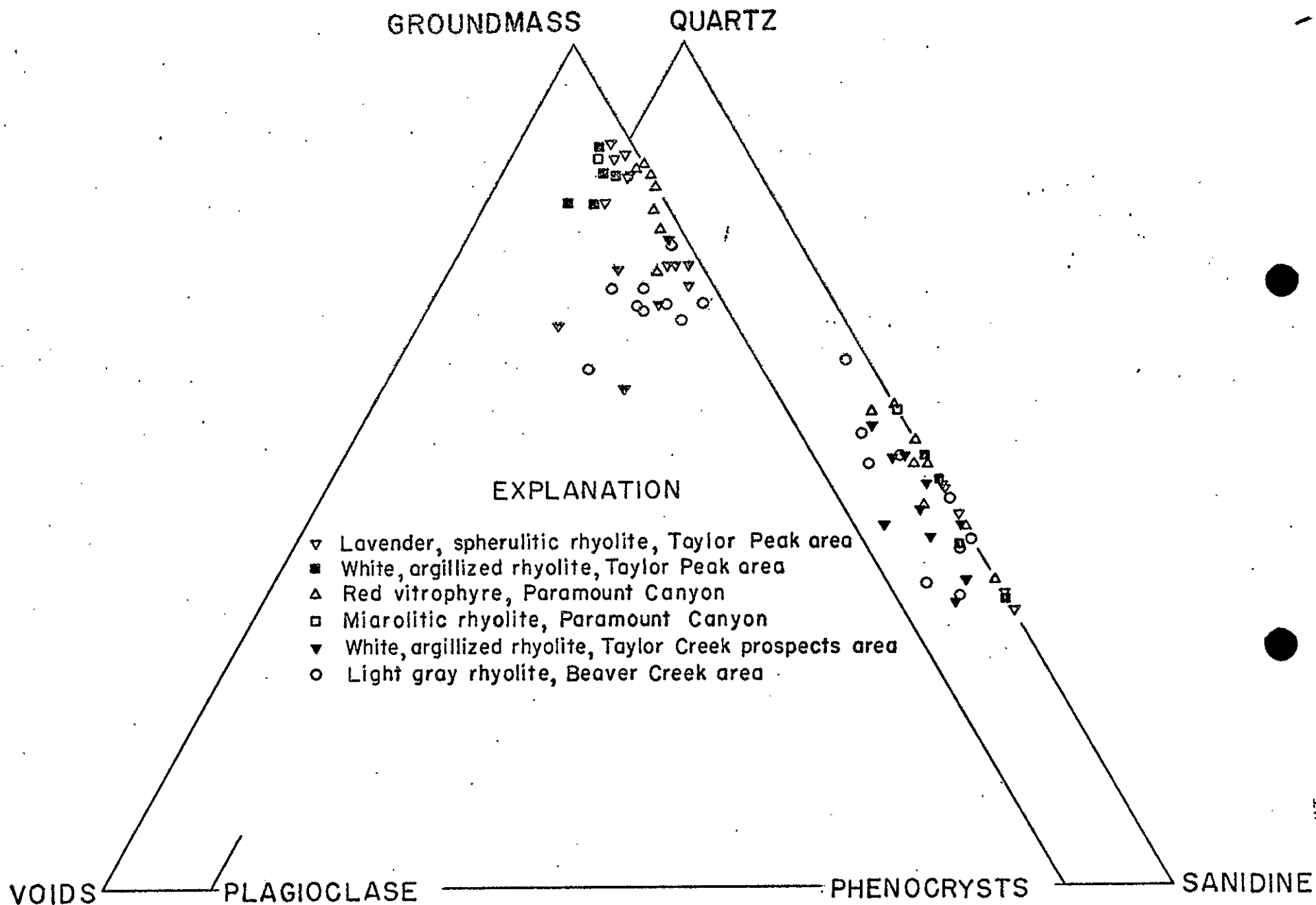
Contacts with other rhyolite facies in the flow-dome generally are gradational, but contacts with interlayered pyroclastic rocks are sharp.

During Pleistocene (?) time, this unit was eroded to form a generally flat upland surface that slopes gently westward. Taylor Creek has dissected the interior of the unit to provide an average of 500 feet of vertical exposure. As much as 800 feet of rhyolite is exposed at Taylor Peak, but here the base cannot be observed. Total thickness of the mass, therefore, is unknown.

#### Petrology

The Taylor Creek Rhyolite is porphyritic, with phenocrysts of sanidine, quartz, and minor plagioclase and biotite set in a felsitic to spherulitic groundmass (Fig. 5). The rock ranges in color from gray to pale red, weathering commonly to shades of gray and lavender. Accessory minerals include titaniferous magnetite, sphene, fayalite (?), zircon, and rarely hornblende. Secondary minerals include predominantly K-feldspar and quartz, with hematite, biotite, topaz, pseudobrookite, clay, and sericite. On the average, phenocrysts constitute 11 percent of the rock, groundmass 86 percent, and voids 3 percent. The sanidine-quartz ratio is about 1.4. Modes and phenocryst ratios are plotted in Figures 3 and 4.

Fig. 3. Rhyolite modes point-counted on stained slabs.



## EXPLANATION

- ▽ Lavender, spherulitic rhyolite, Taylor Peak area
- White, argillized rhyolite, Taylor Peak area
- △ Red vitrophyre, Paramount Canyon
- Mirolitic rhyolite, Paramount Canyon
- ▼ White, argillized rhyolite, Taylor Creek prospects area
- Light gray rhyolite, Beaver Creek area

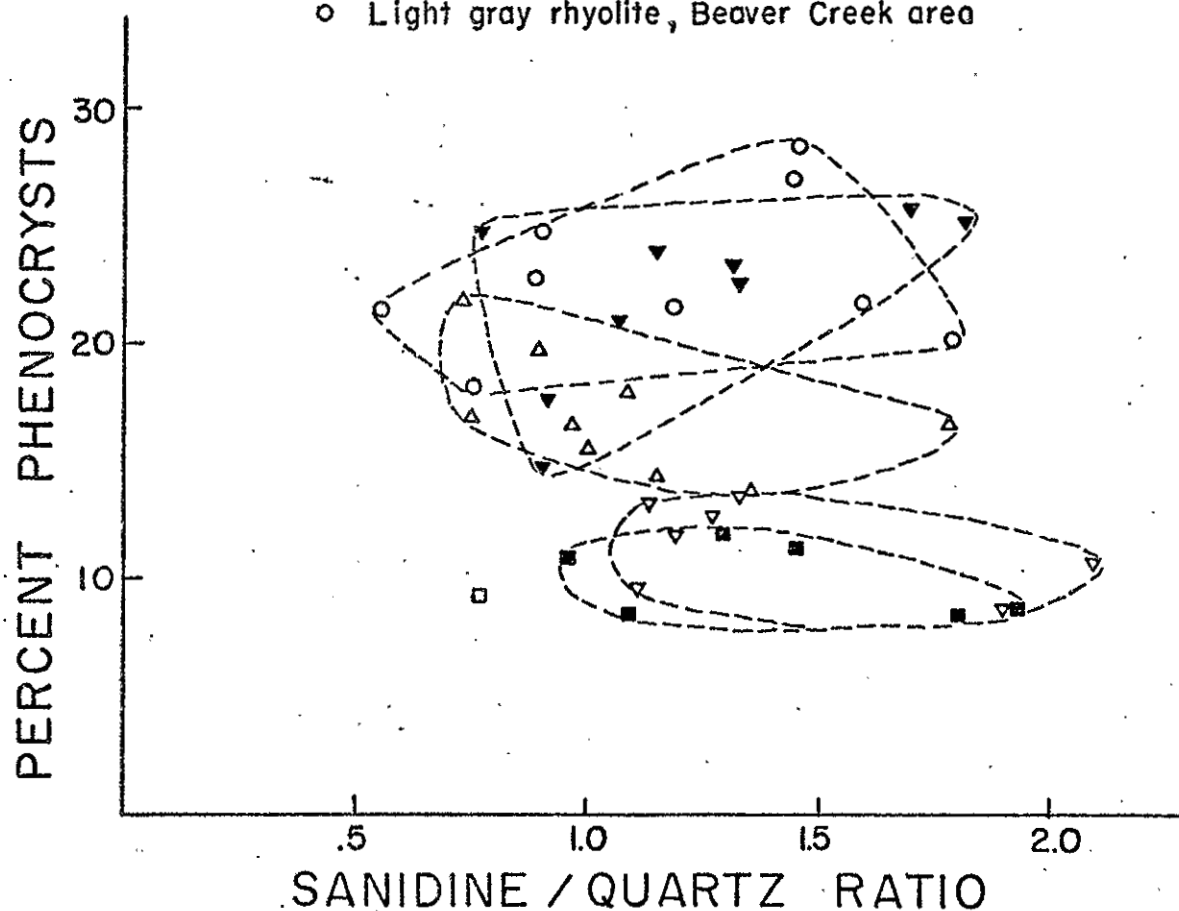


Fig. 4. Sanidine and quartz phenocryst ratios in rhyolite.

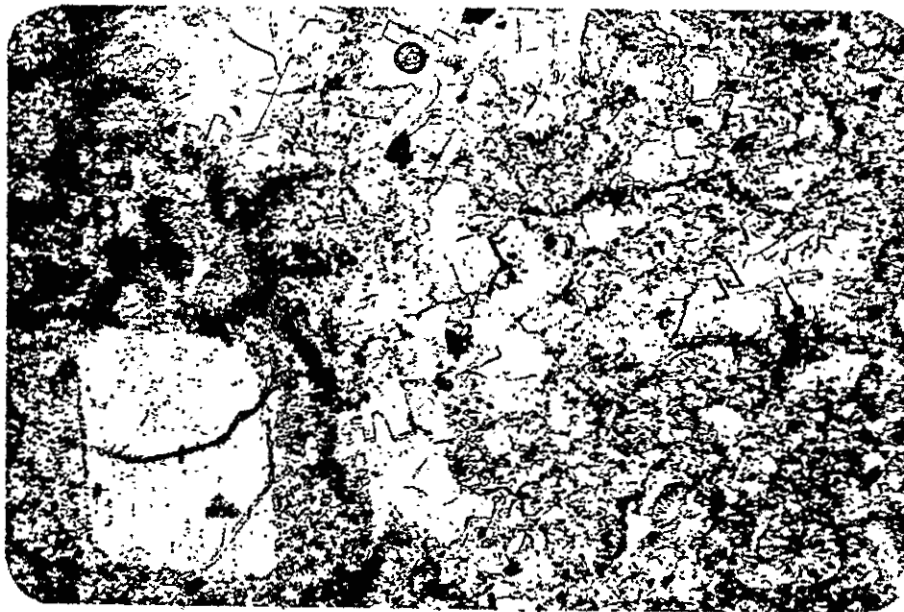


Fig. 5a. Photomicrograph of the Taylor Creek Rhyolite, Taylor Peak area. Sanidine phenocryst enclosed in spherulitic groundmass (left), most of which is devitrified (right) to alkali feldspar and quartz. Plane-polarized light, 72x.

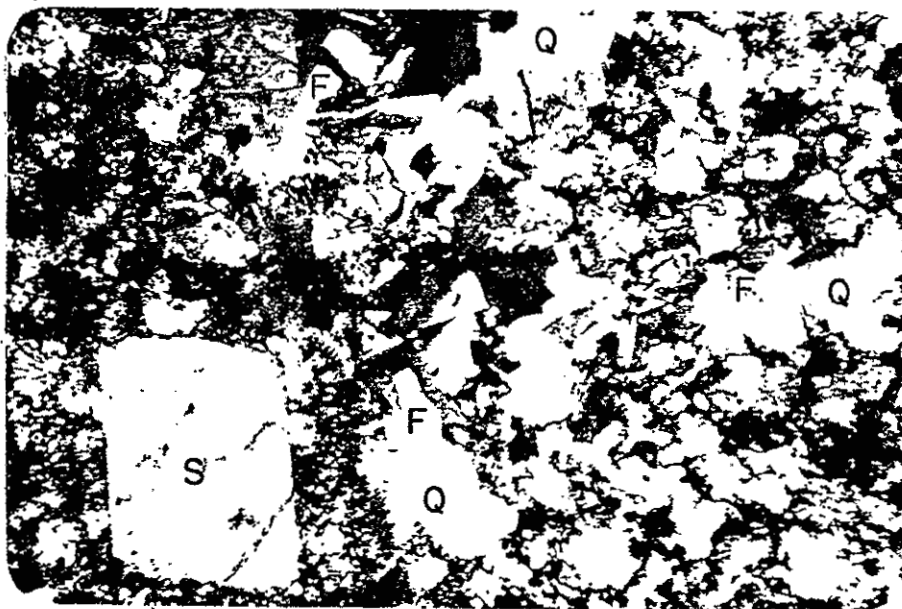


Fig. 5b. Same as above, crossed nicols.

The sanidine phenocrysts are .5 to 2.5 mm in length and constitute 5 to 7.5 percent of the rock, based on point counts of seven stained slabs. The crystals typically are euhedral to subhedral laths, with appreciably recrystallized borders. Carlsbad twinning is common; zoning is rare. Data on structural state and chemical composition of alkali feldspar are discussed farther on.

The quartz, generally smoky, forms subhedral to euhedral bipyramids 1.5 mm or less in diameter. The borders of many crystals are irregular, and appear to reflect corrosion and recrystallization. Some individuals evidently have been enlarged through devitrification of adjacent groundmass, and in one unusual occurrence the inferred enlargement is by a factor of about four. Throughout the rock, the crystals of quartz range from unbroken to highly fractured. Some are weakly biaxial, presumably as a result of strain.

Sodic oligoclase, which rarely exceeds 1 percent by volume of the rock, occurs as small, irregular grains, or as small clusters of several grains intergrown together. The phenocrysts typically are mantled by sanidine and appear to lack any preferred orientation.

The groundmass of the rhyolite consists mainly of K-feldspar and quartz arranged in spherulitic to microcrystalline aggregates, with interstitial silica minerals and zeolites (?). Primary accessory minerals, which amount to less than 1 percent of the rock, include magnetite, sphene, fayalite (?), and zircon. Secondary hematite and biotite are widely distributed in the groundmass. The biotite appears as very small flakes ( $\leq 8\mu$ ) that are pleochroic in shades of yellow, green, and reddish-brown. Zircon commonly occurs as inclusions in phenocrysts of magnetite and biotite, and rarely as individual

microphenocrysts. Fayalite was not positively identified from this locality, but its presence in the Taylor Creek Rhyolite near Seventy Four Draw suggests that it may be characteristic of the rock; a reaction to form hematite probably has obscured its occurrence in the Paramount Canyon area.

Nearly all stages of devitrification can be observed within single thin-sections of rhyolite, and especially that in the Taylor Peak area. Much of the rhyolite groundmass is marked by cloudy patches in which spherulitic fibers of alkali feldspar are present. These grade into expressions of an intermediate stage featuring groups of K-feldspar crystals arranged radially about poikilitic quartz cores. Later-stage aggregates of interlocking feldspar and quartz grains also are abundant. Granophyric intergrowths are commonly observed at the margins of cavities in the rock.

Sequential steps in devitrification of the Taylor Creek Rhyolite are illustrated in Figures 6a, b, and c; all photomicrographs were obtained from one thin-section. The crystallization commonly begins with development of submicroscopic, sheaf-like to spherical bundles of K-feldspar and silica (Fig. 6a), each of which generally develops further into a complete spherulite of feldspar laths radially disposed about a poikilitic quartz core. Some microscopic quartz also can be observed with alkali feldspar in granophyric intergrowths that represent an intermediate step in the transition to coarser-grained radial feldspar laths. In the process of devitrification, the optically continuous quartz blebs within each spherulite begin to crystallize as one grain while the feldspar laths continue to grow outward. This commonly results in a near-perfect "sunflower" pattern,



Fig. 6a. Incipient spherulitic growth of alkali feldspar and silica at early stage in the devitrification of rhyolite glass. Crossed nicols, 720x.

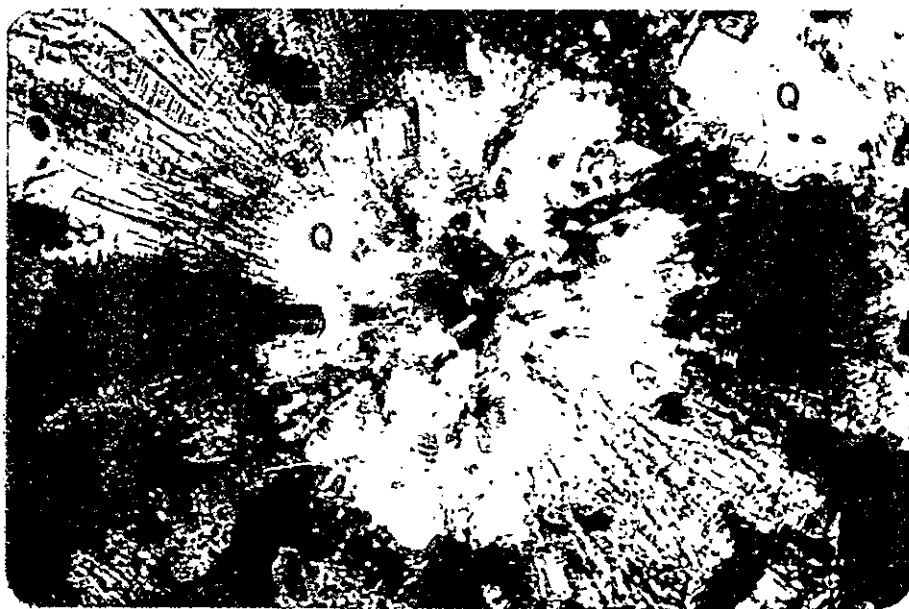


Fig. 6b. Intermediate stage of devitrification, featuring a spherulite rosette of micropoikilitic quartz (Q) surrounded by radial growths of alkali feldspar (F). Crossed nicols, 720x.



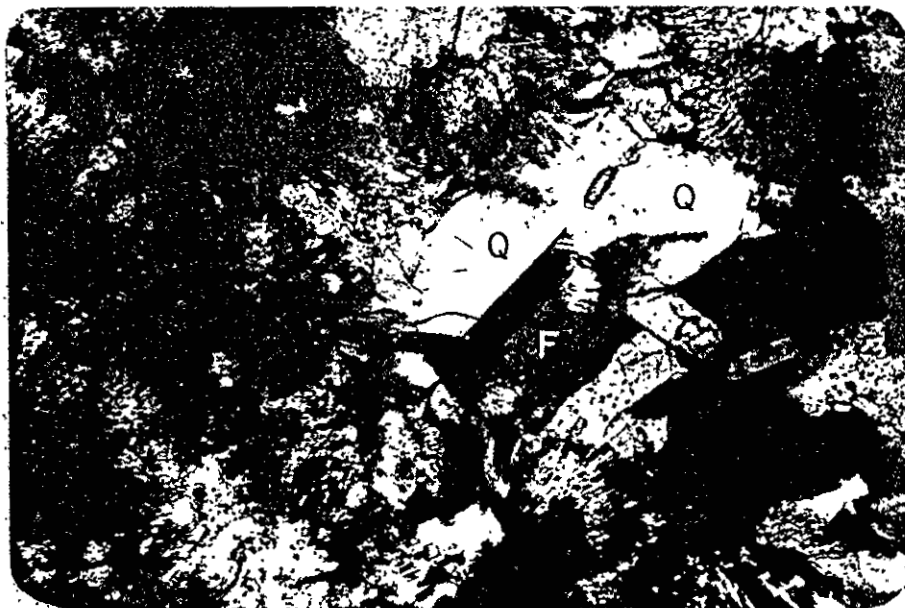


Fig. 6c. Interlocking crystals of quartz and K-feldspar grown interstitially to spherulites. Crossed nicols, 288x.

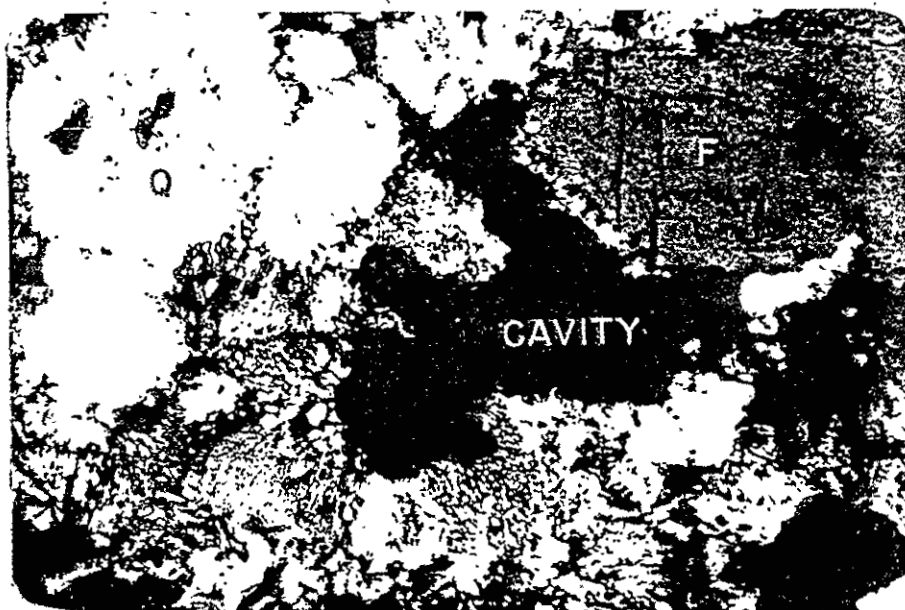


Fig. 6d. Granophyric intergrowths of quartz and feldspar developed at margins of a cavity. Intergrowth appears to have developed directly from spherulitic glass. Crossed nicols, 264x.

or rosette, with a poikilitic quartz core surrounded radially by laths of feldspar (Fig. 6b). Such radially disposed laths commonly remain visible in the quartz core at this stage of spherulitic development, as do inclusions of fine-grained biotite and opaque minerals. Eventually, the core becomes non-poikilitic as it develops into a near-spherical mass of quartz. At a later stage this mass begins to coalesce with other spherulite cores. The radial growth and enlargement of the abundant spherulites defines irregular, pocket-like interstitial areas, where larger individuals of marginal K-feldspar commonly are intergrown with quartz (Fig. 6c). Many of the alkali feldspar crystals lose their prismatic habit in this process of enlargement, and the development of Carlsbad twins and cleavage planes generally is not observed until this stage of growth. Some of these intergrowths may represent vapor-phase crystallization in addition to those formed through the process of devitrification of rhyolite glass.

Many petrologists believe that the end stage in the devitrification process is marked by development of granophyric textures. Although this has not been recognized as an end-stage process in the Taylor Creek Rhyolite, it is interesting to note that the beginnings of a granitic texture can be recognized locally, as expressed by the pocket growths of interlocking fledspar and quartz.

Viscosity has long been regarded as a major factor in the growth and development of spherulites (e.g., Iddings, 1887, 1891; Cross, 1891; Pirsson, 1910). More recently, Keith and Padden (1963, p. 2411) found that "spherulite-forming melts not only have viscosities higher than those of simple liquids--higher by at least two orders of

magnitude--but, in addition, they crystallize much more slowly."

It has been further shown, experimentally, that heat and alkali-rich solutions increase the devitrification rates of rhyolite glass by four to five orders of magnitude in the temperature range 240° to 700°C and at water pressures of .5 to 4 kb (Lofgren, 1968).

Basic principles of spherulite growth have been explained by Keith and Padden (1963) and have been applied by Lofgren (1968) to rhyolite glasses. According to these investigators, a highly viscous, siliceous melt provides the slow crystallization necessary for spherulite growth by creating small coefficients of self-diffusion and low temperature gradients. The growth of radial feldspar fibers, which characterizes spherulites, creates excess 'impurity,' silica, at the crystal-glass interfaces. The silica, in turn, provides a stabilizing effect on initial feldspar fiber growth, while preventing its lateral growth at the same time. Thus silica, which ordinarily crystallizes later on as tridymite or quartz, plays an important role in the outward growth of spherulites. For details on spherulite growth and devitrification, the work of Keith and Padden and its application to silicate glass systems (Lofgren, 1968) should be consulted.

#### Bleached Facies

In general, the bleached and weakly argillized facies occurs in the lowest section of the Taylor Creek Rhyolite. This facies crops out chiefly in two areas. As noted on Plate 2, one area includes the lower rhyolite section as exposed in the north wall of Taylor Creek, extending from the mouth of Paramount Canyon approximately

7000 feet eastward. The other large mass of bleached rhyolite is exposed in the valley immediately east of Taylor Peak.

Contact relations with overlying units, mainly fresh, unbleached rhyolite (Tdtc), are gradational and are delineated on the geologic map by a dotted line that indicates approximately the limit of bleaching. This facies constitutes 300 to 400 feet of the north wall of Paramount Canyon near its junction with Taylor Creek, where it forms a small, arch-like structure. Rocks on the south flank of this structure grade upward through a thin zone of vuggy, spherulitic rhyolite into brecciated and contorted rhyolite. This upper brecciated facies continues westward beyond the map area. From Paramount Canyon eastward, bleached rhyolite exposed along Taylor Creek grades upward into the well-jointed, gray to pale-red rhyolite that forms the canyon rims.

A distinctive feature of the bleached rhyolite facies in Paramount Canyon is shearing, which is most clearly expressed in rocks exposed near the junction with Taylor Creek. Here, subparallel shear surfaces strike northwest and indicate a shear direction to the southwest off the margin of a local, arch-like structure. These shears are local features, whose lengths are measured commonly in a few feet or less. One shear surface is discontinuously exposed for about 300 feet along its length, however. These surfaces are very well defined, and generally are polished and slickensided. They are partly silicified, but not mineralized or iron stained. In some places, individual shear-bounded blocks express backward rotation that is suggestive of slump features formed by gravity sliding. The

amount of movement parallel to these shears is not known, but it does not appear to be great.

The other main exposure of this facies is in the southeast corner of the map area. Here it also forms part of the lowest rhyolite section, which grades upward into unbleached rhyolite. At the eastern margin of the flow-dome, the bleached rhyolite is either juxtaposed against pyroclastic rocks or is overlain by Gila clastic sediments. The strike of flow-layering in the bleached facies generally trends northwesterly, with attitudes ranging up to near-vertical. Locally, rhyolite flowage has resulted in the development of small, asymmetric folds with amplitudes measured in inches.

Mineralogically, the bleached facies closely resembles fresh rhyolite, but differs in weathering characteristics, color, and some aspects of texture. Weak argillization has left the rock noticeably porous and friable. It is gray to white, and commonly weathers into a "honey comb" structure. This "honey comb" or cavernous weathering feature is developed parallel to the flow-layering. The near-vertical walls of these weathering features are typically silicified, and may represent former fractures in the rhyolite that were filled by silica and consequently were resistant to weathering.

Sanidine and quartz are the predominant phenocrysts, and with a little plagioclase they are enclosed in a felsitic, devitrified groundmass. Phenocrysts constitute 10 percent of the rock. The percentage of phenocrysts is somewhat lower than in other rhyolite facies, although practically identical with Tdte (Figs. 3 and 4). The sanidine-quartz ratio is 1.5, higher than in most of the other units.

The principal feature that distinguishes this unit from the unbleached rhyolite is weak argillic alteration, which has been developed largely in the groundmass. Although clay minerals were successfully separated from several samples, no positive identification could be made by X-ray analysis. The clays may be poorly crystallized or they may not be present in sufficient concentration to produce a unique X-ray diffraction pattern. A refractive index of about 1.48 suggests the presence of montmorillonite-type clays. Kaolinite, a common alteration of tuffaceous rocks outside the immediate area, may be present also, but it was not positively identified in this study either.

Clay minerals occur chiefly as interstitial grains throughout the feldspar-quartz matrix. They also can be observed along fractures in sanidine and quartz phenocrysts.

The groundmass appears to be more coarsely crystalline than the unbleached rhyolite facies, resulting in a more granular texture. The fluids responsible for argillization also may have increased the devitrification rate and thereby promoted the development of larger groundmass crystals. Experimental investigations have shown that the presence of aqueous fluids generally increases devitrification rates (e.g., Lofgren, 1968).

#### Porphyritic Vitrophyre

Three small but widely separated masses of rhyolite vitrophyre are exposed within the Boiler Peak dome. The most continuous exposure forms a curvilinear outcrop pattern along the northwest wall of Paramount Canyon (Plate 2). The other outcrop area is in the south-

east map corner along Taylor Creek, where two very small masses are exposed.

The vitrophyre in Paramount Canyon forms a lensoid mass that can be traced more or less continuously for a distance of 5000 feet. At its southern terminus, it appears to pinch out in a thin section of tuff and tuff breccia, although here exposures are poor. At the northern end it thickens and thence disappears in a thicker pyroclastic section. Its contact with the pyroclastic rocks is not observed. The vitrophyric unit is generally less than 50 feet thick, and it reaches a maximum of about 70 feet in the only drainage that crosses the unit. The rock is very brittle, like typical volcanic glass, and is broken by closely spaced vertical joints in groups 1 inch or less wide. A 50-foot section of this vitrophyre near its southern terminus reveals the following: an altered basal vitrophyric breccia, 10 feet thick, overlain by, and in sharp contact with a 6-inch black, porphyritic glass that grades upward into reddish-brown, porphyritic vitrophyre mottled by black lenses elongated parallel to the lower contact (Figs. 7 and 8). The upper section is devoid of color mottling, and is capped by a thin pumiceous rhyolite. Elsewhere, vitrophyre grades upward directly into relatively fresh, flow-layered, lavender-colored rhyolite (Tdtc).

The rhyolite vitrophyre is porphyritic, with phenocrysts of sanidine and quartz enclosed in a glassy but spherulitic matrix. Accessory microphenocrysts include oligoclase, hornblende, biotite, magnetite, and zircon.

Sanidine forms tablets that are .25 to 1 mm long, euhedral to subhedral, and compose 7 to 11 percent of the rock (Fig. 3).



Fig. 7. Basal portion, about 15 feet thick, of color-mottled porphyritic vitrophyre exposed mid-way up the north wall of Paramount Canyon. Unit dips gently to the left (westward) and grades upward into the Taylor Creek Rhyolite.



Fig. 8. Detailed view of vitrophyre, showing lensoid distribution of black color mottling characteristic of the basal 6 feet.



Optically, they are similar to phenocrysts of the other units, but slight differences in exsolution lamellae and optic angles have been noted. The alkali feldspar is discussed farther on.

Quartz phenocrysts constitute 6 to 12 percent of the rock. In all other aspects, quartz is similar to that of other rocks.

Microphenocrysts are accessory, and do not exceed 2 percent of the rock by volume. Hornblende forms euhedral to subhedral crystals .25 to 1.5 mm long. They are both zoned and twinned (Carlsbad), and they contain opaque inclusions. The outer grain margins are typically altered to iron oxide. Zircon is invariably associated with magnetite, commonly in direct contact. Magnetite is altered generally to hematite and limonite or goethite.

The phenocrysts are set in a spherulitic glass matrix, which features local incipient devitrification. The glass is pale yellow-brown to reddish-brown, and it encloses spherulites as much as 2 mm in diameter (generally 1 mm, or less). The spherulites are color zoned, with yellowish brown cores and red-brown rims, and they have a radial structure. Many share mutual polygonal boundaries. Nucleation of spherulites has developed both on crystal faces and edges, and in the glass matrix. As much as 25 percent of the glass has been devitrified to a cryptocrystalline aggregate of unidentifiable material; where crystallized, quartz and alkali feldspar are intergrown.

Flow-layering is conspicuous in thin-section, where it is expressed by color variations in glass, trains of opaque dust, and alternate patches and lenses of glass and devitrified glass. Banding is deflected and contorted around most phenocrysts, with some rotation

30

of quartz and sanidine phenocrysts. Non-concentric perlitic cracks are widely observable in the glassy portions of the rock.

### Flow-Breccia

Rhyolite flow-breccia crops out in the southwest corner of the map area, where two separate, but genetically different masses have been distinguished. One forms a prominent ledge as much as 100 feet thick through most of its exposure, along the south wall of Taylor Creek canyon near its junction with Paramount Canyon (Fig. 9). It dips gently southward and separates gray to lavender rhyolite, which is locally argillized below, from unbleached, lavender-colored rhyolite above. Its lower contact is sharp, but the upper contact is gradational into porphyritic, flow-layered rhyolite (Tdtc).

The flow-breccia is lavender to gray, weathers tan to brown, and contains blocks of pumice and vitrophyric rhyolite. Some of these enclosed blocks are 1 foot or more in diameter (Fig. 10). Pumiceous blocks have weathered out from some exposures, leaving the rock locally vuggy or cavernous, particularly in the upper part of the section.

Based on textural and field relationships, this breccia appears to represent part of a basal flow-breccia, marking a more recent advance of lava outpouring in this area.

The other rhyolite breccia is less well defined. Its lower contact is gradational with porphyritic rhyolite (Tdtc) and the upper contact has been removed by erosion. Like the other breccia, flow-layering is not visible, but it lacks the blocky inclusions of the pumice and vitrophyre. Its stratigraphic position near the western



Fig. 9. Prominent ledge of flow-breccia (right) as exposed in the south wall of Taylor Creek canyon. View looking east-south-east, with Taylor Peak (8288 ft) in background.



Fig. 10. View of flow-breccia in Fig. 9, near top of a ~100-foot section. Note blocks of pumice (P), vuggy appearance, and lack of flow-layering. Hammer for scale.

margin of the dome, and in the upper part of the rhyolite section, suggests that it may represent a more rapidly cooled crust of rhyolite, possibly a "breccia carapace" that was broken and contorted as it was carried along the top of a large, moving mass of rhyolite.

### Miarolitic Rhyolite

Two occurrences of miarolitic rhyolite have been recognized in the study area. The more prominent one is exposed on the north rim of Paramount Canyon near the west edge of Plate 2. Here, the miarolitic unit, delta-shaped in plan, grades upward and downward into dense, porphyritic rhyolite (Tdtc). Portions of the top of this unit have been beveled by erosion, but extensive outcrop is limited to the main canyon wall. Flow-layering, accentuated by the vuggy nature of the rock and by lithophysal structures, dips generally to near vertical on the north side. Judging from the flow-layering, this miarolitic facies appears to form part of the margin of a local dome, or anticlinal structure. And, this structure is related to primary flow, not tectonic activity.

The miarolitic facies is unusual, both texturally and mineralogically, and it provides critical information regarding the genesis of the Taylor Creek tin deposits. The rock is light gray, weathering to pale orange-brown. It is porphyritic, with numerous vugs and lithophysae that are abundant but unequally distributed. The miaroles are irregularly shaped, while the lithophysae ("stone bubbles") are lobe-like in appearance, featuring numerous concentric shells. Both types of cavities typically range from about 8 to 12 mm in

diameter. These features are enlarged somewhat in weathered rock, where they help to define the flow-layering (Fig. 11).

Phenocrysts of quartz, sanidine, and minor plagioclase are set in a devitrified groundmass of the miarolitic facies. The phenocrysts are noticeably smaller than those in the other rhyolite units. Primary accessory minerals include zircon, magnetite, and fayalite (?). Biotite and hornblende are absent. The groundmass is largely devitrified to felsitic or spherulitic aggregates of K-feldspar and quartz, with associated minor cristobalite, tridymite, and chalcedony.

Minerals within the miaroles and lithophysae. An unusual suite of minerals occurs in the miaroles and lithophysae. It includes, in approximate order of decreasing abundance, quartz, alkali feldspar, hematite, bixbyite, pseudobrookite, monazite, cassiterite, and topaz. Zeolites, fluorite, calcite, and andradite were recognized previously (Fries, Schaller, and Glass, 1942), but these phases were not observed during the course of the present study.

Topaz was observed in thin-section, but not in heavy-mineral separates. Probably the best locality in the district for this mineral is Round Mountain, south of the study area, where colorless to pale yellow crystals as much as 2 cm long occur in the rhyolite lithophysae (Ericksen and others, 1970) and other crystals are in the main body of the rhyolite.

An unusually fine specimen of colorless topaz, a crystal 7.5 mm long, was obtained during the present study from jig concentrates at an abandoned mill east of Paramount Canyon in upper Sawmill Canyon. Its sharply defined morphology suggests crystallization within a

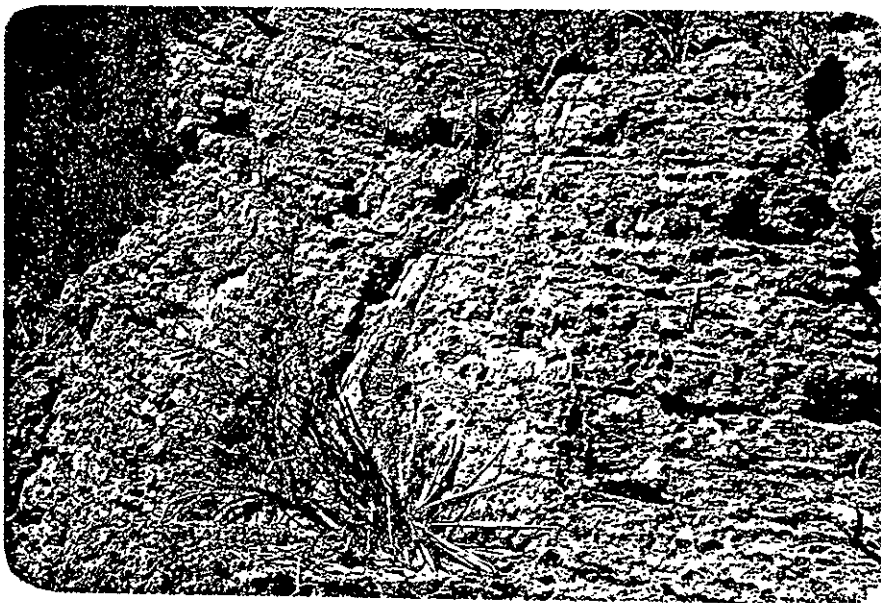


Fig. 11. Miärolitic, lithophysal rhyolite exposed on north rim of Paramount Canyon. Vugs, aligned parallel with the flow-layering, have been enlarged through weathering. Hammer for scale.



Fig. 12. Hand specimen of miärolitic rhyolite, featuring lithophysal structures and a cube of bixbyite, 2 mm on an edge, that has grown within a lithophysal cavity.

rhyolite cavity or veinlet. Cell refinements of this crystal are recorded below. The cell dimensions are closely similar to those of fluorotopaz found in other rhyolite occurrences (e.g., Mexico and Utah). Several investigations of topaz (Rosenberg, 1967; Ribbe and Gibbs, 1971; Deer, Howie, and Zussman, 1962) have shown that the OH:F ratio is the only major chemical variation in the formula,  $\text{Al}_2[\text{SiO}_4][\text{OH},\text{F}]_2$ . Substitution of larger  $\text{OH}^-$  for  $\text{F}^-$  expands the unit-cell, particularly in a direction parallel to the b-cell edge, with a consequent decrease in *ZV* and density. It has been suggested that an increase in OH:F ratio primarily reflects hydrolysis as a function of decreasing temperature (Rosenberg, 1965).

TABLE I

Unit-cell dimensions and optic axial angles  
of some natural topaz crystals

Locality	$a(\text{\AA})$	$b(\text{\AA})$	$c(\text{\AA})$	$V(\text{\AA}^3)$	<i>ZVz</i>
Black Range, N. Mex.	8.390 .002	8.797 .001	4.643 .001	342.69 .17	-
Durango, Mexico*	8.394 .001	8.789 .001	4.652 .001	343.20	68.0°
Topaz Mt., Thomas Range, Utah*	8.394 .002	8.792 .002	4.648 .002	342.99	67.4°
San Luis Potosi, Mexico*	8.396 .001	8.794 .001	4.651 .001	343.40	67.0°

\*Data from Rosenberg, 1967, p. 1891.

The oxide minerals discussed below appear to have crystallized penecontemporaneously within cavities and lithophysae of the rhyolite. Only the upper part of this miarolitic facies, exposed at the canyon rim, contains cavities bearing these minerals. All four species have

not been observed within a single cavity, but pairs such as hematite-cassiterite, hematite-pseudobrookite, and bixbyite-pseudobrookite are common.

Hematite, the most abundant of the oxide minerals, occurs both in cavities and in veinlets of cassiterite and hematite. It is invariably specular, appearing as thin hexagonal plates 1-3 mm in diameter. These plates are fresh and weakly corroded. The hematite commonly is intergrown with cassiterite, which also forms crystalline encrustations on some hematite plates and aggregates of plates.

Six crystals of specularite, associated but not intergrown with cassiterite, from different cavities in the miarolitic facies were analyzed by electron microprobe<sup>1</sup> for tin content, with results recorded in the following table. All these analyzed grains appear

TABLE II

Tin content of hematite, Paramount Canyon

<u>Grain</u>	<u>SnO<sub>2</sub>, wt. percent</u>
A	2.5
B	2.5
C	3.1
D	0.3
E	0.4
F	<u>1.0</u>
Average	1.6

<sup>1</sup>Analyses were made on an Applied Research Laboratories EMX-SM electron microprobe, using high-purity cassiterite as a tin standard. Instrumental errors were corrected, but no matrix corrections were applied.



homogeneous in polished section, and the considerable variation in tin content appears to reflect true differences in composition of the hematite.

Bixbyite,  $(\text{Fe,Mn})_2\text{O}_3$ , is a rare mineral first described from the Thomas Range, Utah, by Penfield and Foote (1897). Specimens were later recognized from the Black Range, and were discussed briefly by Fries, Schaller, and Glass (1942) and by Mason (1943). The bixbyite in the Paramount Canyon area occurs most commonly as cubes as much as 2.5 mm on an edge. Both individual cubes and penetration twins have been found in heavy-mineral separates. Some of the cubes are modified by octahedron faces. Several octahedral crystals of bixbyite that encrust one rhyolite fracture surface are modified by dodecahedral faces.

Most of the larger crystals are sharp and fresh in appearance (Fig. 12), but edges of the smaller cubes commonly are corroded or rounded. Well-defined growth zoning can be observed in polished section; the growth layers generally are parallel to cube faces (Fig. 13). They are expressed by narrow bands of contrasting reflectivity, commonly delineated by linear pits in the polished surface.

The composition of bixbyite recorded in Table III represents an average for one crystal that was found to be inhomogeneous with respect to major elements. The content of  $\text{Fe}_2\text{O}_3$  ranges from 32.8 to 46.6 percent, and that of  $\text{Mn}_2\text{O}_3$  from 49.3 to 63.6 percent. Bixbyite from the Black Range is more manganese-rich than analyzed specimens from the Thomas Range (Fries, Schaller, and Glass, 1942; Staatz and Carr, 1964). In addition, the content of Sn (0.5 percent) is significantly higher than that of Utah bixbyite (.05-0.1 percent Sn),

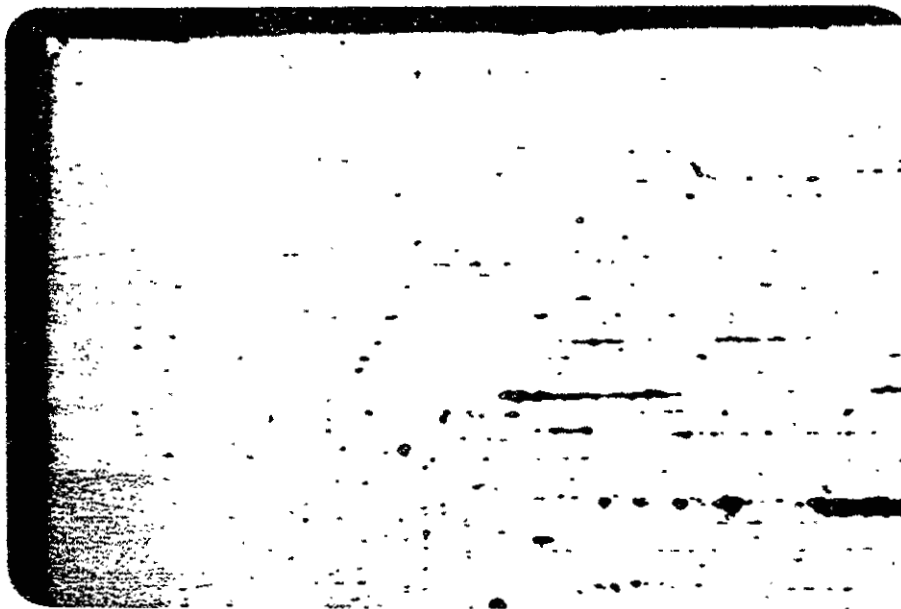


Fig. 13. Photomicrograph of growth zoning in bixbyite, Black Range. Polished section, polarized light, 115x.

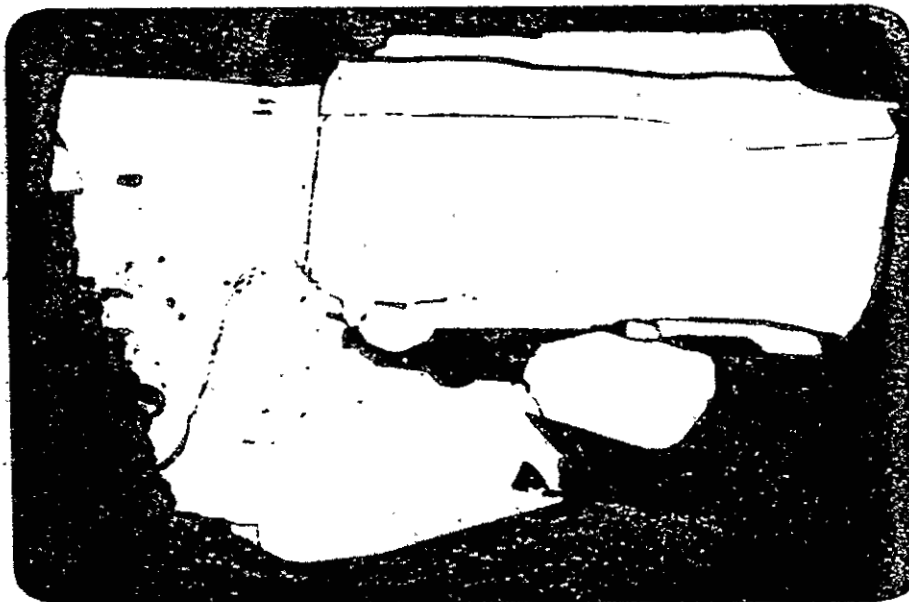


Fig. 14. Hematite blebs in pseudobrookite. Polished section, polarized light, 230x.

which is associated with beryl, garnet, and topaz, but not with cassiterite (Staatz and Carr, 1964).

TABLE III

Composition of bixbyite, Paramount Canyon

Microprobe analysis of one crystal, this study <sup>1</sup>		Approximate analysis (Fries, Schaller, and Glass, 1942)
SiO <sub>2</sub>	-	-
Al <sub>2</sub> O <sub>3</sub>	0.3	0.47
FeO	-	-
Fe <sub>2</sub> O <sub>3</sub>	41.4 <sup>a</sup>	42.54
TiO <sub>2</sub>	1.4 <sup>b</sup>	1.57
Mn <sub>2</sub> O <sub>3</sub>	55.9 <sup>c</sup>	51.92
MgO	-	-
CaO	-	tr.
SnO <sub>2</sub>	0.6	tr.
Insoluble	<u>          </u>	<u>2.21</u>
	99.6	98.71

<sup>a</sup>Total Fe as Fe<sub>2</sub>O<sub>3</sub>

<sup>b</sup>Total Ti as TiO<sub>2</sub>

<sup>c</sup>Total Mn as Mn<sub>2</sub>O<sub>3</sub>

Pseudobrookite (Fe<sub>2</sub>TiO<sub>5</sub>) forms black, acicular crystals .5 to 2 mm long, generally in association with bixbyite. These crystals occur both individually and as tiny semi-radial clusters. Many are striated longitudinally, parallel to the c-axis. Some appear to have been corroded, but most are characterized by sharply defined, lustrous faces.

<sup>1</sup>Bixbyite from the Thomas Range, Utah was used as a standard.

Of the thirty grains of pseudobrookite that were separated and mounted for special study, about one-third contain vermicular blebs of hematite a few microns wide (Fig. 14). This feature, which probably represents exsolution, appears to be most common among the grains forming semi-radial clusters. The hematite is most abundant at the base of the pseudobrookite crystals, where they join to form these clusters.

A microprobe analysis of pseudobrookite from the Paramount Canyon locality yielded the values recorded in Table IV. Individual

TABLE IV  
Composition of pseudobrookite

	<u>Paramount Canyon, Black Range, N. Mex.<sup>1</sup></u>	<u>Thomas Range, Utah (Palache, 1935)</u>	<u>Calculated composition</u>
Fe <sub>2</sub> O <sub>3</sub>	65.7	60.57	66.6
TiO <sub>2</sub>	31.5	38.12	33.4
MnO <sub>2</sub>	2.4	-	
MgO	-	1.26	
SnO <sub>2</sub>	<u>1.3</u>	<u>-</u>	<u>-</u>
	100.9	99.95	100.0

<sup>1</sup>Pseudobrookite from a dacite on Nevis, West Indies, was used as a standard.

crystals of pseudobrookite that lack blebs of hematite are relatively homogeneous. Within an individual grain, the content of Fe and Ti does not vary by more than .5 percent. The tin content, about double that of the bixbyite, probably represents a substitution of Sn<sup>+4</sup> for Ti<sup>+4</sup>.

The composition of Black Range pseudobrookite closely approximates the calculated, ideal formula. Specimens from Utah are relatively rich in titanium, but this may be due to intergrown rutile (Palache, 1935). It has been found that pseudobrookite may also contain appreciable Mg and Mn (Ottemann and Frenzel, 1965). In a microprobe study of 29 specimens, largely from volcanic rocks in western Europe, some pseudobrookite was found to contain as much as 3.9 percent MnO and 20.9 percent MgO.

Cassiterite occurs in cavities, primarily with hematite, and in veinlets with quartz, topaz, hematite, and alkali feldspar. In the cavities it forms stubby to platy crystals that are ruby red and rarely exceed 1 mm in maximum dimension. They are zoned, and twinning commonly is recognizable in polished section (Fig. 15). Most of the twin lamellae are parallel, whereas others intersect to form wedge-shaped patterns. Internal reflection commonly is expressed in shades of yellow, violet, and green.

In its close association with specular hematite, the cassiterite occurs as both overgrowths and intergrowths. In some veinlets it appears to comprise numerous growth plates, stacked one upon another and commonly parallel to underlying plates of hematite.

Cassiterite has not been observed coating, or intergrown with, bixbyite or pseudobrookite. A spectrographic analysis of a clean concentrate of cassiterite from Paramount Canyon indicates the added presence of iron and trace amounts of titanium and silica. The content of  $\text{SnO}_2$  ranges from 92.2 to 97.0 percent.

Temperature of formation of oxide minerals. Phase relations pertinent to occurrences of bixbyite and pseudobrookite have been

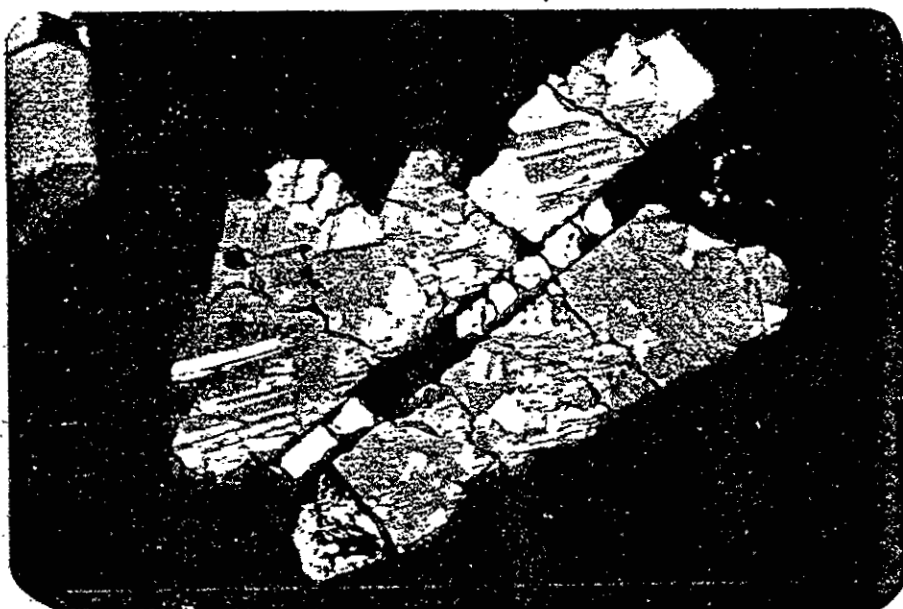


Fig. 15. Twinned crystal of cassiterite with enclosed blade of hematite. Polished section, obliquely crossed polars, 115x.

investigated experimentally during the past thirty years. Principal phases were first established by Mason (1943) for the system  $\text{Fe}_2\text{O}_3$ - $\text{Mn}_2\text{O}_3$  from 400 to 1000°C at a pressure of 1 atm. This study was later improved and extended to 1585°C (Muan and Sömiya, 1962).

The stability field of bixbyite,  $(\text{Mn,Fe})_2\text{O}_3$ , is represented in the lower right corner of Figure 17. At equilibrium, a partial solid solution series between  $\text{Mn}_2\text{O}_3$  and  $\text{Fe}_2\text{O}_3$  is capable of dissolving 40 to 64 weight percent  $\text{Fe}_2\text{O}_3$  in the temperature interval 600-997°C. This series yields  $\text{Mn}_2\text{O}_3$  and tetragonal  $\text{Mn}_3\text{O}_4$ , or spinel solid solution at the composition-sensitive temperatures ranging from 877 to 997°C.

The composition of one bixbyite cube from Paramount Canyon, as determined by microprobe analysis (Table III), is plotted in Figure 16. Crystal inhomogeneity reflects a range of 32.8 to 46.6 percent  $\text{Fe}_2\text{O}_3$ , with an average of 41.1 percent. Considering bixbyite as pure  $(\text{Mn,Fe})_2\text{O}_3$  by adding the amounts of Sn and Ti, which most likely substitute for Fe, to the average  $\text{Fe}_2\text{O}_3$  percentage, the composition becomes  $\text{Fe}_2\text{O}_3 = 44$  percent,  $\text{Mn}_2\text{O}_3 = 56$  percent; this is plotted as the average for this crystal in the binary diagram. Referring to the data of Muan and Sömiya (1962), bixbyite of this composition would yield hematite and  $\text{Mn}_2\text{O}_3$  at 675°C, and above 945°C it would yield spinel and  $\text{Mn}_2\text{O}_3$ ; this establishes a "stability range," for equilibrium conditions, of 270° at 1 atm ( $P_{\text{O}_2} = .25$ ).

Pseudobrookite, a widespread mineral, is found in volcanic rocks ranging in composition from basalt to rhyolite. Members of the pseudobrookite ( $\text{Fe}_2\text{TiO}_5$ )-ferropseudobrookite ( $\text{FeTi}_2\text{O}_5$ ) series generally are oxidation products of titano-magnetite or ilmenite in subsilicic

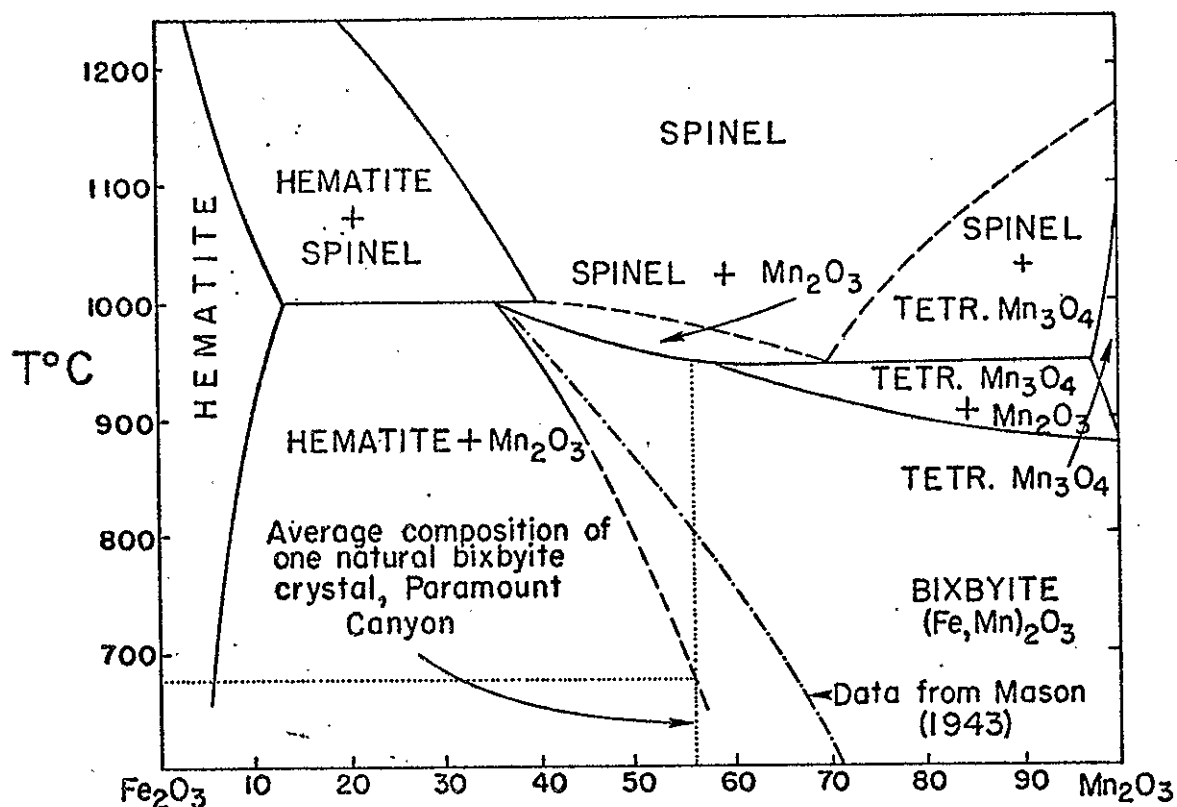


Fig. 16. Phase relations in the system iron oxide-manganese oxide in air. (after Muan and Sömiya, 1962).

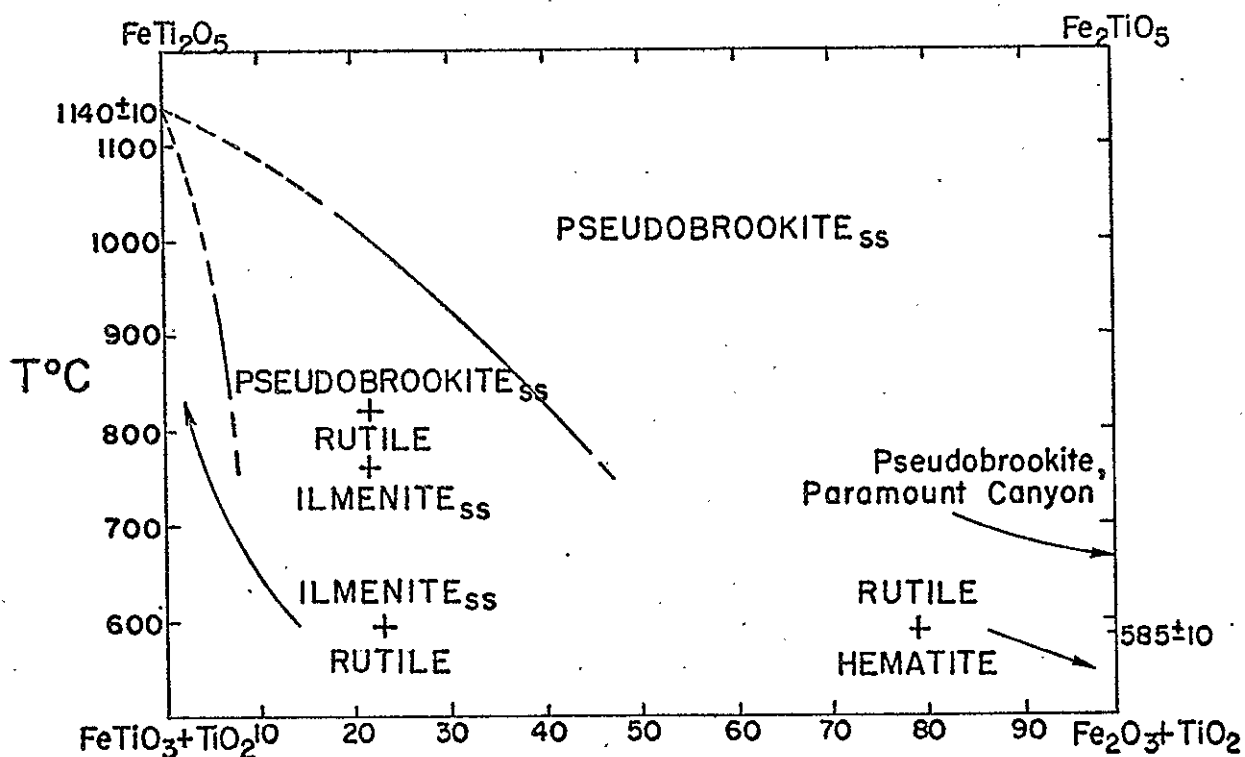


Fig. 17. Phase relations in the ferropseudobrookite-pseudobrookite series (after Haggerty and Lindsley, 1970).



rocks (e.g., Buddington and Lindsley, 1964; Carmichael, 1967; Haggerty and Lindsley, 1970; Ottemann and Frenzel, 1965), or as acicular crystals lining cavities in silicic volcanic rocks (Palache, 1935; Fries, Schaller, and Glass, 1942). Pseudobrookite also has been observed in the flues of a soda factory as an apparent product of sublimation.

Above 1150°C, a complete solid solution series exists between  $\text{Fe}_2\text{TiO}_5$  and  $\text{FeTi}_2\text{O}_5$  in the dry system  $\text{FeO-Fe}_2\text{O}_3\text{-TiO}_2$  (Akimoto, Nagata, and Katsura, 1957). The  $\text{TiO}_2/\text{Fe}_2\text{O}_3$  mol ratio in natural specimens ranges from 1.1 to 3.5 (Ottemann and Frenzel, 1965). In experimental studies, the titanium content of synthetic pseudobrookite has been shown to decrease with lower temperatures of crystallization (Haggerty and Lindsley, 1970). The pure ferropseudobrookite end-member has not been observed in nature. The limits of solid solution have not been closely established at most lower temperatures, owing in part to sluggish reactions in this thermal range (Haggerty and Lindsley, 1970). Phase relations above 1400°C are known to be complex (MacChesney and Muan, 1959).

In determining stability relations from 750° to 1150°C (Fig. 17), Haggerty and Lindsley showed that the solution series is not linear as formerly assumed. The pseudobrookite end-member breaks down to form hematite and rutile at  $585 \pm 10^\circ\text{C}$ , as determined by hydrothermal experiments at 2 kb and with  $f_{\text{O}_2}$  controlled by hematite + hydrogen peroxide buffer. The pseudobrookite from the Black Range is similar in composition to the calculated end-member.

If data from experimental studies of comparable synthetic systems are rigorously applied, a minimum crystallization temperature of 585°C can be assigned to the pseudobrookite and a corresponding minimum temperature of 675°C to the bixbyite. Several complicating factors are apparent, however. Natural crystal inhomogeneities, particularly in bixbyite, complicate any application of results from synthetic studies of homogeneous materials. Nor have the effects of Sn and/or Ti substitution for Fe on the ranges of phase stability of bixbyite and pseudobrookite been determined. Further, the effects of pressure, including  $p_{H_2O}$  and  $p_{O_2}$ , have not yet received enough critical attention for any of the pertinent systems to warrant strict application to the natural mineral assemblage here studied.

Despite the complications inherent in comparing the natural and synthetic systems, it seems reasonable to conclude that the oxide minerals crystallized at temperatures of 600°C or higher. This temperature range is somewhat higher than temperatures reported for most tin deposits. The temperature interval most frequently cited is 300 to 500°C (e.g., Lindgren, 1933; Schneiderhöhn, 1955; Little, 1960). There appears to be less agreement on the temperatures of tin mineralization in rhyolite. For example, in the Mexican rhyolite association, Foshag and Fries (1942) and Valle (1960) have postulated high temperatures (600° and above) for the cassiterite-hematite veinlets, whereas Ypma and Simons (1969) advocate very low temperatures (120°C and lower), based on the association of wood-tin with native bismuth, antimony oxides (?), and lead arsenate. However, the possible occurrence of cassiterite in microlitic cavities in the Mexican

rhyolites has not been discussed by any of the investigators mentioned above.

Discussion. The presence of miarolitic cavities and lithophysae strongly suggests that a gas phase was evolved during cooling of the rhyolite. Also, the penecontemporaneous crystallization of cassiterite with bixbyite, pseudobrookite, and hematite in these cavities establishes a genetic relationship between tin mineralization and the primary cooling history of the rhyolite. This genetic relationship probably extends to the tin-bearing veinlets, which are further discussed in detail below.

The transport of tin and iron in an aqueous gas phase has been verified by field observation and has been investigated experimentally. Fumaroles at Showa-shinzan, Japan show trace quantities of tin. Chemical analyses of fumarolic gases by Nemoto and others (1957) further show an increase in certain metal concentrations with temperature. Tin content in some of these gases at 220°C is .001 ppm and at 760°C is .03 ppm, representing a 30-fold increase. Zies (1924, 1929) found magnetite sublimates in the Valley of Ten Thousand Smokes, Alaska to be enriched in tin (400 ppm at 239°C) and many other metals.

Experimental studies on the vapor transport of tin and iron have emphasized the importance of halides, particularly chlorine, which is believed to form a chloride complex with these metals. This complexing is enhanced by the abundance of HCl in some volcanic gases (e.g., Valley of Ten Thousand Smokes), and by the relatively high vapor pressures of chloride compounds. Iron has been volatilized from clay pots and precipitated as hematite through the action of chloride vapor from 1000 to 1100°C (Merwin and Hostetter, 1919).

Krauskopf (1964) pointed out that tin has appreciable volatility at 827°C, under low partial pressures of oxygen and sulfur, whereas at lower temperatures, significant concentration of tin as  $\text{SnCl}_4$  in vapor would require high partial pressure of oxygen and relatively high HCl pressures. Many fumaroles, however, contain little or no detectable HCl (White and Waring, 1964).

Some experiments suggest that chlorine may not be necessary to transport iron, and perhaps tin as well. The transport of iron in a chlorine-poor aqueous vapor phase has been demonstrated convincingly by Martin and Piwinski (1969). Isothermal and polythermal experiments were conducted on calc-alkaline plutonic rocks between 1.25 and 10 kb  $P_{\text{H}_2\text{O}}$ . In experiments involving a temperature gradient, iron was leached by an aqueous vapor at a temperature of 700°C, transported down the temperature gradient, and deposited as specular plates of hematite at 450 to 500°C. No profound effect of Cl, F,  $\text{CO}_2$ , and S content of the rocks, or of the presence or absence of a melt phase was noted in this study, and "The addition of hydrochloric acid or of alkali chlorides to the system rock-water thus seems unnecessary to produce the fractionation phenomena observed" (Martin and Piwinski, 1969, p. 801).

The crystallization of iron as hematite rather than magnetite within the rhyolite is indicative of a highly oxidizing environment. Data obtained from experiments conducted at 600°C and  $P = 1000$  atm suggest all iron in a vapor phase should crystallize as hematite above  $P_{\text{O}_2} = 10^{-15}$  atm (Krauskopf, 1957).

The apparent concentration of metals, including Sn, Fe, Mn, and Ti, within the microlitic unit near the top of the flow-dome

is analogous to the enrichment of some metals in the cupola areas of granitic stocks, or in the roof portions of some pegmatites.

### Pyroclastic Rocks (Tdp)

In the Taylor Creek district, pyroclastic rocks are widespread, both as interlayered deposits within rhyolite flow-domes and as penecontemporaneous deposits marginal to them. In the map area, pyroclastic rocks found around the eastern margin of the dome are nearly flat-lying and in general are juxtaposed against rhyolite. A partial section of Gila Conglomerate is down-faulted against pyroclastic rocks in the east-central portion of section 30. In this same area, one of the thickest pyroclastic sections (about 105 feet by hand-level measurement) is exposed in the walls of a narrow canyon. The lower 47 feet is massive tuff breccia, white to lavender and weathering dark gray to brown. This unit is overlain by 60 feet of thin- to medium-bedded tuff and tuff breccia, creamy to yellowish and weathering tan to brown. This sequence is overlain by brown, tuffaceous sandstones of the Gila Conglomerate.

The pyroclastic rocks are dominantly crystal-bearing vitric tuffs. The crystal phenoclasts are chiefly sanidine and quartz, with minor plagioclase and the usual rhyolite accessory species. Sanidine and quartz amount to 9 to 12 percent of the rock, with sanidine generally dominant.

The prominent exposure of pyroclastic rocks in northern Paramount Canyon is similar. This section reaches a maximum thickness of about 400 feet, and includes vitric tuff and tuff breccia, pink to cream in color. The tuffs are thin-bedded in the lower part, but

more massive in the middle and upper parts. The total section strikes generally northeast, and dips gently to the northwest.

One other pyroclastic deposit is exposed as a curvilinear band on the northwest wall of Paramount Canyon, southwest of the section just described. It can be traced discontinuously a little more than 200 feet, and pinches out at both ends. A representative section includes the following: 30 feet of basal, thin-bedded tuff, cream to tan, with included fragments of pumice and glass as much as 2 inches in diameter (Fig. 18). The base is covered. This section is channeled and disconformably overlain by approximately 66 feet of breccia, tan to light brown, with boulders of rhyolite 10 feet in diameter. This is overlain, with a sharp contact, by thin-bedded tuff, tan to light brown, with included pebbles of obsidian. The total pyroclastic section is bounded at top and bottom by the Taylor Creek Rhyolite.

#### Gila Conglomerate

The youngest consolidated clastic deposits west of the Continental Divide in the Black Range are referred to as the Gila Conglomerate (QTg) on the state map of New Mexico (Dane and Backman, 1965), although only a small part of the section actually is conglomerate. This formation is exposed in a narrow belt along the eastern margin of the mapped area, but it was not studied in detail. In general the strata are horizontal or dip gently to the east; they overlies tuffaceous deposits or form aprons along the margins of the rhyolite dome.



Fig. 18. Basal part of pyroclastic section, 30 feet thick, that consists of thin- to medium-bedded, cream colored vitric tuff, northeast wall of Paramount Canyon.

In the mapped area, the thickest section of Gila sediments lies immediately north of Greer's Ranch, in the southeast corner of section 30. It is approximately 300 feet thick, and consists mainly of poorly exposed thin- to very thick-bedded, friable, tuffaceous sandstones that are brown in color. Near the base are lenses of pebbly conglomerate with clasts of pumice and silicified rhyolite or vitrophyre. Elsewhere, the basal clastic strata are marked by spheroidal concretions that weather out to form prominent cavities. Chalcedony and opal are abundant in vertical fractures. Midway up the 300-foot section, a conspicuous layer of massive vitric tuff, 15 feet thick, lies between tuffaceous sandstones. It is cream to buff, and friable. This tuff indicates that sporadic acid volcanism continued into the late Tertiary. Gila clastic strata with inter-layered basalt flows have been recognized elsewhere in the Black Range (Elston and others, 1969).

The composition and extent of the Gila sediments suggest that they probably were derived from the weathering of tuffaceous rocks that must have been widespread along the western slope of the Black Range.

#### Holocene Deposits

Unconsolidated deposits rich in volcanic clasts are exposed in valley bottoms and tributary washes, as well as on upland surfaces and steep valley sides throughout the area. These can be subdivided into three units, exposed mainly along Taylor Creek and its tributary washes, that include sand, gravel, and boulders (Qal) along valley bottoms, bouldery rubble and fan gravels (Qft) exposed as lenticular



masses on steeper canyon walls and at mouths of tributary washes, and eluvial sands and gravels (Qel) of slight thickness on upland surfaces, mainly north of State Highway 59. In large part, the unconsolidated deposits are contemporaneous.

Alluvial and eluvial deposits have been prospected in the past as a source of placer tin. In recent years much attention has been given to the tin-bearing sands and gravels of the upper Sawmill Canyon drainage in the northeast corner of the map area.

#### RHYOLITE STRUCTURE AND MODE OF EMPLACEMENT

The body of rhyolite in the Paramount Canyon-Taylor Peak area forms an elongate domain of outcrops, approximately 7 miles north-south and 4 miles east-west. Contact relations are generally obscured at the north end of the body, but they are well exposed on the east and west sides in Taylor Creek, and on the south margin in Alexander Canyon (Plate 1).

The eastern margin of the mass is bordered by Gila sediments and penecontemporaneous pyroclastic strata. In much of this area, rhyolite interfingers with gently-dipping tuffs and tuff breccias, but elsewhere it is overlain with erosional unconformity by nearly flat-lying Gila sandstones. As the contact with pyroclastic rocks is approached, flow-layering in the rhyolite commonly becomes indistinct to brecciated, and silicification is locally conspicuous. In the southeast corner of the map area, flow-layering near the margin of the rhyolite becomes steep to slightly overturned by flow-folding. Elsewhere along the eastern margin, the layers are gently inclined. There is no clear evidence of fusion, or welding of tuffs adjacent

to the rhyolite. Such fusion of tuffs has been recognized in southern Nevada (Christiansen and Lipman, 1966).

The rhyolite is overlain by clastic rocks along its western and northern margins. The contact at the western margin is particularly well exposed in the canyon of Taylor Creek, where tuffaceous sandstones and conglomerates dip gently off the eroded margin at angles of 30 degrees or less. Pyroclastic rocks, common on the eastern side, are generally lacking here.

Contacts at the south margin are well exposed in Alexander Canyon, where the rhyolite also is juxtaposed against pyroclastic rocks. As the contact is approached, the rhyolite becomes increasingly brecciated through a zone that is less than 1000 feet wide in a direction normal to the contact. The breccia interfingers with gently-dipping tuffs at the margin of the dome. Here the flow structure of the rhyolite is flat or dips gently to the east-northeast, except locally where near-vertical dips can be observed. Pyroclastic rocks adjacent to the rhyolite dip  $20^{\circ}$  or less to the northeast. These deposits are overlain by mafic flows, which are widespread in this area but absent around other parts of the Boiler Peak rhyolite mass.

Flow structure throughout the interior of the exposed rhyolite, as characterized primarily by flow-layering, is most consistent in a lower section that is best exposed along the walls of Taylor Creek (Fig. 19). Flow-layers dip gently to moderately, with vertical flow-layering developed only locally along this approximately 4.5 mile cross-sectional area, where the rhyolite averages 400 to 500 feet in thickness. Furthermore, the local exposures of gently inclined

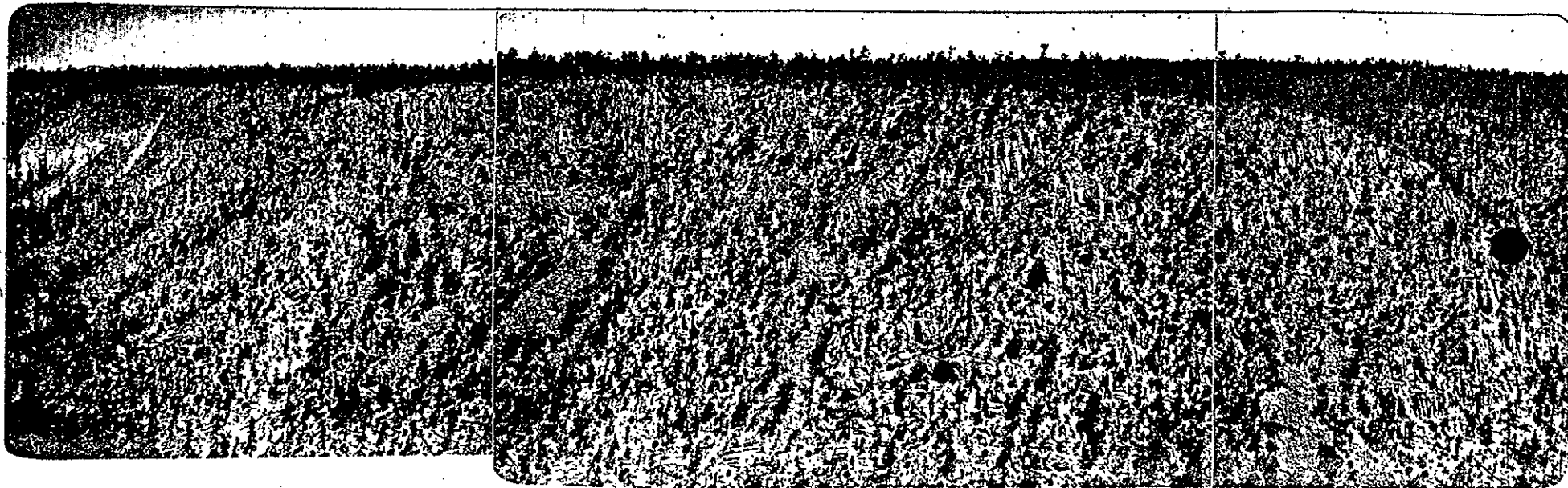


Fig. 19. Panoramic view, from northwest to northeast, of the Boiler Peak dome, as exposed along approximately 4500 feet of the north wall of Taylor Creek. Section in view is 400 to 500 feet thick. Rhyolite, in general, is dipping gently to moderately away from viewer to the north. Note the white bleaching of rhyolite, which is prominent in parts of Paramount Canyon (left) and in the lower rhyolite section in parts of Taylor Creek.

"marker" beds, which include the vitrophyric and pyroclastic lenses in north Paramount Canyon and the flow-broccia in south Taylor Creek canyon, and the steepening of flow-layering along portions of the rhyolite margin characterize a flow-dome structure. The general absence of "vent-like" structures, i.e., vertical flow-layering within the mass interior, and the presence of the best developed vertical joints along the canyon rims, as well as the occurrence of pyroclastic rocks interbedded with, and marginal to, the rhyolite indicate that only the upper part of the dome has been exposed by erosion. The lack of deformation in the marginal pyroclastic deposits suggests further that lateral flow movement of the rhyolite had largely ceased before the pyroclastic rocks were laid down, although these rocks must have been deposited shortly thereafter.

Superimposed on this general framework are numerous local folds, flexures, and other structural irregularities. In Paramount Canyon, several dome-like structures in the rhyolite do not exceed 2000 feet in diameter. The elongate exposure of bleached, argillized rhyolite in the southeast corner of the map area delineates an eroded anticlinal flexure in this vicinity.

Flow-layering mapped on the partially eroded top of the dome, on the other hand, reveals a more complicated structural pattern. Over most of this area the layers dip at angles of 50 degrees or more. The existing combination of flow-layering, large-scale flow-folds, and local "marker" beds permits reconstruction of flow directions within the Boiler Peak dome (Plate 3). The eastern half of the rhyolite mass appears to represent primary flowage that was radial to a part of the complex centrally located between Boiler Peak, Paramount

Canyon, and Taylor Peak. The western half is complicated by evidence of more than one major flow unit of rhyolite. South of Taylor Creek, in the southwest map area, the poorly exposed lower rhyolite section is overlain by a flow-breccia that does not appear on the north wall of Taylor Creek. This relationship, together with an east-west strike of flow-layering that dips to the south, suggests a local direction of flowage toward the north for the breccia unit. In the underlying rhyolite, as exposed immediately south of the "gooseneck" in Taylor Creek, a prominent recumbent fold indicates flowage toward the northwest.

In Paramount Canyon, a basal vitrophyre with laterally associated pyroclastic rocks crops out midway up the north wall of the canyon. The occurrence of vitrophyre and the pyroclastic rocks, which cannot be recognized on the south wall of the canyon, suggests that a second, more recent rhyolite flow advanced to the southeast from a vicinity north of Highway 59.

The mode of emplacement of the Boiler Peak dome can be inferred from the distribution and relationships of the volcanic units, their estimated physical properties during flow, inferred directions of flowage, and from a comparison with structural features of other volcanic piles. The association of rhyolite with interlayered pyroclastic deposits and the occurrence of vitrophyric and flow-breccia facies within the total volcanic section indicate that emplacement and development of the dome was not one uninterrupted event of rhyolite upwelling, but instead was marked by periods of explosive activity, followed by renewed, local outpourings of lava in different directions from separate vents beneath the dome.

The viscosity of the rhyolite magma during formation of the dome must have been very high. The factors known to influence the fluidity of a melt are chemical composition, water content, and heat. Hydrostatic pressure per se has little effect on viscosity (Shaw, 1965), but is important in that it controls the retention or escape of volatile constituents.

The viscosities of several silica-rich glasses of different compositions have been determined by several investigators. These glasses, which contain about 71 to 76 weight percent  $\text{SiO}_2$ , range from  $10^6$  to  $10^7$  poises over the temperature interval, 700 to 800°C. The viscosity of a melted obsidian sample is reported to be  $10^6$  poises at 1400°C and 1 atm pressure (Clarke, 1966).

Water generally reduces the viscosity of a melt. The maximum possible water content, in turn, is controlled by the lithostatic load on the melt. If the mean density of rhyolite glass is taken as 2.37 g/cc (e.g., Tilley, 1922), a column of this material, 1 inch square and 1000 feet thick, would weigh approximately 1020 lbs. At the base of this column, the lithostatic pressure would be approximately 70 bars. At this pressure, a rhyolite could hold a maximum of about 3 percent water at 400°C, and about 1 percent water at 900°C (Friedman and others, 1963). The water content, of course, would decrease upward in this column of melt with the decrease in load. With 3 weight percent dissolved water, the viscosity of a granitic magma, at its "ternary minimum" composition, would be on the order of  $10^7$  to  $10^8$  poises (Shaw, 1965). The viscosity of a dry melt of the same composition would be  $10^{10}$  or higher.

Increasing the temperature has the similar effect of reducing viscosity. Experiments on siliceous glasses suggest that viscosities are generally reduced by .5 to 1 order of magnitude for every 100 degree increase in temperature over the interval, 500 to 1400°C (e.g., Clarke, 1966). The temperature of the Taylor Creek Rhyolite during extrusion is not known, but estimates of rhyolite temperatures in general fall in the range, 750 to 950°C (Lovering, 1955; Battey, 1966; Fyfe, 1970; Carmichael, 1967).

The general horizontal structure observed in the Boiler Peak dome is not common in most dome structures described in the literature, although many of these domes are andesitic and dacitic rather than rhyolitic in composition. The Peléan type (Fig. 20), with distorted and crude concentric layering, is most common among the andesitic domes (Williams, 1932). Domes of silicic composition, however, commonly display a "fan-structure" (Fig. 21), in which the flow-layering diverges outward from the vent area. This structure characterizes some of the rhyolite domes of Inyo County, California (Chesterman, 1956), and the Novarupta dome, Alaska (Williams, 1932).

The gross structure of the Taylor Creek Rhyolite resembles, in a general way, the experimental form developed by Reyer (1888; reproduced in Williams, 1932), who created dome shapes and structures by squeezing viscous material through a narrow aperture (Fig. 22). Domes with horizontal flow-structure were thereby produced, and steeply inclined to recumbent flow-folding was developed at the margins of the domes as the material spread laterally beyond the vents. A similar situation could well have obtained during extrusion of the rhyolite at Taylor Creek, but it probably was complicated by several local vents

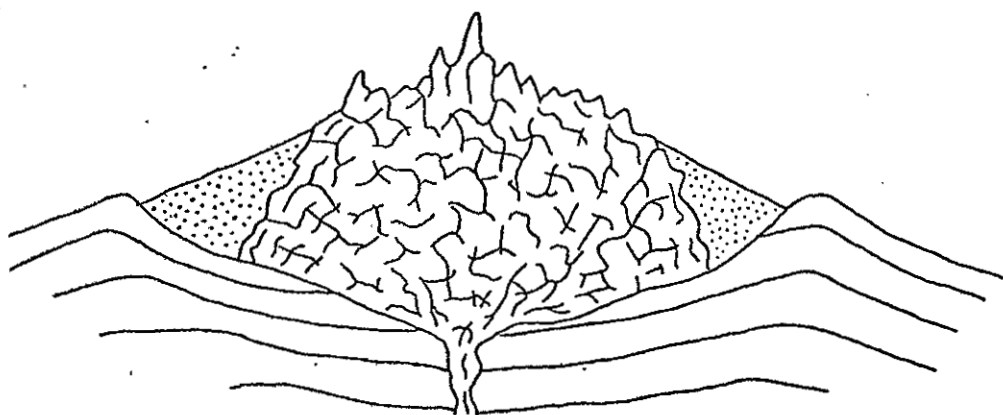


Fig. 20. Diagrammatic sketch of Peléan-type dome, the most common, featuring crude concentric banding and irregular fissures (after Williams, 1932).

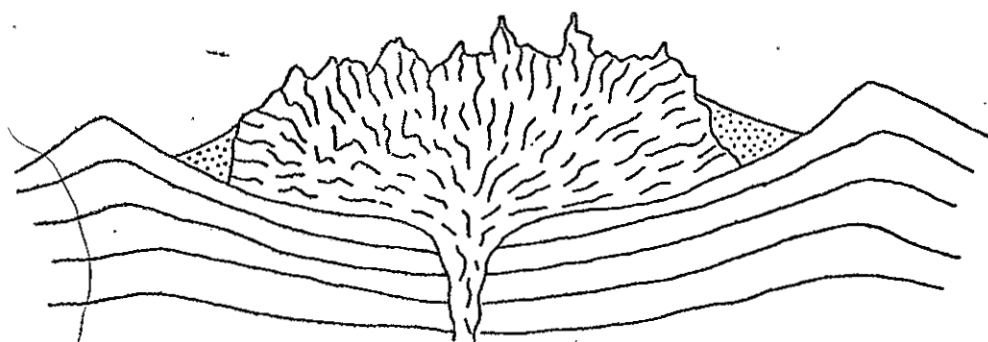


Fig. 21. Sketch of fan-structure in a volcanic dome (ibid.).

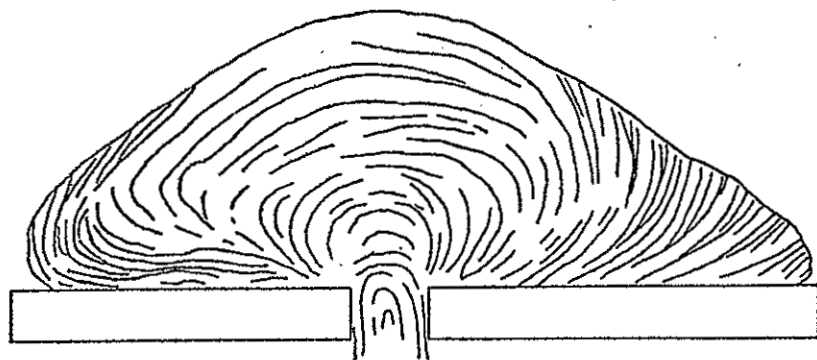


Fig. 22. Experimental dome formed by squeezing viscous material through a narrow aperture (after Reyer, 1888; in Williams, 1932).



beneath the present outcrop area, as well as by intermittent explosive activity. Unfortunately, it is not possible to establish the locations of the inferred vents.

## TAYLOR CREEK PROSPECTS

### Introduction

One of the finest exposures of tin-bearing veinlets in the district is on Taylor Creek, about 3 miles above its confluence with Beaver Creek in the southwestern part of the district (Plate 1). This area has been mapped in considerable detail by Fries (1940) and by Jahns (1957-62, unpubl.). Their mapping, with only minor details added, is presented as Plate 4. Between 1939 and 1943, the U. S. Bureau of Mines conducted a sampling program, which was confined to the known mineralized areas at Taylor Creek and elsewhere in the district (Volin and others, 1947).

During the course of the present study, this area was examined for a period of approximately two weeks. Emphasis was placed on observations of the rhyolite structure, alteration, and localization of the tin-bearing veinlets.

### General Features

The Taylor Creek area features excellent outcrops that provide a three-dimensional exposure of the western edge of another flow-dome (Plates 1 and 4), here referred to as the Taylor Creek dome.

Six lithologic units, more than 700 feet in aggregate thickness, are present in the area. They range in age from mid-Tertiary to

Holocene, and include, in order to decreasing age, the Datil Formation, andesitic flows, Gila Conglomerate, terrace deposits, and older and younger alluvial deposits. The Datil Formation consists predominantly of Taylor Creek Rhyolite and minor flow-breccia units, which are confined to the dome margin. The Taylor Creek Rhyolite, Oligocene in age, is a gray, porphyritic rock that is bleached white near the margin of the dome. Here also, the rhyolite is underlain and overlain locally by small masses of flow-breccia. Andesitic flows unconformably overlie the younger flow-breccia unit in the northwest part of the map area. More than 300 feet of consolidated and unconsolidated clastic rocks in turn overlie the volcanic section. The sequence consists primarily of the Gila Conglomerate (tuffaceous sandstones), Plio-Pleistocene in age, and it in general overlies the Taylor Creek Rhyolite in the southern part of this area. Holocene terrace deposits and alluvium of slight thickness complete the stratigraphic succession. The terrace deposits include volcanic sands and gravels on elevated surfaces adjacent to Taylor Creek. The younger alluvial deposits are confined to small washes and to Taylor Creek and its tributaries.

The volcanic section is dominated by more than 400 feet of flow-layered, Taylor Creek Rhyolite in which flow-layering strikes north to northwest and dips gently to moderately toward the east to northeast. Part of the rhyolite section has been down-dropped by a high-angle, normal fault north of Cox Canyon, preserving a partial section of Gila clastic sediments. To the northeast, immediately north of the Taylor Creek "gooseneck," a prominent recumbent flow-fold is present in the rhyolite body (Fig. 23a, b). This fold appears to express the motion of a rhyolite mass spreading laterally from east to

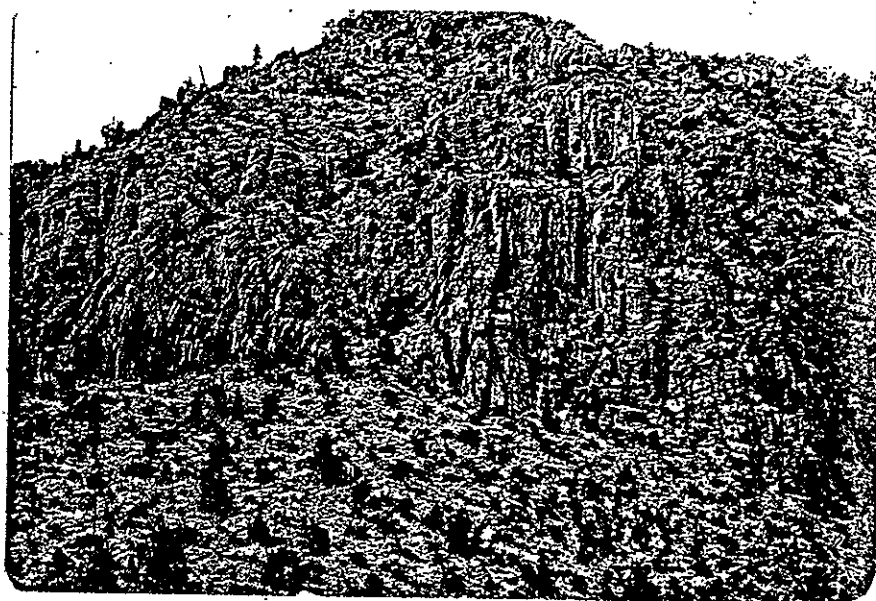


Fig. 23a. A prominent recumbent flow-fold near the margin of a rhyolite dome in the Taylor Creek prospects area. Vertical exposure is about 400 feet.

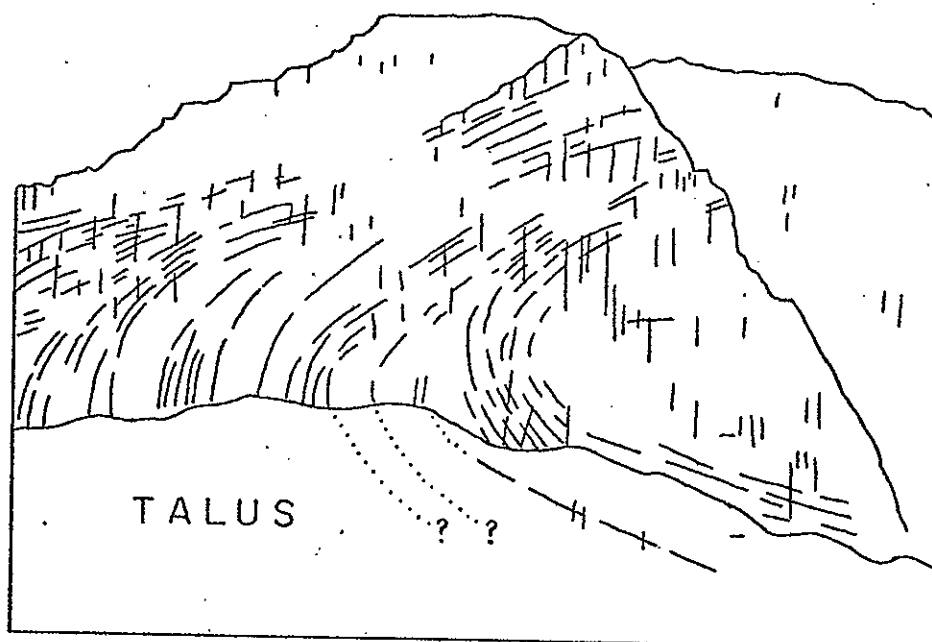


Fig. 23b. Delineation of structural details above, including flow-layering and vertical joint planes.

west. Near-vertical flow-layering associated with portions of this fold can be traced southward, and formerly was believed to mark a vent area of the rhyolite and related tin mineralization (Fries, 1940). Observations on moving lava and debris flows indicate that steep to overturned flow-layering is not uncommon at their margins, or snout regions, and indeed should be expected in view of the forward-rolling motion of viscous material as it spreads laterally in a manner somewhat analogous to the motion of a tractor tread.

#### Taylor Creek Rhyolite

The gray, porphyritic rhyolite and its bleached facies (Fig. 24) are similar in most respects to the rhyolitic rocks of the Paramount Canyon-Taylor Creek area, except that they are generally coarser grained. Phenocrysts of sanidine and quartz, with minor plagioclase and biotite, are set in a microcrystalline to spherulitic groundmass of quartz and alkali feldspar. Accessory minerals include fayalite (?), hematite, magnetite, sphene, pseudobrookite, and zircon. Quartz is dominant among the silica minerals, but opal, tridymite, cristobalite, and chalcedony are present in the groundmass.

A narrow band of bleached and weakly argillized Taylor Creek Rhyolite, 200 feet thick or more, crops out near the western margin of the dome. This facies is white and friable. The phenocrysts of quartz and sanidine are fresh, but the groundmass includes widely scattered patches of clay minerals. The argillized rock is further characterized by numerous shear zones, not found in the less altered rhyolite. Individual shear surfaces, which commonly are slickensided, can be traced for only a few feet in outcrop.

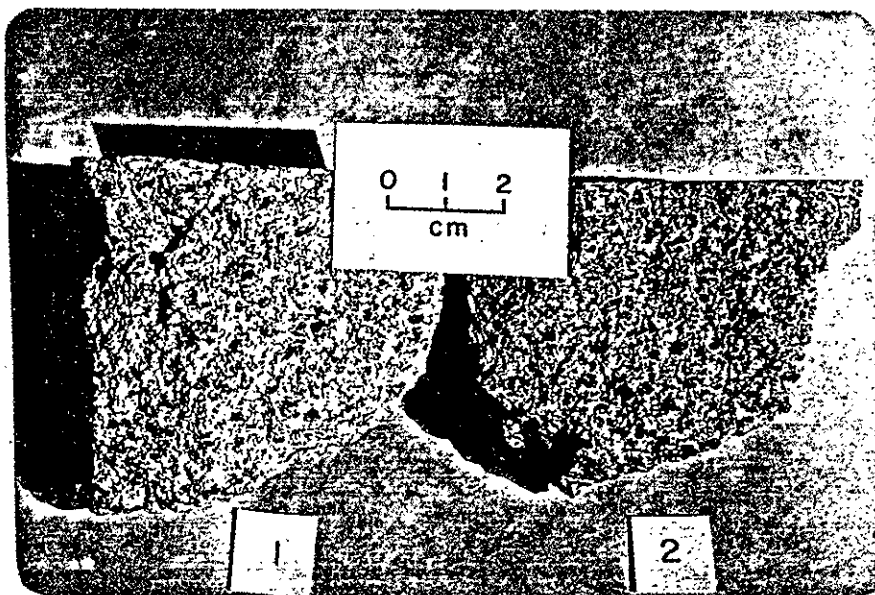


Fig. 24. Representative samples of Taylor Creek Rhyolite as exposed in the Taylor Creek prospects area. Gray, porphyritic rhyolite (#2) and its bleached white, argillized equivalent. Phenocrysts of quartz and sanidine constitute about 22 volume percent of the rock.

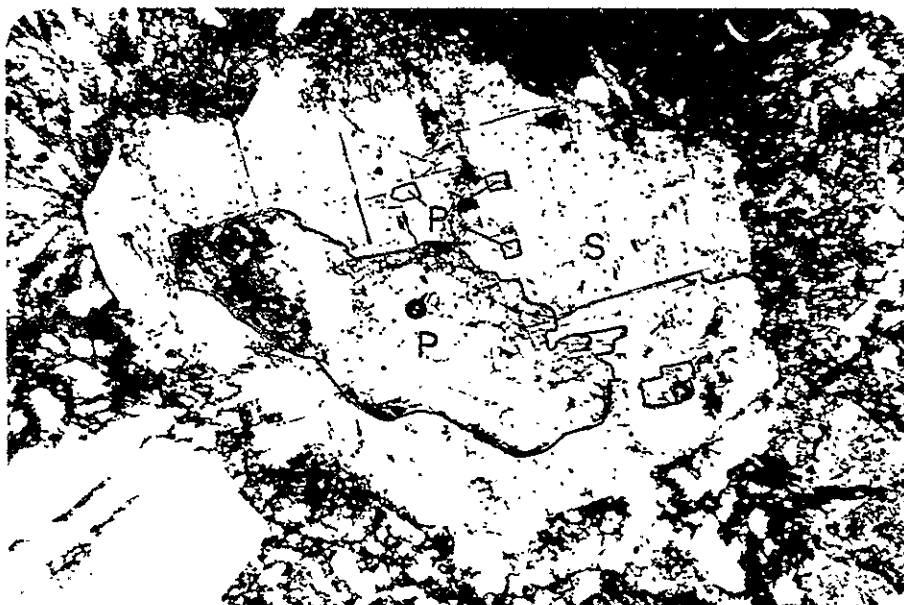


Fig. 25. Sanidine (S) phenocryst mantling plagioclase (P)--a feature commonly observed in the Taylor Creek Rhyolite. Crossed nicols, 72x.

Sanidine phenocrysts separated from the gray, porphyritic rhyolite at Taylor Creek yield potassium-argon age dates from  $24.0 \pm 0.5$  m.y. (Elston, 1971, written comm.) to  $25.1 \pm 1.0$  m.y. (Kottlowski, 1970, written comm.), which places the Taylor Creek Rhyolite on the Oligocene-Miocene boundary.

Sanidine and quartz are the dominant phenocrysts, constituting 25 percent or less of the rock (Figs. 3 and 4). Sanidine, in crystals .5 to 4 mm long, is optically similar to the sanidine of other units, but within the argillized facies it exhibits a peculiar fracture mosaic that is expressed as a "quilt-like" extinction pattern under the microscope. Small portions of these phenocrysts apparently have been moved or rotated slightly relative to adjacent portions. This observation suggests a slight micro-granulation, yet the external crystal boundaries seem to be undeformed.

The  $2V_x$  of the sanidine ranges from  $27$  to  $56^\circ$ , with an average of  $40^\circ$ . These values are somewhat higher than those for sanidines in the rhyolite from Beaver Creek ( $34.5^\circ$ ) and in the porphyritic vitrophyre of Paramount Canyon ( $34.5^\circ$ ). Figure 36 provides data for comparison.

Amethystine quartz, euhedral to subhedral crystals, and 5 mm in maximum diameter, composes approximately half of the total phenocryst volume. Much of it is fractured, with recrystallized borders.

Sodic oligoclase,  $An_{17}$ , occurs both as individual phenocrysts 1.25 mm or less in diameter and as clustered grains. It commonly is mantled by sanidine (Fig. 25). Only a few grains are present in a typical thin-section.

Accessory minerals, generally present as small grains, include biotite, fayalite (?), sphene, hematite, magnetite, and zircon. Anhedral to wedge-shaped grains of spheno, .6 mm or less in diameter, are typically altered to iron oxide, as is most of the biotite. Zircon, less than 10 microns long, is included within, and clustered around, rims of magnetite crystals.

The bulk of the groundmass is devitrified glass, in general a microcrystalline aggregate of quartz and alkali feldspar. The feldspar occurs in spherulitic growths and in mosaics as prismatic to tapered crystals, .5 mm or less in length. Tridymite and cristobalite are present also in the groundmass, but are not common.

#### Alteration

Alteration of the rhyolite is dominantly argillic, with very local silicification and sericitization. The alteration is mainly in the groundmass, where clay minerals appear as scattered patches interstitial to groundmass feldspar and silica minerals. Phenocrysts of feldspar and quartz are fresh, except for very minor sericitization and clay alteration along fracture and cleavage surfaces. The clay minerals could not be identified positively using standard techniques of clay separation, concentration, and X-ray analysis.

#### Tin-Bearing Veinlets

Hematite-cassiterite veinlets are well exposed at the Taylor Creek locality, although less than twenty veinlets are now visible. Many have been mined out, judging from the number of prospect pits in the area. The veinlets are discontinuous, and cannot be traced for

distances of more than a few feet in any one outcrop. Their exposed width rarely exceeds 8 mm.

Veinlets are restricted to the argillized facies of rhyolite, which is exposed along the western margin of the flow-dome. They generally strike northwesterly, and dip steeply to the southwest. They consist dominantly of specular hematite, with quartz, alkali feldspar, cassiterite, topaz, and less commonly, cristobalite. A typical veinlet is shown in Figure 26. The veinlets are zoned on a micro-scale, and three zones commonly can be recognized. In typical succession inward from the veinlet walls, these zones include: (1) a sanidine-rich layer with hematite, cassiterite, and topaz, (2) an intergrowth of hematite and quartz, with or without disseminated cassiterite, and (3) nearly solid specular hematite with minor disseminated cassiterite. Sanidine generally forms radial clusters along the walls of a given veinlet, and it is generally sericitized and iron-stained. In at least one sample (TCW-36), alkali feldspars from the veinlet were found to be considerably more potassic, and of higher structural state, than the groundmass or phenocryst phases from other rhyolite samples (Fig. 37).

Topaz forms individual prisms and rosette-like crystal clusters included in K-feldspar (Fig. 27a), generally in zone 1 adjacent to the veinlet wall. It is not abundant. The occurrence of well-crystallized topaz in a feldspar host is suggestive of replacement, although there is no clear criterion to prove that feldspar has been replaced by topaz. The formation of topaz at the expense of alkali feldspar is typical of greisenization, so common in tin deposits of plutonic affiliation.



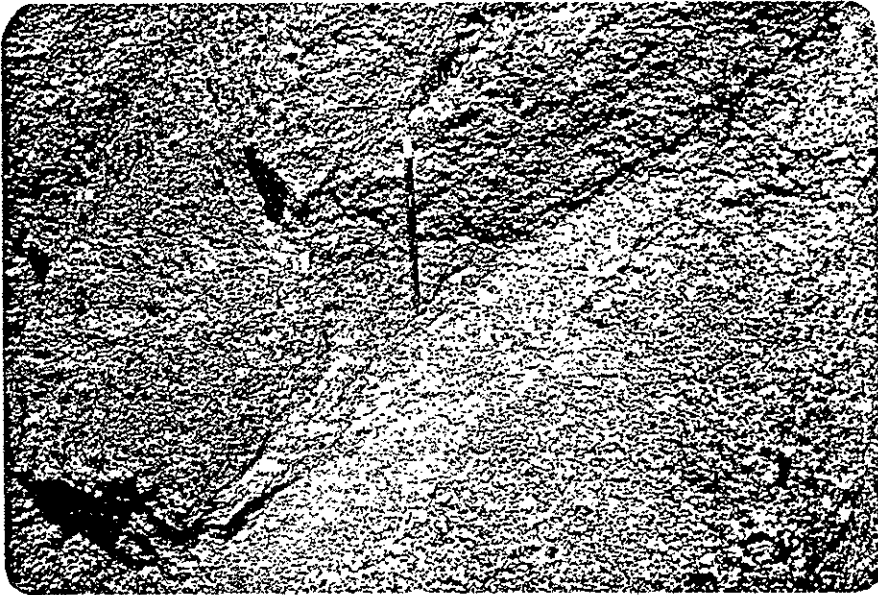


Fig. 26. Typical cassiterite-hematite veinlet exposed in the Taylor Creek prospects area. Six inch pencil for scale.

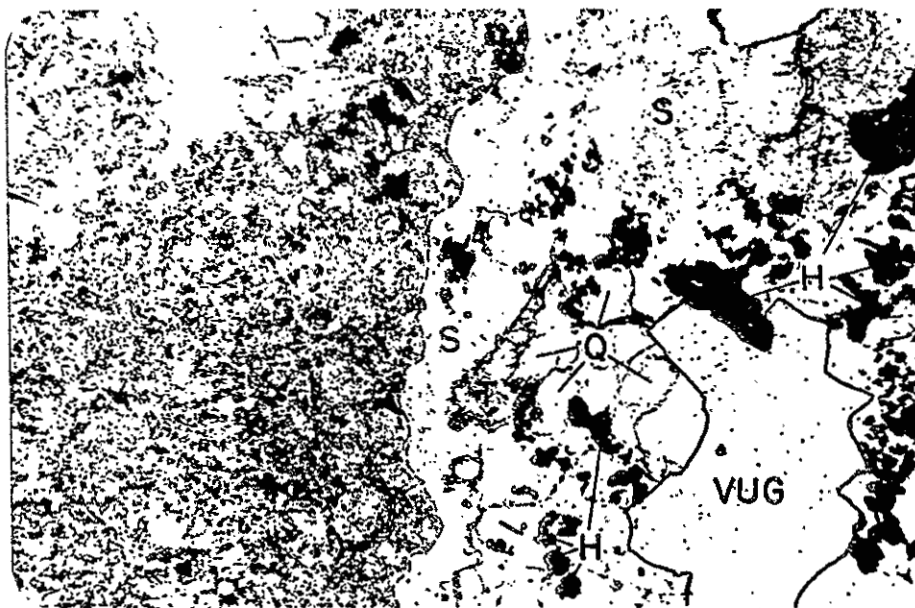


Fig. 27a. Sharp contact between rhyolite groundmass (left) and tin-bearing veinlet. Sanidine (S), and less commonly, topaz (T) line the veinlet wall. The sanidine is sericitized. Quartz (Q) and hematite (H) commonly encrust the sanidine-rich zone. The hematite-rich zone is absent from view (right). Plane-polarized light, 72x.

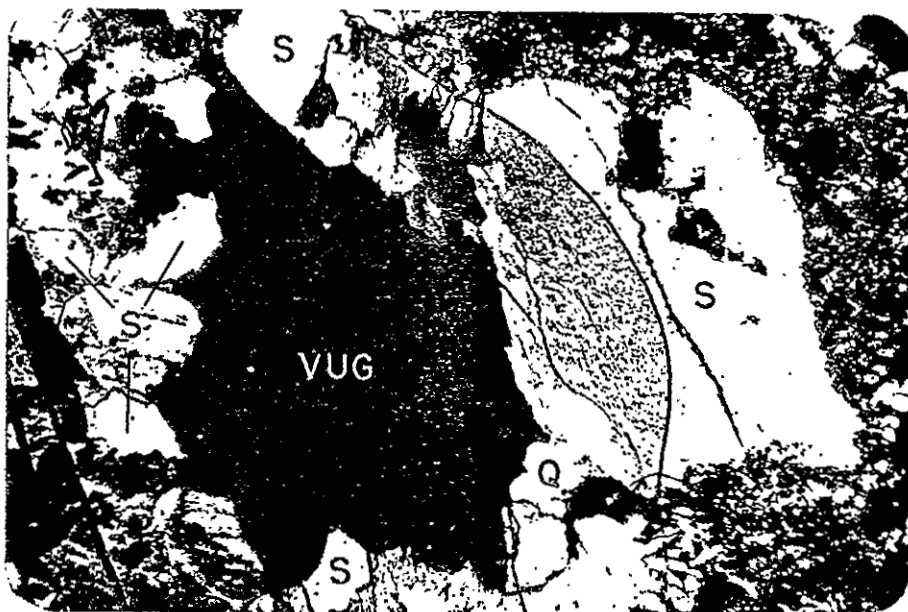


Fig. 27b. Sericitization embayment of sanidine (S) phenocryst adjacent to veinlet wall, suggesting that the movement of altering fluids was outward from the veinlet. Crossed nicols, 72x.

Cassiterite occurs as minute red crystals that are honey yellow to yellow-brown in thin-section. These grains are non-pleochroic, indicating that they have a low tantalum content. They are scattered in all three zones of the veinlet association, but are most abundant within the hematite-rich zone. Cassiterite also is disseminated within the rhyolite groundmass, but only immediately adjacent to the veinlets.

Sericitization of alkali feldspar is very local and does not extend for more than a few millimeters from the veinlet into the wall rock. A sharp sericitization "front" is shown in Figure 27b. The altering fluids have formed a very local sericite embayment, that is convex into the sanidine crystal. The sanidine phenocryst, which represents an early crystalline phase of the rhyolite, is unaltered outside the sericite zone. The sericite embayment, convex into the feldspar crystal, suggests that the altering fluids migrated from the veinlet fracture into the wall rock.

#### Rhyolite Chemistry

Bulk chemical and trace-element analyses were obtained from samples of relatively fresh, devitrified rhyolite (TCW-28A), as well as weakly argillized, bleached rhyolite (TCW-6, 20, and 24). Sample locations are indicated on Plate 5, and the analytical results are recorded in Table VI.

The major compositional differences among these samples lie in their alkali and lime contents. The argillized facies, as might be expected, has been enriched in potash (6.4 versus 4.1 percent  $K_2O$ ), and depleted in  $CaO$  (0.40 versus 1.31 percent) relative to the fresher

rhyolite. Most of the potash metasomatism probably is expressed in the formation of secondary K-feldspar within the groundmass and veinlets. The veinlet feldspar from one argillized sample, as determined by X-ray, was found to be the most potassic of all feldspar phases studied. Similar K-metasomatism has been recognized in the Mexican tin-bearing rhyolites (Ypma and Simons, 1969).

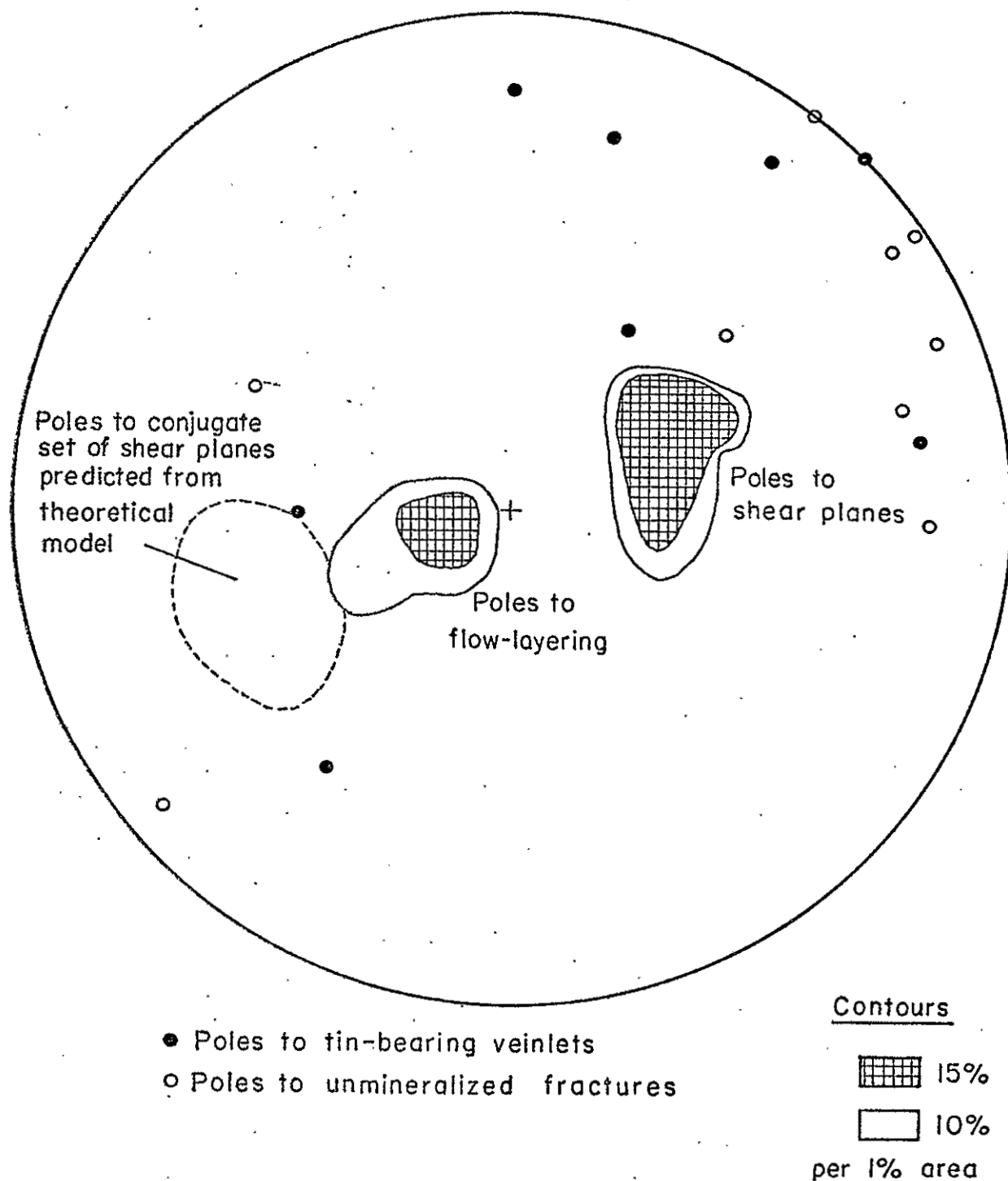
Trace-element contents between fresh and argillized facies of rhyolite appear to be similar.

During World War II, the U. S. Bureau of Mines sampled both lode and placer deposits for analyses of tin content only (Volin and others, 1947). Lode deposits east of Nugget Gulch and between Taylor Creek and Cox Canyon were sampled by means of trenches, shafts, crosscuts, and one adit. The samples generally were taken at 5- to 10-foot intervals, covering more than 1800 feet of excavations in mineralized areas. Locations of these test pits and corresponding tin values, compiled from the U. S. B. M. Rept. Inv. 4068, are recorded on Plate 5. The tin content of channel samples across mineralized areas generally is less than .05 weight percent.

#### Rhyolite Structure and Localization of Veinlets

Considerable structural detail within the tin-bearing rhyolite has been provided by the mapping of Fries (1940) and Jahns (1957-62, unpubl.). Structural records from their maps, including orientations of rhyolite flow-layering and shear planes, have been plotted as poles on a Schmidt equal-area net, lower hemisphere (Fig. 28). Poles to the tin-bearing veinlets and shear fractures measured during this study also are plotted in Figure 28.

Fig. 28. Pole projections of structural features in rhyolite, Taylor Creek prospects area. Schmidt net, lower hemisphere.



Flow-layering is the most conspicuous planar feature consistently developed in the rhyolite. Where accentuated by weathering, it resembles the layering in sedimentary rocks, with individual "layers" ranging from less than an inch to several inches thick. As shown in Plate 4, and Figure 29, the flow-layering is gently inclined in most places. It strikes north to northwest, and dips gently east to northeast.

Nearly all the shear planes are confined to argillized, white rhyolite, and they generally are restricted to the rhyolite near the dome margin. Distinctive slickensides along the shear planes rake  $30^{\circ}$  or less (Fig. 30). The surfaces commonly are iron-stained but not mineralized, and they intersect flow-layering at an angle of about 40 degrees. They typically dip west-southwestward at angles near 30 degrees. Individual shears can be traced a few tens of feet, at most, in the outcrop. Amounts of movement along these surfaces could not be determined, but they are believed to be small due to their limited extent, and general lack of associated brecciation.

The fractures and mineralized veinlets are not planar features, but instead are irregular and branching. As evidenced in Figure 28, there is considerable scatter in orientation of the fractures. In general, however, they strike northwest, and 70 percent of those measured dip southwestward at angles of 60 to 90 degrees. Displacements along these surfaces generally cannot be recognized. Slickensides and brecciation are absent. In thin-section, phenocrysts along fracture walls show no visible evidence of shear or granulation.

Age relations between the shear surfaces and the tin-bearing veinlets are not known, for these features do not intersect each

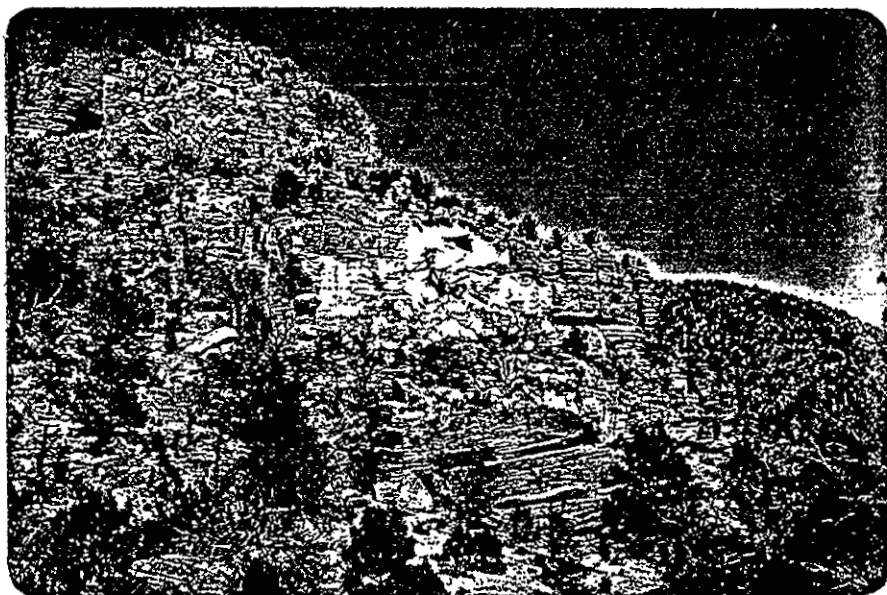


Fig. 29. Well-defined flow-layering in argillized portion of Taylor Creek Rhyolite at Taylor Creek. Flow-layering dips gently eastward away from viewer. The prominent ledge (white) is about 25 feet thick.

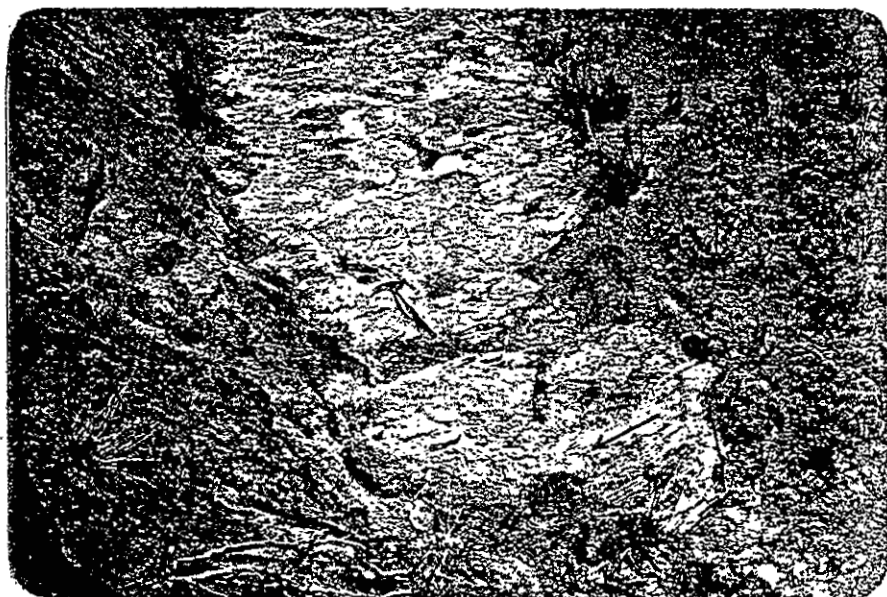


Fig. 30. Shear surface dipping westward toward viewer at an angle of about 35 degrees. Slickensides (→) rake approximately 30 degrees. Same locality.

other. The projected angle of intersection between shears ( $\sim 30^\circ$ ) and veinlets ( $\sim 75^\circ$ ) is about 45 degrees.

At least two different modes of origin can be postulated for the tin-bearing fractures. They might represent one set of shear planes, or slip planes developed in a partly cooled rhyolite dome as it moved laterally. Alternatively, they might represent tensional features developed in rhyolite during cooling after the lava movement has ceased. Relative to the first possibility, it is known that the veinlets are concentrated near the margin of the dome, where the rhyolite probably was cooler during flow and presumably where it behaved nearly as a solid or plastic material. Further, the veinlet fractures are inclined about 45 degrees to the shear planes, so that the veinlets might be considered as another set of shear or slip planes within the rhyolite. According to this interpretation, the veinlet fractures and shear fractures form conjugate sets of breaks that correspond to conjugate sets of shear planes in a plastic material. The difference between the veinlet fractures and shear fractures thus would be related to the different amounts of slippage along the two sets of planes; more slippage is recorded along the shear fractures than along the veinlet fractures.

This interpretation of the fractures can be compared, in a gross way, with the calculated pattern of shear planes in the margin of a theoretical rhyolite dome. If it is assumed that the rhyolite behaved much as a Coulomb plastic substance at the time when the veinlet fractures and shear fractures were formed, the shear stress then was:

$$\tau = c + \sigma_n \tan \phi, \quad (1)$$



where  $\tau$  is shear stress,  $c$  is cohesive strength,  $\sigma_n$  is stress normal to the shear planes, and  $\phi$  is angle of internal friction. According to Coulomb theory of plastic flow, shear or slip planes intersect each other at angles of  $90^\circ - \phi$  or  $90^\circ + \phi$ ; these planes are oriented at an angle of  $\pm 45^\circ - \phi/2$  to the direction of maximum compression.

The use of Coulomb's model to describe the mechanical behavior of rhyolite is supported by some indirect evidence. For example, Shaw and others (1968) noted that Hawaiian basalt has a yield strength, which is the fundamental aspect of Coulomb's law. Further, Pollard and Johnson (in press) have suggested that the behavior of a mush of crystals and silicate melt should be similar to the behavior of a mixture of clay slurry and suspended clasts. When the clasts exceed about 30 volume percent of the mixture, they begin to interact and produce "friction" such as described by the angle of internal friction in Coulomb's law (Hampton, 1970; Pollard and Johnson, in press).

The procedure for calculating the orientation of the slip planes in the snout of a dome of Coulomb plastic consists of establishing the form of the profile of the dome and then of establishing the pattern of slip lines below this profile. The theoretical form of the profile in two dimensions has been computed by Johnson (1965, and pers. comm.), and is given by the equations:

$$y = \frac{-2k}{\gamma} \ln [\sin(\theta)] \quad (2)$$

and

$$x = \frac{2k}{\gamma} \left[ \sqrt{\exp\left(\frac{\gamma y}{k}\right) - 1} \right] - \arctan \left[ \sqrt{\exp\left(\frac{\gamma y}{k}\right) - 1} \right], \quad (3)$$

where

$$k = \tan(45^\circ + \phi/2)$$

ln = natural logarithm

exp = exponential (e)

$\gamma$  = unit weight (density times acceleration of gravity)

$\theta$  = slope angle, measured counterclockwise from the plus x-direction

x = horizontal coordinate

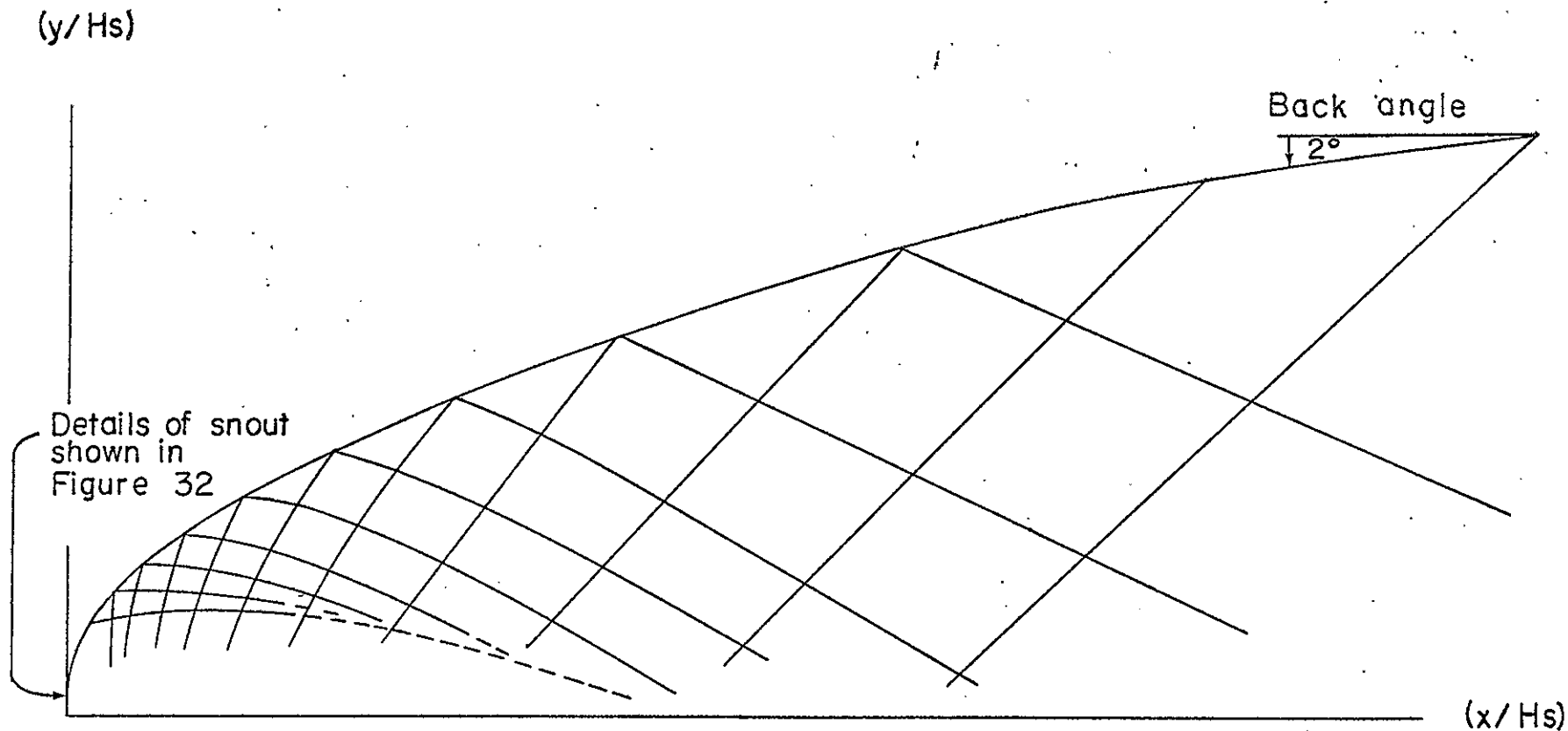
y = vertical coordinate

The profile of the snout of a theoretical dome of large diameter is shown in Figure 31. Here the x- and y-coordinates have been plotted in dimensionless form ( $y/H_s$ ), ( $x/H_s$ ), where  $H_s$  is the maximum height of the snout. The theoretical shear planes sketched in Figure 31 dip at relatively gentle angles along the back of the snout, where  $x/H_s$  is greater than 1.0. At the tip of the snout, one shear set dips at steep angles, and the other at gentle ones, a relationship similar to that present in the Taylor Creek dome. The calculated slip lines for the tip of the snout are shown in detail in Figure 32 for friction angles of 0, 15, and 30 degrees. The friction angle ( $\phi$ ) for rhyolite under any given set of flow conditions is not known, so that this estimate cannot be checked independently.

In the theoretical models, the two sets of shear fractures intersect each other at angles from 60 to 90 degrees, dependent upon the angle of internal friction. One of the shear sets dips away from the snout region, while the other set dips steeply into the snout (Fig. 32).

Shear fractures in the natural rhyolite (about 30° dips) could fit into any one of the three theoretical models. The veinlet fractures in the existing rhyolite, however, dip steeply away from, rather than

Fig. 31. Slip-line pattern beneath stress-free surface of a theoretical dome of large diameter, with the following boundary conditions: snout angle,  $90^\circ$ , back angle,  $2^\circ$ , and internal friction angle,  $(\phi)$ ,  $15^\circ$ .



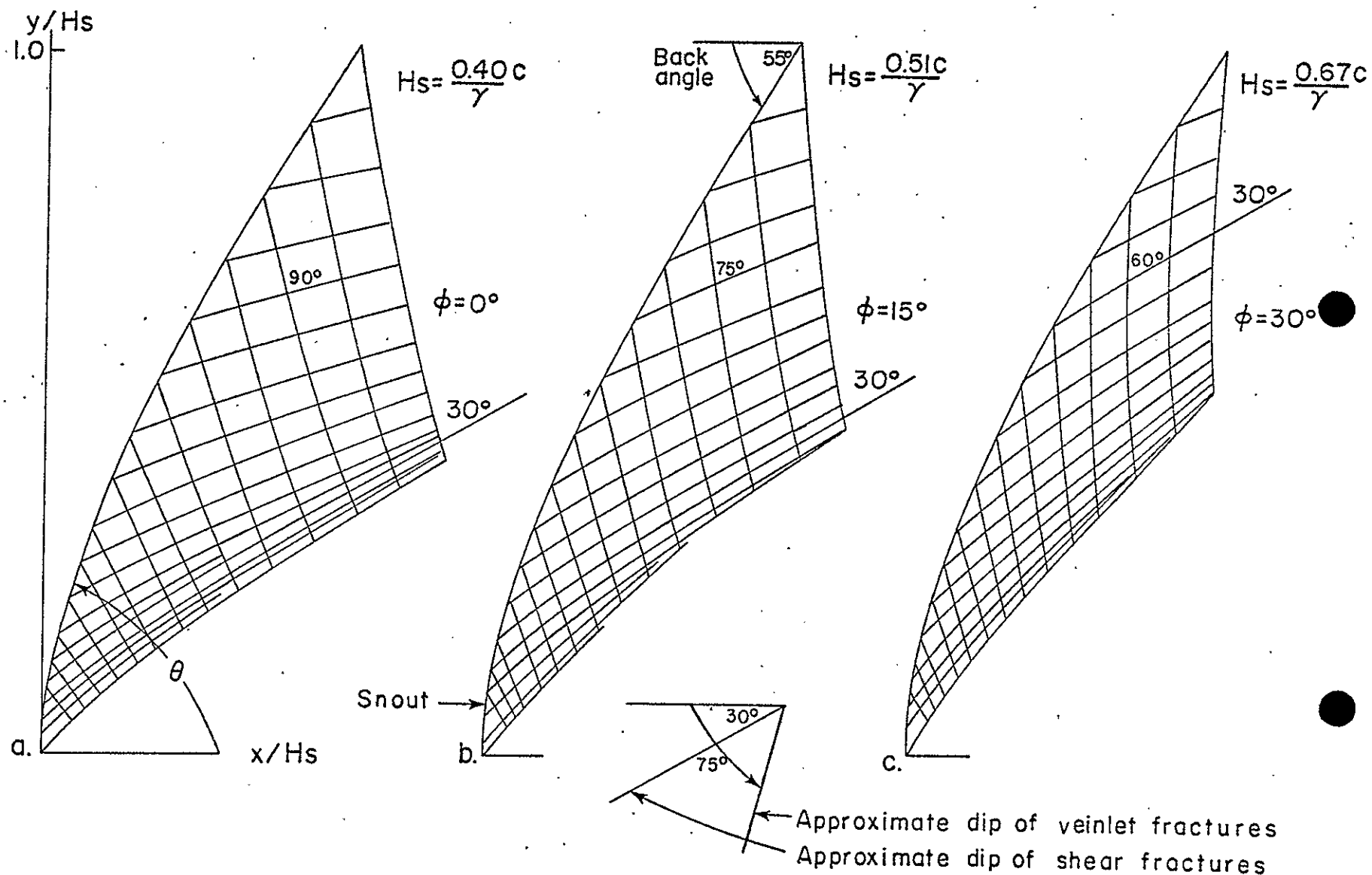


Fig. 32. Details of 2-dimensional slip-line pattern beneath stress-free surface of the snout region of a theoretical dome with the following boundary conditions: snout angle,  $90^\circ$ , back angle,  $55^\circ$ , and internal friction angle, ( $\phi$ ),  $0^\circ$ ,  $15^\circ$ , and  $30^\circ$ .

into the snout of the dome. Furthermore, the veinlet fractures intersect the shear fractures in the rhyolite at angles near 45 degrees, not 60 to 90 degrees. Obviously, the orientation of structural features calculated by the theoretical model does not fit the pattern observed in the Taylor Creek Rhyolite.

If the foregoing assumptions and calculations are correct, it must be concluded that the veinlet fractures are not shear fractures developed in consequence to flow. They instead appear to be tensional features formed during cooling of the rhyolite, and the absence of shearing parallel to these surfaces supports this view. It also is interesting to note that the veinlet fractures are not planar, whereas most primary joints in the rhyolite along the canyon rims of Taylor Creek are planar and vertical. The irregular, branching, non-planar characteristics of the veinlets may well be related to the slight micro-granulation (not brecciation) of the rock developed as a consequence of flowage. The granulation and increased porosity probably contributed to the development of the veinlets as irregular fractures, rather than as planar fractures.

A possible explanation for the concentration of low-angle shear planes developed in the argillized facies is that they represent surfaces on which gravity-sliding took place. This would be favored in the argillized facies, which is more porous and considerably less coherent than the other flow rocks exposed here. If sliding occurred, however, it was local and probably took place over short distances only. Similar low-angle shears also can be observed in argillized rhyolite near the mouth of Paramount Canyon (Plate 2).

### Source of Tin and Mineralizing Fluids

Any explanation concerning the origin of lode tin deposits at Taylor Creek must account for the following observations: (1) the concentration of tin-bearing veinlets around the margins of the rhyolite flow-domes, including the Boiler Peak and Taylor Creek domes, (2) the lack of tin mineralization in younger units overlying the rhyolite, including the andesites and the Gila Conglomerate, (3) the enrichment of cassiterite in miarolitic, lithophysal rhyolite facies, commonly in the upper parts of the rhyolite domes, (4) the association of high-temperature oxides with cassiterite, and (5) the apparent movement of altering fluids from the veinlets into the country rock.

Whether the ultimate origin of lode tin at Taylor Creek lay in the mantle or in crustal rocks, more immediate possible sources include the following: (1) the tin and associated iron were derived via volcanic vents from deeper sources unrelated to the rhyolite, as suggested by some earlier investigators (e.g., Fries, 1940), or (2) the tin was derived from the rhyolite, having been incorporated in groundmass glasses or in relatively early-crystallizing phases such as biotite and sphene, and subsequently released and concentrated by the action of late-stage fluids (the "deuteric-release" hypothesis), or (3) the tin was a constituent of the rhyolite magma, was concentrated in residual fluids, and then was precipitated in fractures or cavities at a late stage in the cooling history of the rock.

Relative to the first hypothesis, detailed field mapping in the study area has failed to reveal what logically could be termed a "vent area." Flow-layers in the vast bulk of the lower rhyolite section are gently dipping. Near some of the margins of the rhyolite

masses, recumbent flow-folds in the rhyolite are developed and are associated marginally with flow-breccia, particularly in the Taylor Creek prospects area. These relationships are indicative of laterally-spreading, viscous flow. In general, vertical flow-layering in volcanic rocks has been cited commonly as evidence for vertical flowage upward from below, i.e., a vent. The development of a clearly recognizable flow-fold, in three-dimensions, at Taylor Creek near the margin of the dome (Fig. 23a) makes the vent interpretation for this structure untenable. Without the aid of the third dimension, this structure probably would not have been recognized. Bleaching, argillization, and tin mineralization are not closely associated spatially with vertical flow-layering in the rhyolite, but are removed laterally by 1000 to 1500 feet. If tin mineralization were related to possible vent structures, one might expect a close spatial relationship. This is not the case at Taylor Creek.

The miarolitic, tin-bearing facies exposed in Paramount Canyon grades downward into relatively fresh, lavender rhyolite. If this unit were connected by a possible vent, the underlying rhyolite would have been affected almost certainly by ascending hydrothermal fluids. There is no evidence of this.

The lack of tin mineralization in the younger, overlying units, the presence of tin in miarolitic, gas-rich layers of the rhyolite, and the absence of any association with recognizable vent structures strongly suggest a genetic relationship of tin to the rhyolite magma. Whether significant amounts of tin were incorporated in the glass or in early crystallizing minerals of the rhyolite according to the second hypothesis is questionable. The general scarcity of biotite

(less than 1 percent), whose structure provides possible sites for the incorporation of tin during early stages of crystallization, does not enhance this argument. Indeed, biotite is absent from the miarolitic rhyolite, which contains concentrations of cassiterite in Paramount Canyon. When present in the rhyolite, the biotite invariably is altered to hematite and magnetite, so no comparison could be made relative to the tin contents between fresh and altered biotites.

Sphene, known to contain detectable amounts of tin in some skarn deposits and in some granites, is less abundant than biotite. Sphene could not be effectively removed from the rock using heavy-mineral separation techniques.

Residual glasses are not common in the Taylor Creek Rhyolite. Nearly all the rhyolite has been devitrified to aggregates of quartz and alkali feldspar, hence no meaningful comparisons could be made relative to the concentration of tin in rhyolite glass and the possible leaching of tin during, or following the devitrification of the glass. Tin was not detected, using the emission spectrograph, in one thin, porphyritic vitrophyre mapped in Paramount Canyon. However, silicic glasses in the Nacimiento volcanic subprovince (Fig. 42), of which this district is a part, contain an average of 13 ppm Sn (R. R. Coates, 1970, pers. comm.). Thus, the possibility does exist that tin could have been extracted from rhyolite glass in the Taylor Creek area during devitrification, or hydrothermal activity, but the extent to which such processes might have contributed to the formation of the tin deposits is not known. It is clear from the alteration pattern in the individual tin-bearing veinlets (Fig. 28) that the mineralizing fluids moved into the country rock from the sites of fractures, so that the



immediate host rock probably was not the source of tin via some kind of "lateral secretion."

Evidence to support the third hypothesis, that tin was a constituent of the rhyolite magma, and was concentrated in residual fluids and then was precipitated in fractures or cavities, is derived, in part, from the miarolitic facies exposed in Paramount Canyon. The occurrence of tin in vapor cavities within the rhyolite suggests that tin was concentrated in gas-rich layers, as evidenced by the abundance of lithophysae and miaroles. The presence of miarolitic rhyolite near the tops of the domes indicates that only certain portions of the rhyolite became water-saturated, and near the tops of the domes, gases were free to escape under the reduced lithostatic pressures near the surface of the mass. This is analogous to the concentration of volatile and metal constituents in the cupola areas of many plutons.

The more extensive bleaching of rocks in the Taylor Creek prospects area, where miarolitic cavities are absent, indicates that a great volume of hot fluids moved through this part of the volcanic complex. The fluids must have continued to permeate the rhyolite at least until the bulk of this rock was sufficiently solid and brittle to be fractured. The fact that tin is concentrated in veinlets, rather than in miaroles, adjacent to the dome margin, suggests that there was a greater concentration of volatiles emitted at the margins of the dome, and that fracturing was sufficiently developed to permit escape of the contained gases. The concentrated release of tin-bearing fluids near the margin of the Taylor Creek dome, where veinlets and bleaching are abundant, would be expected and would be in good

agreement with reported observations of moving lava flows. In his descriptions of lava movement at Parícutin, Krauskopf (1948) noted that emissions of gas were strongest near the edge of a flow, where morainal blocks of lava commonly were altered. The formation of a surface crust, or "breccia carapace" on a body of lava undoubtedly serves to retain gases that otherwise would escape from the flow during and after gross movement.

The late-stage, or deuteric fluids responsible for the tin mineralization probably also contributed to the bleaching and weak argillization invariably associated with the tin deposits. There is widespread argillization, however, where no tin deposits are found. The low thermal ranges of stability of clay minerals in general (e.g., Hemley and Jones, 1964; Roy and Osborn, 1954; Sand, Roy, and Osborn, 1954) suggest that the alteration was not simultaneous with deposition of the cassiterite. White mica, rather than clay minerals, occurs within the tin-bearing veinlets themselves. In a cooling rhyolite mass, argillization of the groundmass most likely would follow tin mineralization as the temperature of deuteric fluids dropped to values within the stability ranges of the clay minerals--300°C as an approximate upper limit. Post-metal hypogene argillization, expressed primarily by formation of dickite, has been reported from the tin deposits at Lost River, Alaska (Sainsbury, 1960).

To summarize briefly, the mineralization and argillization of the Taylor Creek Rhyolite are viewed here as parts of a continuous process extending from tin deposition at temperatures of approximately 600°C to rock alteration at lower temperatures (less than 300°C) during cooling of the rhyolite and its contained fluids. The localization

of tin in microlitic rhyolite at Paramount Canyon in the upper part of a rhyolite dome, as well as in the argillized, bleached rock found mainly in the lower rhyolite section and near the dome margins at Taylor Creek and elsewhere, suggests that the tin was inhomogeneously distributed at an early stage during formation of the flow-domes, probably within aqueous-rich gases in different parts of the bodies. Where favorable temperature gradients were developed, such as along the margins of the domes or near their tops, tin, iron, and locally manganese and titanium could migrate or be transported to favorable sites of deposition in the rhyolite.

#### SOUTH KEMP MESA-BEAVER CREEK AREA

##### General Features

The small, rectangular area mapped in the western part of the tin district is  $3/4$  by 1 mile in plan (Plate 6). It is immediately south of Kemp Mesa, a flat upland underlain by andesitic lava flows. The area is deeply dissected by the drainage of Beaver Creek, which joins Taylor Creek a few miles downstream to form the Gila River. Beaver Creek has cut a box-like canyon to points 300 to 400 feet below the generally flat mesa surface, providing excellent exposures of flow-layered Taylor Creek Rhyolite and overlying andesite and basalt (?) flows. This section in part overlies and in part is juxtaposed against the Taylor Creek Rhyolite.

Five units have been distinguished in the immediate area. The oldest is the Taylor Creek Rhyolite (Datil Formation), Oligocene in age, and it is overlain unconformably by andesite of Miocene (?) age.

This volcanic section is overlain by unconsolidated deposits of Holocene age, which include terrace deposits and floodplain alluvium along Beaver Creek and its tributaries, as well as fan and talus deposits at mouths of tributary washes and on several steep slopes. Eluvial deposits form a thin, discontinuous cover on rhyolite and andesite in much of the upland area.

### Taylor Creek Rhyolite

The Taylor Creek Rhyolite appears in an arcuate outcrop belt about 3800 feet long (east-west) and 400 to 2000 feet wide (north-south). In the vertical dimension, approximately 300 to 400 feet of this elongate mass is exposed along the easterly canyon wall of Beaver Creek (Fig. 33). As the rhyolite is traced in outcrop from east to west, the strike of flow-layering shifts progressively from east-west to nearly north-south, conforming to the general arcuate shape of the exposed mass. The dip of the layering correspondingly steepens to near vertical, and broad, slightly overturned flow-layering occurs in places along the western wall of the Beaver Creek canyon.

On the west and southwest margins of the body, andesite butts against rhyolite with near-vertical flow-layering. The contacts here are sharp, and the rhyolite groundmass has been discolored to an orange-brown. Effects of baking do not extend more than a few inches into the rhyolite in this vicinity.

Along its northerly border, as exposed on the north wall of Beaver Creek, the rhyolite is unconformably overlain by andesite (Fig. 33), but the two units become laterally juxtaposed as their contact is followed westward. The southerly border of the rhyolite

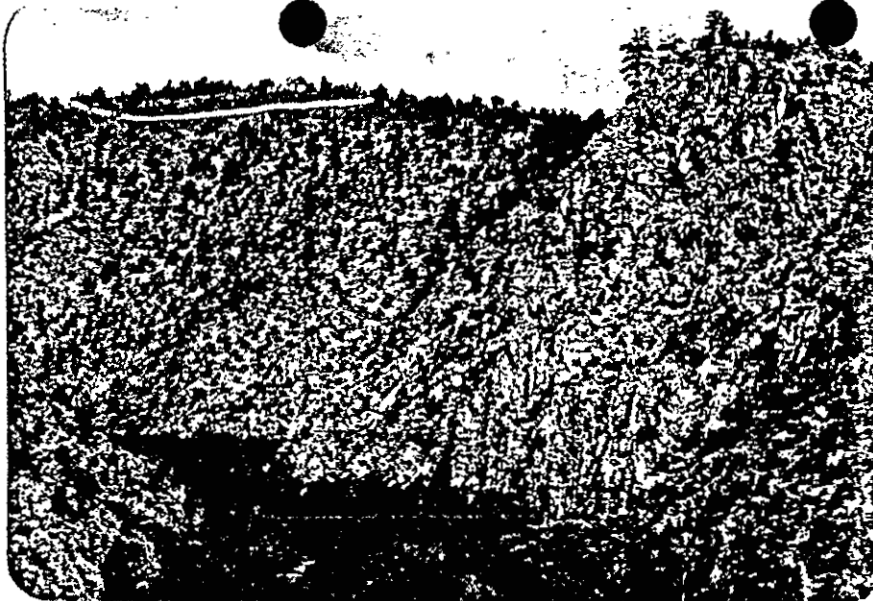


Fig. 33. View looking northeast across Beaver Creek at the Taylor Creek Rhyolite. Flow-layering strikes northeast and dips steeply to the northwest. Note the thin ledge of andesite that caps the rhyolite in the background.

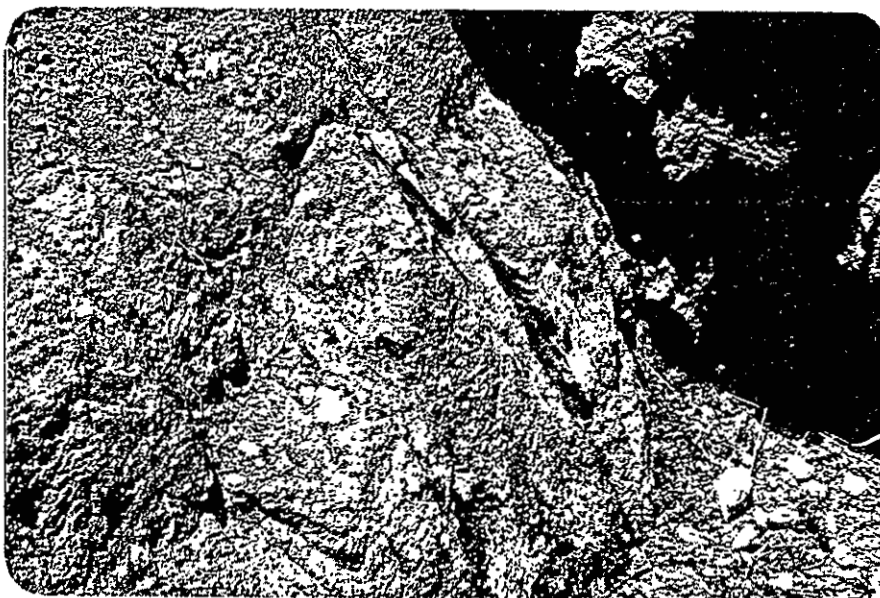


Fig. 34. Typical cassiterite-hematite veinlet exposed in the Beaver Creek area. The veinlet encrusts a parting surface that is parallel to the flow-layering dipping steeply to the right (south). White cristobalite encrusts the black specular hematite. Hammer for scale.

has been only approximately located. In the few places where it is well exposed, the rhyolite has been altered in a zone 15 to 20 feet wide, and locally has been brecciated. Here the rhyolite groundmass has been recrystallized and discolored orange-brown by introduced iron oxides. Semi-spherical relict clots of unaltered rhyolite, less than .5 inch in diameter, are present in a fine-grained matrix of quartz and alkali feldspar.

The mineralogy of the rhyolite is similar to that already described for the argillized rhyolite at the Taylor Creek Prospects, but the phenocrysts generally are larger. Sanidine crystals as long as 12 mm have been observed, and the quartz phenocrysts range from 1 to 5 mm in diameter. Phenocryst modes and sanidine-quartz ratios for this unit are recorded in Figures 3 and 4.

The groundmass, which consists predominately of K-feldspar and quartz, is interrupted by pockets in which these minerals are more coarsely crystallized, and by cavities lined with opal and chalcedony. The groundmass has been altered in varying degree to mixtures of sericite and clay, leaving the rock porous. Sericite, the more abundant alteration mineral, is irregularly disseminated and locally is concentrated in patches. In silicified parts of the rhyolite, sericite is sparse or absent, and colorless to pale brown chalcedony is the dominant silica mineral.

Accessory minerals include oligoclase, biotite, sphene, pseudobrookite, titaniferous magnetite, hematite, and zircon. Both the occurrence and appearance of the biotite and pseudobrookite are unusual. The biotite is the freshest of any seen in thin-sections of the rhyolites in the district. It also is in larger crystals that

are strongly pleochroic, with Z = red-brown, X = straw yellow. These crystals commonly have opaque rims. The more typical biotite, as observed elsewhere in the district, is very weakly pleochroic, is pale brown, and has been almost completely altered to hematite and magnetite.

Whereas pseudobrookite occurs in cavities in the rhyolite of Paramount Canyon, it here appears in the groundmass of the rhyolite as acicular prisms. These prisms are orange-brown to deep red, and commonly are marked by longitudinal striations. They occur both as individual crystals and as reticulated clusters, 8 microns or less long.

#### Tin-Bearing Veinlets

Several cassiterite-hematite veinlets are present in the rhyolite. Their mineralogy is like that of the veinlets discussed earlier, except that cristobalite is fairly abundant. They also differ in their relationship to the flow-layering of the rhyolite. Where they are most abundant, in the central part of the rhyolite body, the veinlets are localized parallel to the flow-layering and appear to have been deposited as crusts on parting surfaces (Fig. 34). Elsewhere, the mineralization is in steep fractures along which lateral movement has occurred. Near the southerly margin of the exposed rhyolite immediately east of Beaver Creek, for example, a near-vertical shear zone 5 to 20 feet wide is weakly mineralized. At the western end of this shear zone, a shear surface dips southeastward about 80°, and slickensides on this surface rake 50° to the west. A tunnel, U. S. Bureau of Mines Adit #8, was driven northeastward for a distance

of about 180 feet into the rhyolite along this shear zone. Seven samples collected by the Bureau in a traverse along the tunnel contained an average of less than .05 percent Sn (Volin and others, 1947).

### Andesite

Andesitic flows that are more than 500 feet in aggregate thickness nearly surround the small mass of tin-bearing rhyolite. They may have been derived from sources in the Black Mountain area 6.5 miles to the west, where a great thickness of intermediate to basic (?) rocks is present. The rocks exposed along Beaver Creek have not been dated, but they are thought to be temporal equivalents of similar rocks of the Bearwallow Mountain Formation, the age of which has been determined as about 21 million years (W. E. Elston, 1971, written comm.).

A few samples were collected, but no attempt was made to subdivide these rocks in the field. More basic rocks may be present within the section mapped as andesite. These flows in general are dense to vesicular pyroxene andesites, light gray to dark gray and with a platy weathering habit. A chemical analysis obtained for one of these rocks indicates a rather high silica content of 63 percent. A complete chemical analysis of the andesite is recorded in Table VI.

The andesite is aphanitic in the hand specimen, but under the microscope tiny phenocrysts of andesine and pyroxene constitute as much as 32 percent of the rock. These are set in a matrix of black glass or microlitic plagioclase. Two pyroxenes, augite and hypersthene, are present both as microphenocrysts and in the groundmass. The augite has pale green to pinkish pleochroism, and it commonly is



mantled by yellowish-brown hornblende. The groundmass pyroxenes are generally altered to biotite.

In the vesicular rocks of the andosite section, zeolites and chalcedony are present as cavity fillings. Stilbite appears to be the dominant zeolite.

#### Holocene Deposits

Unconsolidated deposits of unknown thickness cover approximately one quarter of the map area. Thin eluvial deposits are the most widespread, and consist of sand, gravel, and bouldery debris derived from underlying andesite and rhyolite. Gila Conglomerate may underlie the eluvial blanket to the south, although no outcrop of that formation was observed in the area studied. Younger stream and fan deposits are confined to the present floor of Beaver Creek. Minor accumulations of talus and slide debris occur on the steep valley sides.

#### Summary

Relationships between the Black Range lode tin deposits and the Taylor Creek Rhyolite discussed in the previous sections can be summarized briefly here as follows: (1) the tin-mineralized rhyolite forms several conspicuous flow-domes in the Tertiary volcanic section of the Black Range, (2) lode tin occurs in miarolitic cavities within porphyritic rhyolite and also in cassiterite-specularite veinlets that traverse the rhyolite. In the miarolitic rhyolite occurrence, such as that found in Paramount Canyon, cassiterite occurs primarily in vugs and lithophysal cavities in association with hematite, quartz,

alkali feldspar, bixbyite, pseudobrookite, topaz, and monazite. More commonly, tin is present as cassiterite in veinlets that are confined to the argillized facies of the rhyolite; moreover, these veinlets generally crop out around the margins of the flow-domes. The tin-bearing veinlets are zoned and consist dominantly of specular hematite, with quartz, alkali feldspar, cassiterite, topaz, and cristobalite. The alkali feldspar commonly is sericitized adjacent to the veinlet walls, and (3) the orientation of veinlets and the general lack of shearing parallel to the walls of the tin-bearing fractures suggest that the veinlets are tensional features which formed at a late stage in the cooling history of the rhyolite, and (4) the tin deposits are thought to be genetically related, or indigenous to the host rhyolite. The presence of cassiterite inmiarolitic cavities suggests that tin was precipitated from a gas phase that was evolved during emplacement of the rhyolite. Where the rhyolite was sufficiently fractured, and where the tin-bearing fluids could readily escape, such as around the margins of the flow-domes, tin was precipitated in fractures in the rhyolite. The association of cassiterite with the high temperature oxide minerals, bixbyite and pseudobrookite, indicates that at least some of the cassiterite was deposited at high temperatures, about 600°C; the veinlet occurrences may have been deposited at somewhat lower temperatures.

## ALKALI FELDSPARS

### Introductory Statement

A reconnaissance study of the alkali feldspars was undertaken to determine the extent to which these feldspars differ in their

optical properties, structural state, and composition in the areas studied, to learn what effects, if any, argillic alteration has had on structural state and composition of these feldspars, and to compare compositions among several generations of alkali feldspar, including those in phenocryst, devitrified groundmass, and veinlet assemblages.

Toward these ends, unit-cell parameters were determined for unhomogenized alkali feldspar phenocrysts that were hand picked from nine samples of rhyolite, as well as for groundmass feldspar from two of these samples. The feldspar samples were ground under acetone in an agate mortar, and then were X-rayed, using spinel as an internal standard ( $a_0 = 8.0833 \text{ \AA}$  at  $25^\circ\text{C}$ ). The Guinier-DeWolff focusing camera and  $\text{CuK}\alpha$  radiation were employed, with film exposures of 41 hours, or less. Unit-cell parameters were calculated, using the least squares program developed by Evans and others (1963). Calculated patterns of sanidine cell dimensions from Borg and Smith (1969) were used as starting parameters for the refinement program, using the fixed index option. In addition,  $2\theta_{(\bar{2}01)}$  spacings were obtained by X-ray diffraction for alkali feldspars from eighteen samples of porphyritic rhyolite, including phenocryst and associated groundmass phases. From one of these samples three generations of feldspar were obtained, including phenocryst, groundmass, and veinlet phases. Their compositions were determined by measuring the difference between  $2\theta_{(\bar{2}01)}$  of feldspar and  $2\theta_{(10\bar{1}0)}$  of quartz, following the method of Tuttle and Bowen (1958, p. 12).

### Phenocrysts

The alkali feldspar phenocrysts are sanidine. They generally are 2 mm or less in length, but some are as much as 12 mm long (e.g., at the Beaver Creek locality). Carlsbad twinning is common, and the crystals appear to be unzoned. The sanidine is microperthitic, with exsolved units of soda-rich feldspar that generally can be resolved at 80x magnification or less (Fig. 35). This exsolution probably contributes to the beautiful, pale-blue "moonstone" chatoyancy of most crystals. The albitic phase has been exsolved parallel to (001) of the host sanidine, and it forms discontinuous stringers across the width of individual crystals.

Minute inclusions of biotite and opaques, as well as apatite (?), are present in the phenocrysts. All the sanidine phenocrysts are fresh, with only slight argillization and sericitization along cleavage and fracture surfaces.

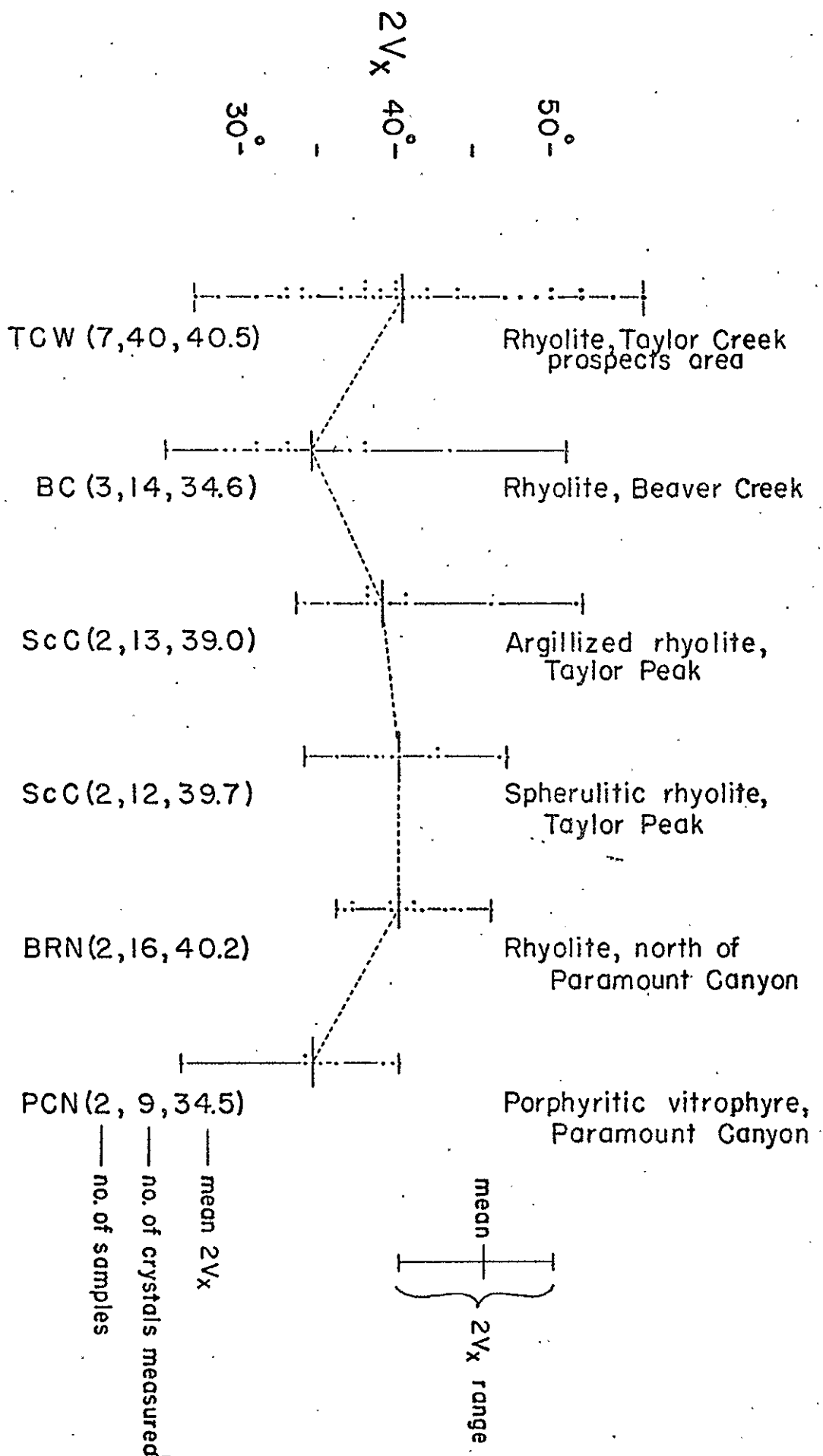
Optic angles ( $2V_x$ ) were measured in thin-section for more than 100 crystals from eighteen samples, utilizing the universal stage. Measurements of 9 to 27 crystals were made for each sample, and these are recorded in Figure 36. Considerable range in  $2V_x$  is noted among the phenocrysts, even in one thin-section. An average range of  $12^\circ$  was found per thin-section overall. From one sample to another, the greatest range ( $29^\circ$ ) was found among the seven samples from the Taylor Creek Prospects area (Plate 4). Generally, only two samples were used from each area.

Of the six areas sampled, four yielded an average of  $40^\circ$ , with a mean of  $2V_x = 35^\circ$  for sanidine phenocrysts from rhyolite at Beaver Creek and porphyritic vitrophyre, Paramount Canyon.



Fig. 35. Photomicrograph of sanidine phenocryst, showing albite exsolution lamellae parallel to (001). The phenocryst is present in a porphyritic vitrophyre, Paramount Canyon. Obliquely crossed polars, 288x.

Fig. 36. Optic angles of sanidine phenocrysts, Taylor Creek Rhyolite.



A comparison also was made between sanidines of bleached, argillized rhyolite and fresh, non-argillized rhyolite, although in both rock types the phenocrysts appear to be unaltered. The samples were taken from rhyolites near Taylor Peak. Optic angles for sanidines from the argillized rhyolite average  $39^\circ$ ; for the non-argillized unit,  $2V = 40^\circ$  (Fig. 36). Apparently, the argillization process has had no effect on the optic angles of these K-feldspar phenocrysts. Hydrothermal activity may have some effect on the optics of alkali feldspars. For example, Chapin (1965) found that post-emplacement vapor-phase or hydrothermal activity formed a zone of higher  $2V$  along the edges of some sanidine crystal fragments in two ash flows of the Thirtynine Mile Volcanic Field, Colorado.

#### Structural State

The unit-cell dimensions of alkali feldspars from several samples of Taylor Creek Rhyolite are recorded in Table V. Sample numbers followed by (P) denote phenocrysts, (G) groundmass, and (V) veinlet feldspar. Following the suggestions of other investigators (e.g., Wright and Stewart, 1968), cell refinements with a standard error, SE, greater than  $2\theta = .02^\circ$  are deemed unacceptable. These are marked by an asterisk (\*) in Table V. On this basis, half the refinements fall outside the acceptable standard error. Locations for the above samples are indicated on Plates 2, 5, and 6, and rock types are discussed farther on.

Cell edges are further recorded on a reference b-c plot (Fig. 37). The axial dimensions of most phenocrysts are clustered, and they plot off the high albite-high sanidine equivalent series.

TABLE V

Unit-cell dimensions of alkali feldspars from  
the Taylor Creek Rhyolite, Black Range, New Mexico

Sample	N <sub>Or</sub>	a(Å)	b(Å)	c(Å)	$\beta(^{\circ})$	V(Å <sup>3</sup> )	SE ( $^{\circ}2\theta$ )	Ref.
BC-19P	.79	8.5618 0.0013	12.9726 0.0014	7.1611 0.0008	116°04.39 0.7	714.43 0.13	0.009	18/20
BC-19G*	.87	8.5848 0.0049	12.9775 0.0058	7.1618 0.0035	115 52.70 3.3	717.89 0.48	0.039	19/20
TCN-7P*	.85	8.5844 0.0069	12.9613 0.0098	7.1595 0.0044	115 50.13 4.6	716.98 0.77	0.039	11/11
TCW-36V*	.875	8.5641 0.0052	13.0140 0.0055	7.1725 0.0033	116 01.95 3.5	718.29 0.54	0.039	18/18
BRN-11P	.805	8.5826 0.0039	12.9502 0.0063	7.1622 0.0041	116 05.17 2.8	714.95 0.49	0.027	17/19
PC-1P*	.79	8.5960 0.0059	12.9183 0.0104	7.1565 0.0057	116 01.22 4.7	714.15 0.71	0.047	19/26
PCN-47P	.785	8.5515 0.0021	12.9744 0.0035	7.1620 0.0016	116 02.52 1.2	713.95 0.22	0.018	23/24
PCS-31P	.78	8.5681 0.0027	12.9651 0.0061	7.1559 0.0019	116 07.41 1.4	713.72 0.33	0.018	15/15
ScC-26P	.81	8.5764 0.0029	12.9631 0.0044	7.1598 0.0030	116 02.70 1.7	715.17 0.31	0.018	16/19
ScC-26G*	.87	8.5901 0.0062	12.9695 0.0083	7.1665 0.0036	115 54.97 3.0	718.11 0.53	0.040	18/18
ScC-35P*	.86	8.5802 0.0050	12.9672 0.0122	7.1744 0.0056	115 59.41 3.3	717.51 0.76	0.029	11/11
TCW-11P	.82	8.5732 0.0033	12.9711 0.0043	7.1607 0.0027	116 01.35 1.7	715.57 0.36	0.022	14/17

N<sub>Or</sub> - Mol fraction  $\text{KAlSi}_3\text{O}_8$ , calculated from the expression  $N_{\text{Or}} = A + BX + CX^2$  (Luth and Querol-Suñe', 1970) using Orville's data (1967) where A, B, C are constants and X is cell volume.

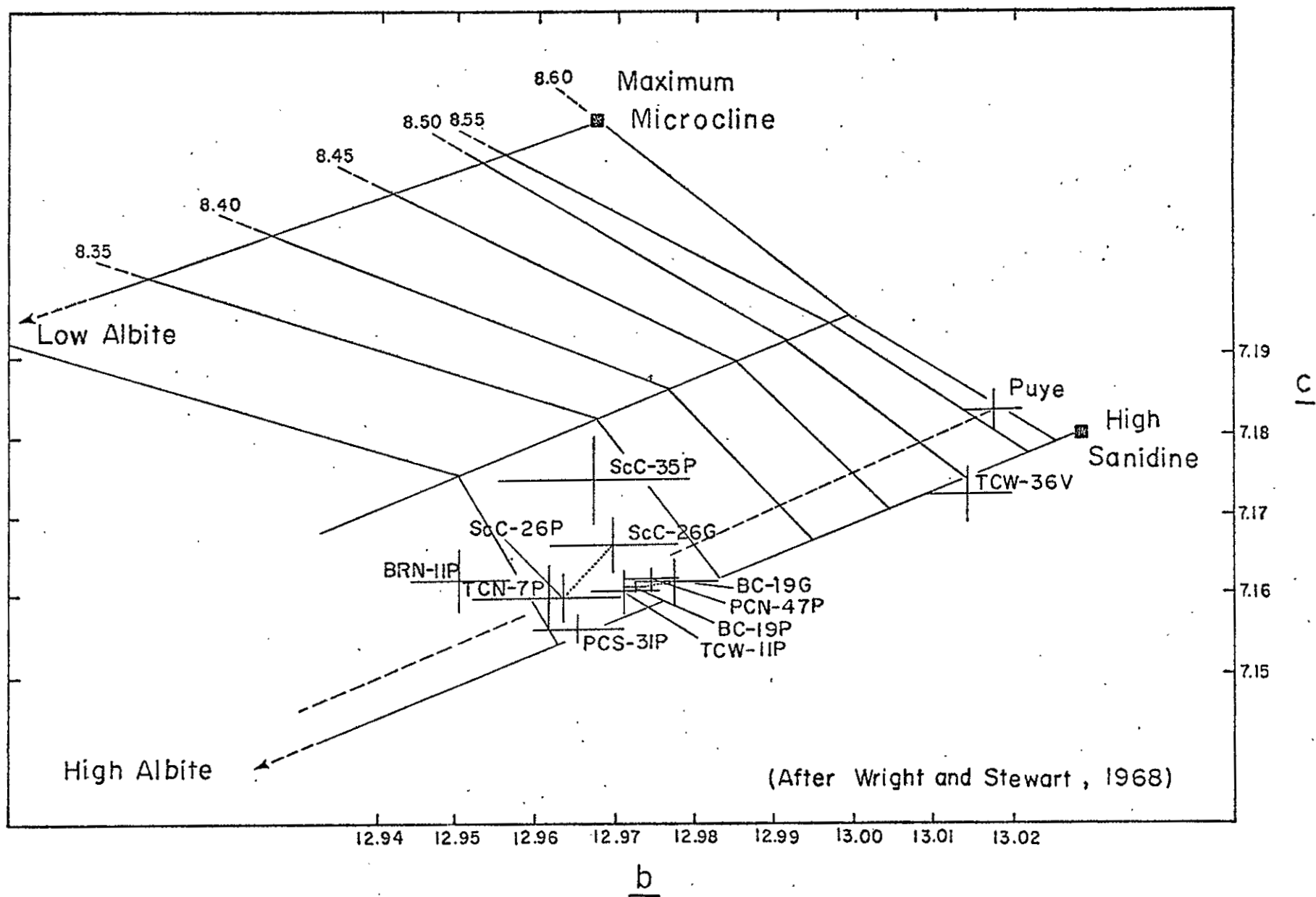
SE - Standard error of observation of unit weight.

Ref - n/m, number of lines used in refinement/number of input diffraction lines.

\* - SE too high for acceptable refinement.



Fig. 37. b-c plot of alkali feldspars, Taylor Creek Rhyolite.



Following the terminology of Wright and Stewart (1968), these feldspars represent the "low sanidine" structural state and are "anomalous" ( $\frac{a}{b}$  refined -  $\frac{a}{b}$  estimated from  $\frac{b}{c}$  plot exceeds  $0.2 \text{ \AA}$ ). Phenocrysts from samples ScC-35 and BRN-11 plot noticeably removed from the cluster, which probably reflects a high standard error (.027-.029) in cell refinement rather than actual differences in structural state.

Plots for four of the phenocryst samples cluster about the K-exchanged series of the Puye sample, a low sanidine from the Bandelier Tuff, Jemez Mountains, New Mexico. Three of these samples, PCN-47, BC-19, and TCW-11, which yield nearly identical cell dimensions, are diverse both in geographical location and rock type. PCN-47 represents phenocrysts from a thin unit of reddish porphyritic vitrophyre in Paramount Canyon, TCW-11 white, argillized rhyolite from the Taylor Creek Prospects, and BC-19 sanidine phenocrysts from a small mass of light gray rhyolite at Beaver Creek (Plate 6), along the western edge of the district.

Cell refinements for two samples of groundmass feldspar, BC-19 and ScC-26, involve a high standard error (.039-.040). It is nevertheless surprising that the groundmass phases are similar in structural state to their associated phenocrysts. During the devitrification of glass, which presumably takes place at lower temperatures than the crystallization temperatures of phenocrysts, one might expect greater Si/Al ordering in the feldspar structure. Yet, experimental devitrification of rhyolitic glass is known to produce alkali feldspar of similarly high structural state. Based on the limited number of samples and the generally poor refinement of the groundmass phases, no firm conclusions can be drawn regarding these similarities.

The b-c cell dimensions of a veinlet alkali feldspar (TCW-36) indicate sanidine that differs from the phenocryst and groundmass feldspars in that it plots on the opposite side of the high sanidine-high albite series, corresponding to the position of the synthetic feldspar series of Luth and Querol-Suñé (1970). Unfortunately, it also has a high standard error of refinement (.039), yet the shift to a slightly higher structural state could be expected for this occurrence, assuming a more rapid growth in a high-temperature, low-pressure gas medium. This feldspar, which is sericitized and associated with hematite, cassiterite, and topaz, probably is more significant from the standpoint of composition than structural state.

#### Composition

The compositions of the unhomogenized, microperthitic phenocrysts discussed above were determined from both refined cell volumes (Table V) and  $\bar{2}01$  reflections from XRD data. Because all feldspars studied were found to be "anomalous," the a-cell dimension cannot be used to accurately determine composition. However, following the suggestion of Wright and Stewart (1968, p. 71), "cell volume. . . is particularly useful in estimating the composition of anomalous phases, on the premise that the atoms occupy the same volume regardless of the configuration of the unit cell." Therefore,  $N_{Or}$ , the mol fraction of  $KAlSi_3O_8$  in the host potassic phase, was calculated from the polynomial expression,  $N_{Or} = -17.261 + 2.03625X + 0.009805X^2$  (Luth and Querol-Suñé, 1970), where  $X$  = unit cell volume. Constants were taken from the work of Orville (1967), and  $N_{Ab}$  (mol fraction of  $NaAlSi_3O_8$ ) of the albitic phase was estimated from Orville's graph

(1967, p. 75). Compositions are nearly identical among the phenocryst phases.  $N_{Or}$  ranges from 78 to 82 percent for the feldspar refinements that are considered reliable. However,  $N_{Or}$  would be expected to decrease by about 10 to 15 mol percent following homogenization. In two samples of groundmass feldspar, BC-19 and ScC-26, the Or content (about 87 percent in each) was found to be higher than that of phenocrysts (79 and 81 percent, respectively) from the same hand samples. Alkali feldspar from one tin-bearing veinlet, similarly, is highly potassic ( $Or \approx 88$  percent).

Compositions also were determined, but less satisfactorily, by X-ray diffraction, using the  $\bar{2}01$  reflection of phenocryst, groundmass, and veinlet feldspars according to the method of Tuttle and Bowen (1958, p. 12). Compositions determined by this method indicate the presence of both potassic and sodic phases in the groundmass also. Errors in estimating Or composition by this method, generally 4 to 11 mol percent higher than in compositions calculated from refined cell volumes, are believed due, in large part, to the lack of sharp, well-defined  $\bar{2}01$  reflections in many samples. Because of this problem, little difference was noted between the orthoclase content of groundmass and that of phenocryst phases, in contrast to results from the cell refinement method. The compositions derived from cell volumes are believed to be more accurate.

#### Discussion

The apparent similarities in composition and structural state among the alkali feldspar phenocrysts from several different localities within the district, representing vitrophyric, devitrified, and other

textures, suggest a similar early compositional and thermal history. Furthermore, the absence of seriate texture of the phenocrysts, and their apparent lack of zoning in thin-section support the notion of intratelluric crystallization within a common magma chamber. Post-emplacement processes, including the devitrification of glass and argillization within the groundmass, appear to have had little effect on the alkali feldspar phenocrysts. The three geographically separate rhyolite masses discussed earlier may well have been derived from the same magma source. This conclusion is further supported by modal analysis of these rocks, and by bulk chemical data discussed farther on. The relatively high structural state of these feldspar phenocrysts is to be expected in a volcanic environment characterized by high temperatures and relatively rapid crystallization, and implies the lack of extensive recrystallization at low to moderate temperatures.

The more potassic composition and apparently high structural state of the groundmass feldspar is unexpected, if in fact these differences are real. During fractional crystallization of a potassic granite melt, alkali feldspar phenocrysts ideally would be more potassic than the liquid from which they are being formed (Tuttle and Bowen, 1958; Carmichael, 1963). Assuming that the liquid was quenched sometime after phenocryst crystallization, the groundmass thus should be more sodic than the phenocrysts, and this difference should be reflected by the compositions of groundmass feldspars formed by devitrification. However, alkali exchange is common in silicic rocks, and it can be expected to alter their original compositions (e.g., Noble, 1965, 1967; Noble, Smith, and Peck, 1967; Orville, 1963).

The presence of sanidine in veinlets, in association with cassiterite, hematite, and topaz, is compatible with the high temperatures inferred for the tin mineralization in miarolitic cavities at Paramount Canyon. Yet, it is recognized that several other variables influence the alkali feldspar ordering and composition, including pressure and chemical environment (e.g., Luth and Tuttle, 1966; Martin, 1969; Luth and Querol-Suñé, 1970). At relatively low pressures and at temperatures above and below the solidus, the vapor phase in equilibrium with granite is depleted in potassium relative to crystallized phases (Luth and Tuttle, 1969). A vapor-deposited feldspar more potassic than phenocryst and groundmass compositions therefore would not be expected if the vapor were in equilibrium with the already-crystallized phases. Of course, a relatively potassic composition might result under non-equilibrium conditions by alkali exchange, perhaps at other times, between vapor and groundmass or phenocryst phases. Orville (1963) has shown that fractionation of alkalis between water vapor and feldspar crystals in the system  $\text{KAlSi}_3\text{O}_8$ - $\text{NaAlSi}_3\text{O}_8$ - $\text{NaCl}$ - $\text{KCl}$ - $\text{H}_2\text{O}$  is strongly dependent upon temperature. And, because the alkali ratio in the vapor phase varies with temperature, a compositional gradient is produced. In experiments conducted at 700°C, 2 kb water pressure, and involving a temperature gradient, Orville found that  $\text{K}^+$  preferentially moved down the temperature gradient, enriching the cool end of the bomb in K-feldspar, while  $\text{Na}^+$  moved to the hot end.

Certainly, a relatively high temperature gradient would exist in a cooling lava flow between the interior and its surface. Therefore, a more potassium-rich feldspar could be expected to precipitate

in veinlets through alkali transfer between vapor and crystallized phases, or magma, provided the rhyolite were vapor-saturated and that the above experimental data can be extrapolated to surface pressures.

## CHEMISTRY OF THE VOLCANIC ROCKS

### General Statement

The results of bulk chemical and trace-element analyses of volcanic rocks sampled in the Taylor Creek area are recorded in Table VI. Norms, based on these analyses and calculated by computer, also are listed. The fourteen analyzed samples represent parts of the three rhyolite masses that were studied; samples from two pyroclastic sections and one andesitic sequence also are included. Some of the individual analyses that are recorded represent several rock samples that were collected on a traverse over a given unit. These samples were homogenized to provide a reasonably representative sample of each unit. Sample locations and traverses are noted on the geologic maps, Plates 2, 5, and 6.

An important objective in the analyses of the rhyolitic rocks was to trace chemical changes that were involved in the bleaching and weak argillization of considerable volumes of rock. Several sample pairs, representing both fresh but devitrified rhyolite and bleached rhyolite equivalents, were obtained from parts of the Boiler Peak and Taylor Creek domes.

TABLE VI

Chemical, normative, and trace-element analyses of volcanic rocks,  
Taylor Creek and Beaver Creek areas, Black Range, New Mexico<sup>1</sup>

Field No. <sup>2</sup>	BC- 11-18	TCW- 28A	TCW- 6-24	A- 15-16	A- 17-18	A- 19-23	A- 13-14	A- 8-12	PC- Cr	A- 1-7	ScC- 23-30	ScC- 34-38	ScC- 300	BC- 203
N.M.B.M. Lab. No.	17237	17234	17236	17225	17223	17226	17231	17227	17229	17228	17235	17232	17230	17224
Sample No.	1	2	3	4	5	6	7	8	9	10	11	12	13	14
SiO <sub>2</sub>	74.8	77.1	75.0	74.4	75.7	76.0	75.2	73.14	73.3	75.5	74.71	75.7	73.76	63.08
Al <sub>2</sub> O <sub>3</sub>	12.4	11.8	11.9	12.0	13.7	12.4	12.8	13.66	12.1	12.5	11.21	12.7	12.69	17.4
TiO <sub>2</sub>	0.17	0.27	0.16	0.17	0.03	0.15	0.15	0.12	0.17	0.15	0.18	0.22	0.15	1.37
Fe <sub>2</sub> O <sub>3</sub>	1.24	1.50	1.47	1.91	1.36	2.06	2.12	1.81	5.02	1.81	1.59	2.10	1.88	4.71
FeO	0.04	0.06	0.04	0.05	0.12	0.07	0.06	0.08	-	0.07	0.05	0.07	0.08	2.05
MnO	0.06	0.05	0.05	0.08	0.05	0.06	0.05	0.07	0.16	0.07	0.04	0.08	0.06	0.09
MgO	0.41	0.33	0.55	1.85	0.62	0.52	0.33	0.33	0.25	0.45	1.07	0.17	1.02	0.98
CaO	0.68	1.31	0.40	1.67	0.49	0.46	0.39	0.95	0.50	0.56	1.05	0.33	2.16	5.13
Na <sub>2</sub> O	3.64	4.43	3.55	2.46	3.65	3.81	4.06	3.93	3.48	3.84	5.05	5.20	2.03	3.66
K <sub>2</sub> O	6.54	4.10	6.40	3.90	3.80	4.10	4.10	4.20	4.60	4.30	4.10	4.50	2.40	2.90
H <sub>2</sub> O	0.10	0.21	0.13	1.14	0.29	0.26	0.18	0.20	0.10	0.12	0.61	0.11	2.81	0.45
P <sub>2</sub> O <sub>5</sub>	0.02	-	0.01	0.01	0.01	-	0.08	0.04	0.04	0.04	0.02	0.01	-	0.02
Total	101.10	101.16	99.66	99.64	99.82	99.89	99.52	98.53	99.72	99.41	99.68	101.19	99.04	101.84



TABLE VI (cont'd.)

## CIPW Norms

Sample No.	1	2	3	4	5	6	7	8	9	10	11	12	13	14
Ns	-	-	-	-	-	-	-	-	-	-	0.62	-	-	-
Q	28.07	33.70	29.64	38.90	37.98	36.38	34.79	31.79	34.12	34.95	29.68	28.49	46.62	13.90
C	-	-	-	0.76	2.19	0.86	1.16	1.02	0.58	0.61	-	-	2.33	-
Or	38.65	24.23	37.82	23.05	22.46	24.23	24.23	24.82	27.18	25.41	24.23	26.59	14.18	17.14
Ab	27.37	37.49	25.58	20.82	30.89	32.24	34.36	33.26	29.45	32.49	34.84	40.27	17.18	30.97
An	-	0.20	-	8.12	2.37	2.28	1.42	4.45	2.22	2.52	-	-	10.72	22.49
Ac	3.02	-	3.93	-	-	-	-	-	-	-	4.60	3.28	-	-
Wo	1.27	2.41	0.72	-	-	-	-	-	-	-	2.01	0.58	-	1.18
En	1.02	0.82	1.37	4.61	1.54	1.29	0.82	0.82	0.62	1.12	2.66	0.42	2.54	2.44
Fs	-	-	-	-	-	-	-	-	-	-	-	-	-	-
Mt	-	-	-	-	0.46	-	-	0.14	0.03	0.02	-	-	0.02	2.93
Ht	0.20	1.50	0.11	1.91	1.04	2.06	2.12	1.71	5.00	1.80	-	0.96	1.87	2.69
Il	0.21	0.23	0.19	0.28	0.06	0.28	0.23	0.23	0.32	0.28	0.19	0.32	0.23	2.60
R	-	-	-	0.02	-	-	0.03	-	-	-	-	-	-	-
Ap	0.05	-	0.02	0.02	0.02	-	0.19	0.09	0.09	0.09	0.05	0.02	-	-
Cc	-	-	-	-	-	-	-	-	-	-	-	-	-	-
Sp	0.14	0.36	0.15	-	-	-	-	-	-	-	0.19	0.13	-	-
Total	100.00	100.95	99.53	98.48	99.00	99.63	98.33	99.34	99.62	99.29	99.07	101.08	96.23	101.39

TABLE VI (cont'd)  
Trace-elements  
(in parts per million)

Sample No.	1	2	3	4	5	6	7	8	9	10	11	12	13	14
Ag(1)	1	2	1	-	-	1	-	-	5	-	4	1	1	-
B(1)	3	1	6	1	3	4	8	15	75	20	5	8	-	-
Be(1)	1	1	1	5	5	2	2	5	2	1	2	3	-	-
Ce(500)	-	-	-	-	-	-	-	-	-	-	-	-	-	-
Co(10)	-	-	-	-	-	-	-	-	-	-	-	-	-	-
Cr(10)	-	-	-	-	-	-	-	-	10	-	-	-	-	-
Cu(.5)	1	1	1	-	1	1	1	-	-	1	1	1	-	-
In(1)	-	10	-	10	5	50	1	10	50	10	10	10	-	-
Nb(5)	35	7	30	-	-	35	35	40	15	100	60	20	-	-
Ni(1)	1	10	3	-	-	10	10	-	-	3	-	-	-	30
Pb(1)	90	10	30	30	10	10	10	30	30	50	30	100	-	1
Re(50)	50	-	-	-	-	-	-	-	750	-	275	300	-	50
Rh(50)	-	-	-	-	-	-	-	-	100	-	50	50	-	-
Sn(3)	-	-	-	-	-	4	4	-	1000	-	10	4	-	-
Sr(5)	-	-	-	300	-	-	-	-	-	-	-	-	300	300
Ta(10)	-	30	-	-	-	-	-	-	10	-	20	275	20	-
V(5)	30	20	30	25	25	30	30	30	30	25	30	30	20	400
W(20)	-	-	-	-	-	-	-	-	-	-	100	-	-	-
Zn(3)	-	-	-	-	-	-	-	-	150	-	-	-	-	-
Zr(10)	60	150	100	70	500	60	60	75	80	100	60	100	35	500

TABLE VI (cont'd.)

<sup>1</sup>Wet chemical and trace-element analyses were performed in the laboratories of the New Mexico Bureau of Mines and Mineral Resources, Socorro; Mrs. Lynn Brandvold, analyst. Trace-element analyses of volcanic rocks are semiquantitative and were determined by emission spectrograph; number in parentheses indicates the lower limit of sensitivity for that element. CIPW norms were calculated by computer, using a program devised by C. Kelsey, U. S. Geological Survey.

<sup>2</sup>Rock sample localities are shown on Plates 2, 4, 5, and 6.

<u>Sample No.</u>	<u>Classification</u>	<u>Description and Locality</u>
1.	rhyolite	Gray, porphyritic rhyolite, with phenocrysts of sanidine and quartz, and minor plagioclase and biotite in a matrix of alkali feldspar and quartz; slightly argillized and porous; Beaver Creek area.
2	rhyolite	Gray, porphyritic, dense; phenocrysts of sanidine and quartz, with minor plagioclase and biotite in a groundmass of alkali feldspar and quartz; Taylor Creek prospects area.
3	rhyolite	Argillized equivalent of #2 (above); white, porous; Taylor Creek prospects area.
4	tuff breccia	Light gray, massive; contains about 10 percent crystals of sanidine and quartz in matrix of glass fragments; Paramount Canyon.
5	vitrophyre	Reddish, porphyritic vitrophyre, with phenocrysts chiefly of sanidine and quartz enclosed in spherulitic glass matrix; Paramount Canyon.
6	rhyolite	Lavender, porphyritic rhyolite; phenocrysts of sanidine and quartz, with minor biotite and plagioclase in a dense matrix of alkali feldspar and quartz; Paramount Canyon.
7	rhyolite	Similar to sample #6; rim of Paramount Canyon.

TABLE VI (cont'd.)

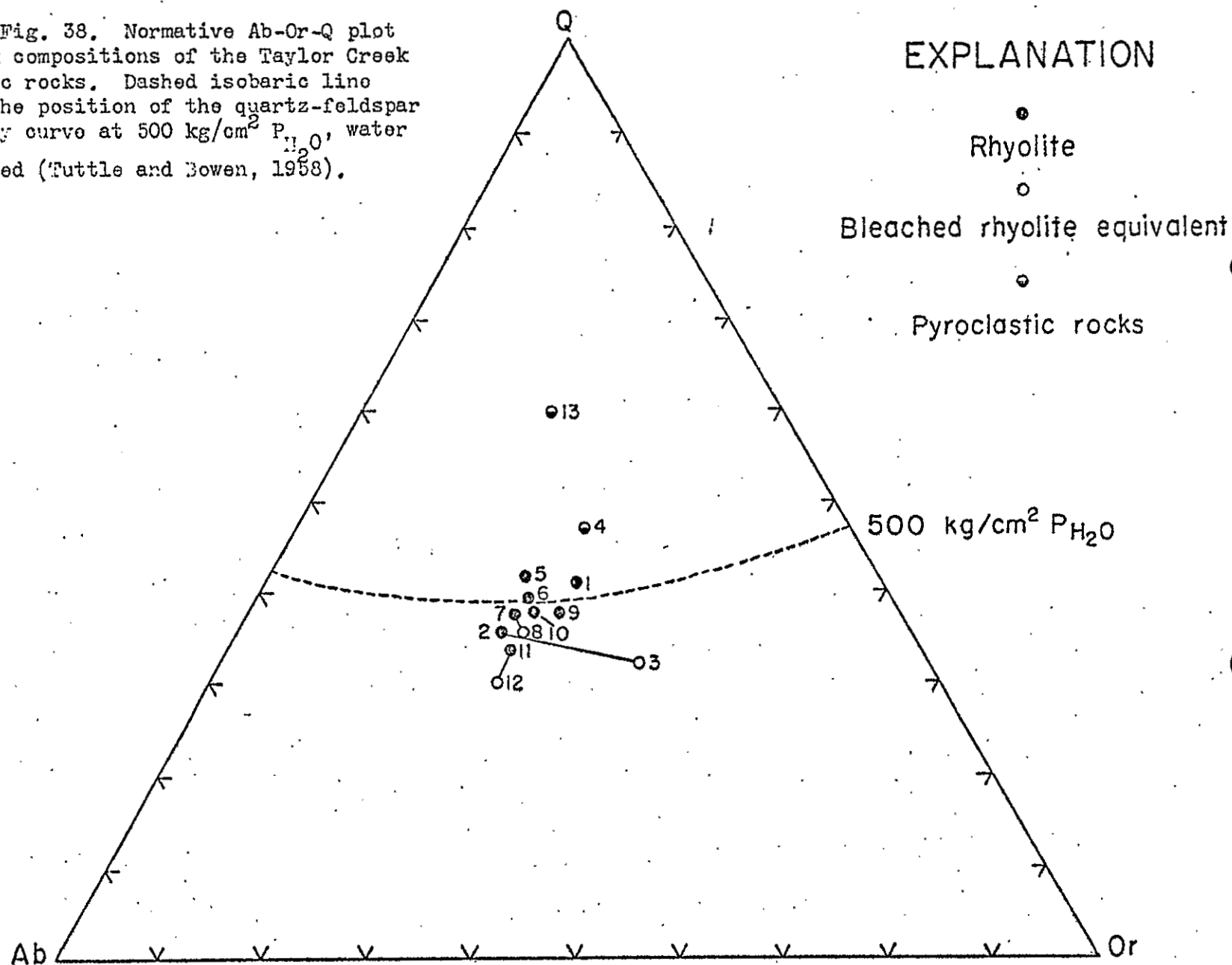
<u>Sample No.</u>	<u>Classification</u>	<u>Description and Locality</u>
8	rhyolite	Bleached and slightly argillized equivalent of sample #7; white, porous and weathers into "honeycomb" pattern; Paramount Canyon.
9	rhyolite	Light gray, microlitic and porphyritic rhyolite, with lithophysal structure; contains megascopic crystals of bixbyite, pseudobrookite, hematite, and cassiterite in cavities; Paramount Canyon.
10	rhyolite	Same as sample #9, without visible oxides in cavities.
11	rhyolite	Lavender, porphyritic rhyolite, with phenocrysts of sanidine and quartz, and minor plagioclase and biotite; dense; Taylor Peak.
12	rhyolite	Bleached equivalent of sample #11; white, porous, and slightly argillized.
13	tuff	White to cream, vitric tuff; contains about 10 percent crystals of sanidine and quartz, friable; east margin of Boiler Peak dome.
14	andesite	Dark gray, dense; contains microphenocrysts of augite and hypersthene; Beaver Creek area.

Major Elements

The Taylor Creek Rhyolite is similar in composition to Nockolds' average alkali rhyolite (Nockolds, 1954). The silica content, about 75 percent, is slightly higher, but alumina, alkalies, and total iron are nearly identical to the average alkali rhyolite. The content of potash commonly is a little higher than soda. A normative Q-Ab-Or plot (Fig. 38) reveals a close similarity among rhyolitic samples of the district, with the exception of the pyroclastic rocks (samples 4 and 13). Samples #2 and 3, 7 and 8, and 11 and 12 are pairs representing fresh and bleached rhyolite equivalents. Samples #3, 8, and 12, all from the bleached rhyolite facies, show an increase in alkalies relative to their fresh rhyolite equivalents. Two of the three samples from the bleached rhyolite show enrichment in normative orthoclase.

In the sample pair, #2-3, there is considerable difference between the two analyses, with #3 highly skewed toward Or compared with the other samples. Some of the differences in analyses, however, may not properly reflect true chemical differences, owing to lack of agreement between some of the samples in the total oxide analysis. For example, in sample #2, the oxides total 101.16, whereas those of #3 total 99.96. By adding the difference, 1.50, to the silica content of #3 and apportioning part of the alkalies, the two analyses become almost identical. Thus, too much numerical emphasis should not be placed on the apparent chemical differences. There is a suggestion from the chemical analyses, however, that alkali enrichment has accompanied the bleaching and argillization processes in the rhyolite.

Fig. 38. Normative Ab-Or-Q plot of bulk compositions of the Taylor Creek volcanic rocks. Dashed isobaric line marks the position of the quartz-feldspar boundary curve at 500 kg/cm<sup>2</sup> P<sub>H<sub>2</sub>O</sub>, water saturated (Tuttle and Bowen, 1958).



In two of the three sample pairs just cited, the enrichment has been more potassic than sodic. Alkali enrichment in the bleached rhyolite might be reflected in the compositions of some of the groundmass and veinlet alkali feldspars previously discussed, or in the formation of the clay minerals.

The sample that probably represents most closely the composition of the rhyolite magma which gave rise to the Boiler Peak dome is a reddish porphyritic vitrophyre, sample #5, from Paramount Canyon. This rock contains an average of 17 percent phenocrysts, principally sanidine and quartz, with accessory plagioclase, biotite, hornblende, and opaques enclosed in a spherulitic glass matrix. The whole-rock analysis, projected onto the anhydrous base in the system Ab-Or-Q-H<sub>2</sub>O (Fig. 38), plots near the thermal minimum, on the quartz side, at 500 kg/cm<sup>2</sup> P<sub>H<sub>2</sub>O</sub>.

Pyroclastic rocks, including tuff breccia from Paramount Canyon and tuffs from the eastern margin of the Boiler Peak dome, differ primarily from the rhyolites in their higher contents of lime and water, and in their lower contents of alkalis. These differences in porous rocks can be partly accounted for by ground-water leaching of alkalis and hydration of pumiceous glass.

The mafic rocks, which are widespread in the northwestern part of the district, were not studied in detail. One sample (#14) from the Beaver Creek-Kemp Mesa area (Plate 6) was analyzed. Its silica content is 63 percent. Following the chemical classification of volcanic rocks used in a study of the Black Range Primitive Area (Ericksen and others, 1970), this rock would be classified as an andesite (58 to 64 percent SiO<sub>2</sub>), however, it is more siliceous than

most andesites. Further detailed study of the dark-colored flows in this general area may well reveal a compositional range from basalt to andesite for the rocks formerly mapped as "basalts" (Fries, 1940).

To determine whether tin-bearing rhyolites might be distinguished from tin-free rhyolites by major element distributions, numerous rhyolite analyses were examined from the published record. Most of these represent rocks from the western United States, but some refer to rhyolites from parts of Mexico, New Zealand, and Iceland. Norms, calculated by computer from these analyses were plotted with those of the New Mexico samples in standard triangular diagrams for Q-Ab+An-Or and Al-Alk-CFM (Figs. 39 and 40).

The best known tin-bearing rhyolites of North America are restricted, geographically, to part of Mexico (primarily in Durango, Zacatecas, and Guanajuato), the Black Range of New Mexico, and northern Nevada (Lander County). All are Tertiary in age. Little is known about possible tin-bearing rhyolites in Canada. One recognized occurrence is the tin deposit at Mt. Pleasant, 22 miles north of St. George, New Brunswick, which is in altered rhyolites and associated pyroclastic rocks. There is some doubt, however, as to the relation of tin mineralization to the rhyolites. "These volcanic rocks have been mapped as Mississippian, but there is some doubt as to their age, consequently as to whether the deposit may be genetically related to the Devonian granite of the region or must be younger. The process of mineralization may be genetically related to the rhyolitic volcanic rocks themselves or intrusive hypabyssal phases. . . ." (Mulligan, 1966, p. 21).



Fig. 39. Normative Q-Ab+An-Or plot of rhyolite analyses.

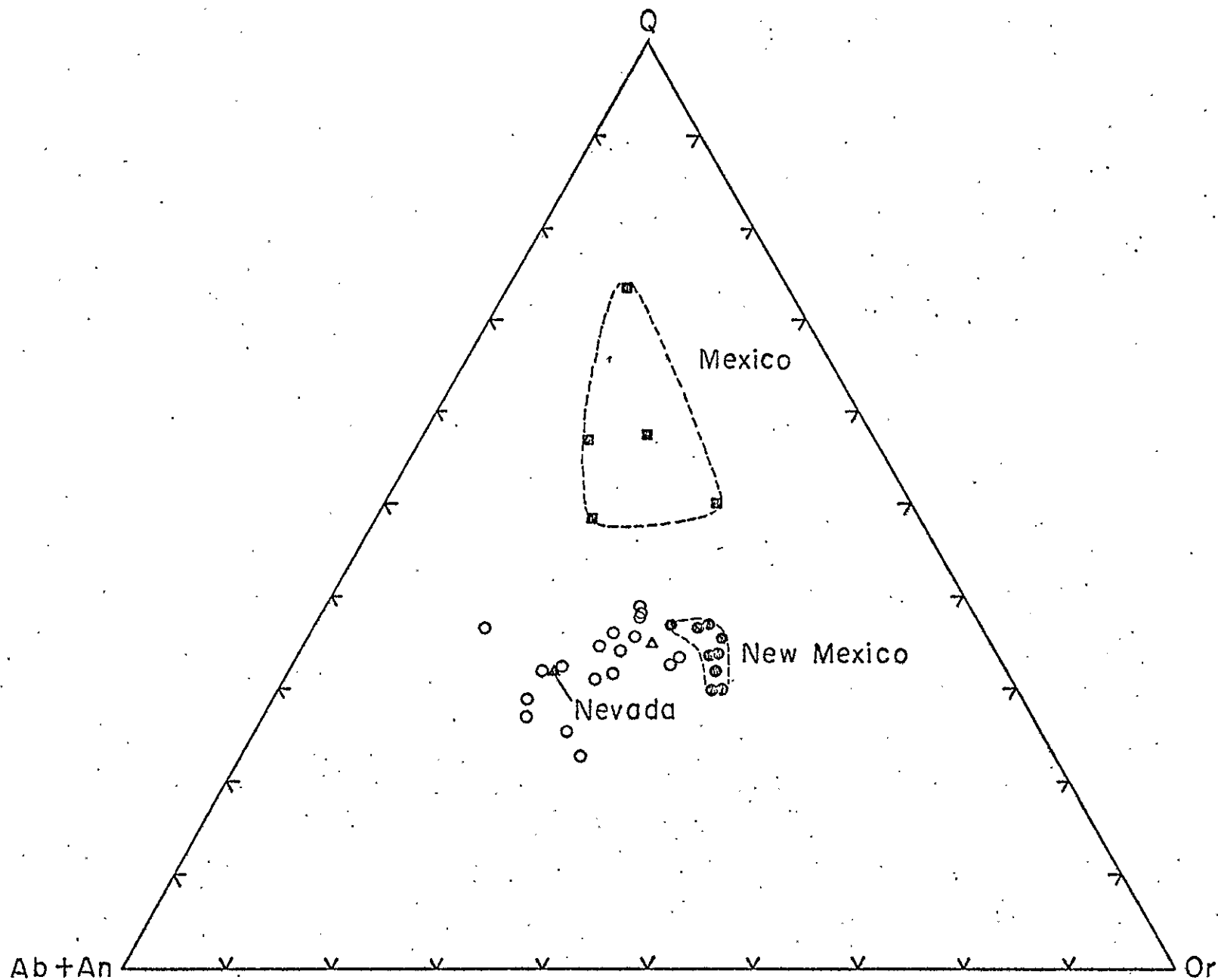
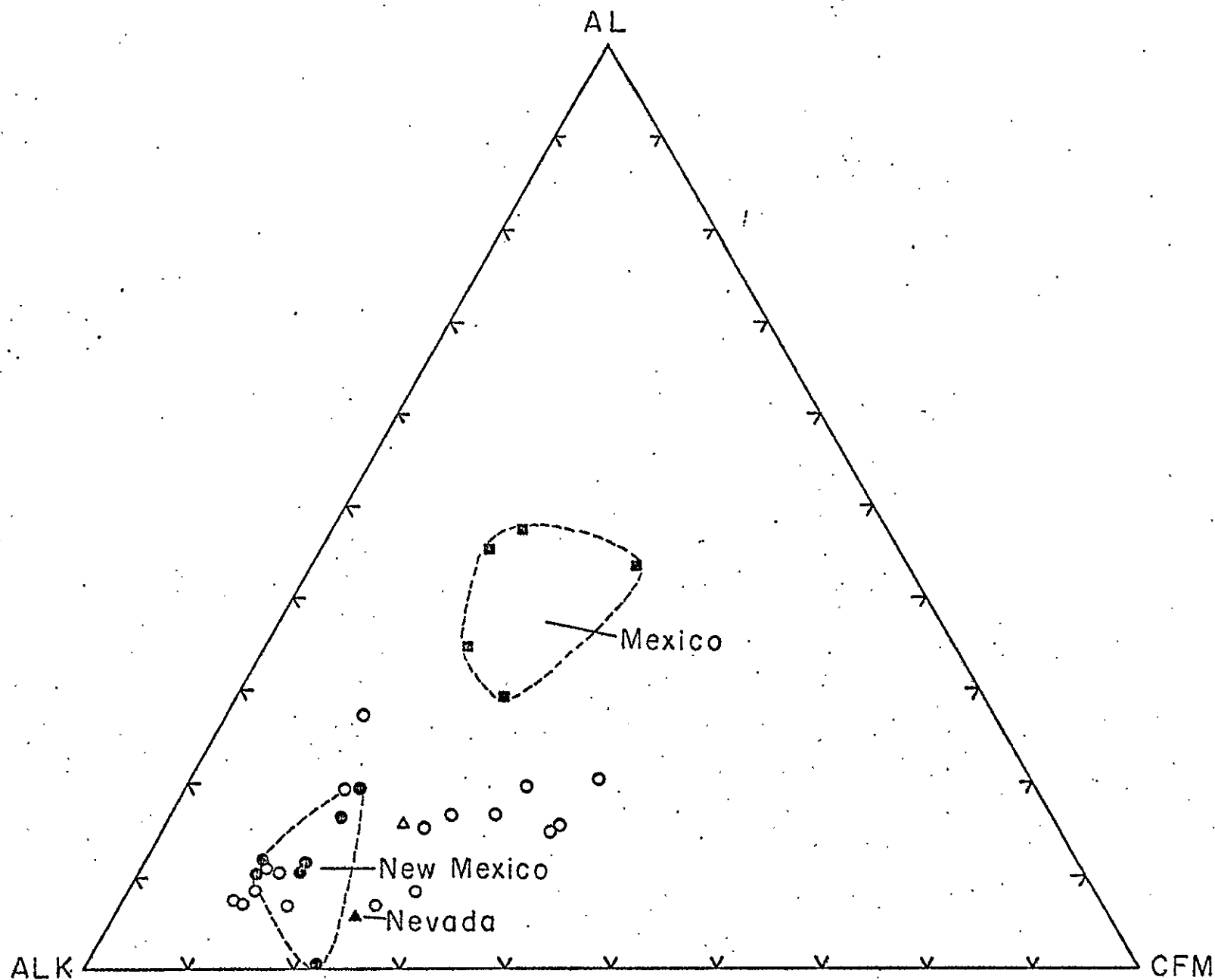


Fig. 40. Normative Al-Alk-CFM plot of rhyolite analyses.



Analyses of the tin-bearing rhyolites here compared include five from Zacatecas, Mexico (J. L. Leo, 1970, written comm.), nine from the Black Range, and one sample collected by the writer in northern Nevada. From Figures 39 and 40, it is clear that no unique composition characterizes these rhyolites. For example, the Mexican rhyolites are unusually high in alumina (about 14 percent), and relatively "low" in alkalis and silica. The general notion that tin-bearing rocks are silica-rich, therefore, is not wholly correct. The compositional skewing of the Mexican rocks toward the normative quartz apex (Fig. 39) is due primarily to a low alkali content (about 5 percent) rather than to a high silica content (average of about 72 percent).

The Taylor Creek Rhyolite and the Nevada "tin-rhyolite" are close in composition to the average alkaline rhyolite, but skewed in opposite directions from this average value.

Since tin of volcanic occurrence is closely associated in space and time with the crystallization of hematite, a plot was made of  $\text{FeO}/\text{FeO} + \text{Fe}_2\text{O}_3$  ratios for the rhyolites discussed above (Fig. 41). These ratios show a wide scatter between 0 and .92. It is interesting to note, however, that the Taylor Creek Rhyolite has the lowest ferrous-ferric iron ratios ( $<.1$ ), much lower than in the average calc-alkaline rhyolite (.37) or alkaline rhyolite (.43). The unusually low iron ratios indicate a more oxidizing environment. The incorporation of the bulk of the iron in hematite, rather than in biotite or amphibole, might possibly be the result of initially high magmatic temperatures which prevented mafic silicates, including biotite and hornblende, from crystallizing in significant amounts, and causing

## EXPLANATION

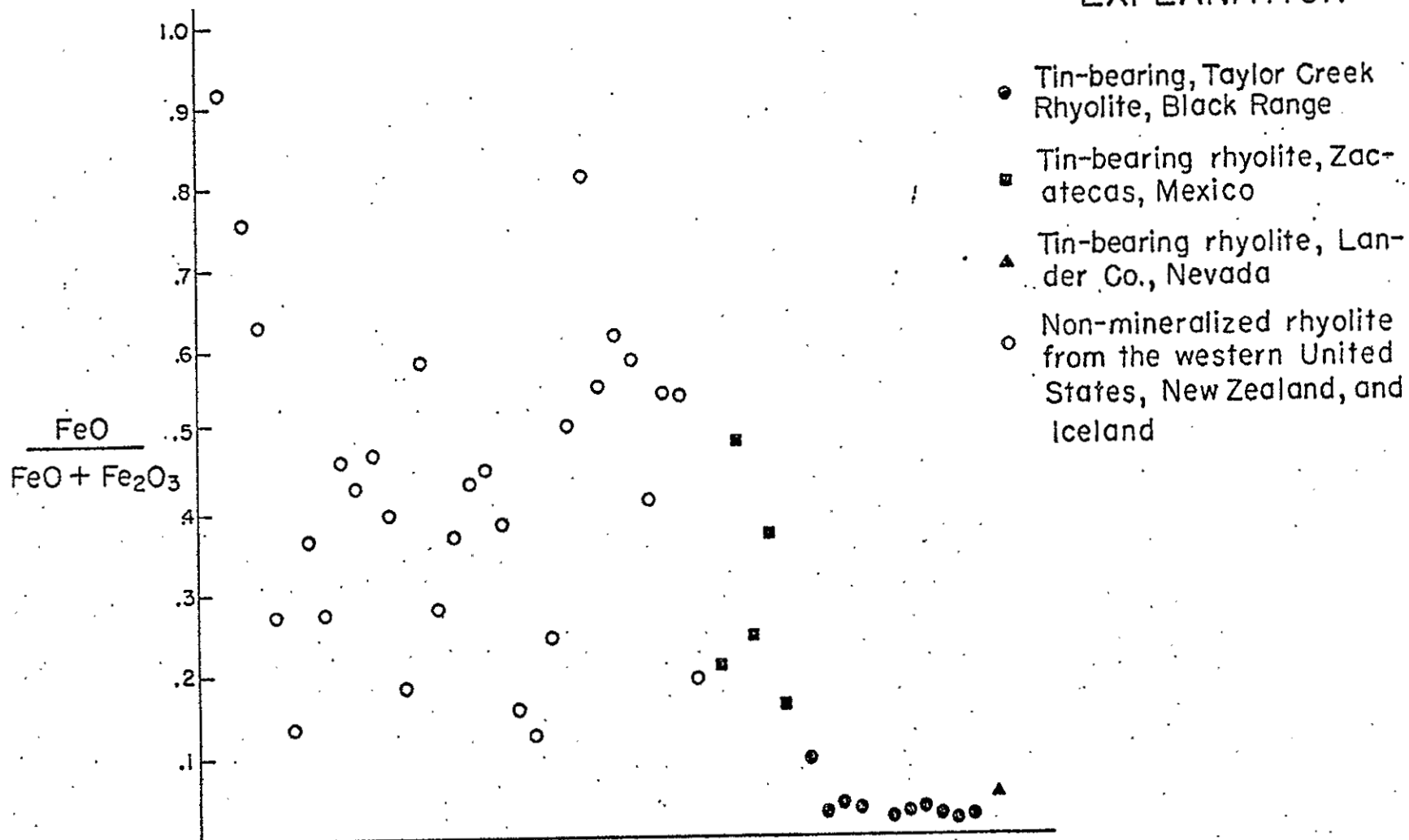


Fig. 41.  $\text{FeO}/\text{FeO} + \text{Fe}_2\text{O}_3$  ratios in some rhyolites.

iron (and other metals) to crystallize as oxides at a later stage when conditions became more oxidizing.

To summarize briefly, the comparison of tin-bearing rhyolites with other rhyolites suggests that no major-element trend uniquely characterizes the tin-bearing rhyolites. The greatest compositional differences can be recognized among the tin-bearing rhyolites themselves, as these rocks range from typically siliceous, alkaline types to much more alumina-rich types.

#### Trace Elements

The results of semiquantitative analyses determined by emission spectrograph for 20 trace elements in the above 14 rocks are recorded in Table VI. When these rocks are compared with rocks of similar bulk composition, no unusual concentrations (except tin locally) or deficiencies of trace elements are apparent.

A traverse extending upward on the northern wall of Paramount Canyon (Plate 2) yielded successive samples of tuff breccia, prophyritic vitrophyre, dense gray porphyritic rhyolite, and light gray microlitic and lithophysal rhyolite. Significantly, the microlitic unit is enriched in Sn, In, B, Pb, Zn, Nb, and Re relative to the other rhyolite facies. Other rare earths, in addition to In, are probably present (but below detection limits) in accessory monazite, which was not found in the other rhyolite units.

Tin was detected in six of eleven rhyolite samples from the Taylor Creek area. The greatest concentration, other than in samples of tin-bearing veinlets, was found in the microlitic rhyolite (0.1 percent Sn, or less), but the tin appears to be concentrated within a

very small part of the unit. For example, Sn was not detected in a traverse including seven samples (A1-A7) over most of this same unit. Other values recorded from bleached, white rhyolite are typically about 4 ppm Sn. Tin was not detected in the vitrophyric rhyolite exposed in Paramount Canyon.

Beryllium, molybdenum, and tungsten, metals associated with many of the world's tin deposits, do not occur in unusual concentrations, although the lower sensitivity limits of the emission spectrograph used in this study for Mo (10 ppm) and W (20 ppm) are well above the concentrations of these metals (about 2 ppm each) normally found in granitic rocks (Taylor, 1964).

Beryllium does not exceed 5 ppm in the rhyolite samples. A somewhat higher concentration, however, was reported from an earlier study; a grab sample obtained by Warner and others (1959) near the U. S. Bureau of Mines adit 1N, Taylor Creek Prospects site, contained 0.002 percent BeO, or about 11 ppm Be. A mean of 3.6 ppm Be has been reported for silicic volcanic glasses of the western United States (Coats and others, 1962).

In the Black Range Primitive Area, immediately south of Taylor Creek, the tin-bearing rhyolite is enriched in beryllium (5 ppm, recorded as the 50th percentile of analyzed samples) and molybdenum (5 ppm) relative to other rhyolites in this part of the Black Range (Ericksen and others, 1970). Contact metamorphic deposits of beryllium and tungsten (Jahns, 1944a, b) are associated with shallow-seated granitic rocks at Iron Mountain in the Sierra Cuchillo, a fault-block range immediately east of the Black Range.

The results of the molybdenum analysis were not considered reliable, and therefore are deleted from Table VI. Tungsten was detected in only one sample of rhyolite.

Regionally, the Black Range is part of the Nacimientos subprovince of Coats and others (1963), in which the volcanic rocks are enriched in tin and fluorine relative to those of adjacent provinces (Fig. 42). Average values for the Nacimientos subprovince (Table VII) indicate that Sn is slightly enriched relative to the Rio Grande subprovince and 3 times that of the Mohave subprovince. Scatter diagrams for each province (Figs. 43, 44, and 45) indicate that there is some correlation between Sn and F within the Nacimientos subprovince, but that no apparent correlation exists for the other two subprovinces (R. R. Coats, 1970, pers. comm.). Most of the samples analyzed in the present study fall below the Sn mean (13 ppm) reported by Coats for silicic glasses in this subprovince. Reasons for this discrepancy, other than sampling or analytical error, are not immediately clear. Fluorine determinations were not made in this study.

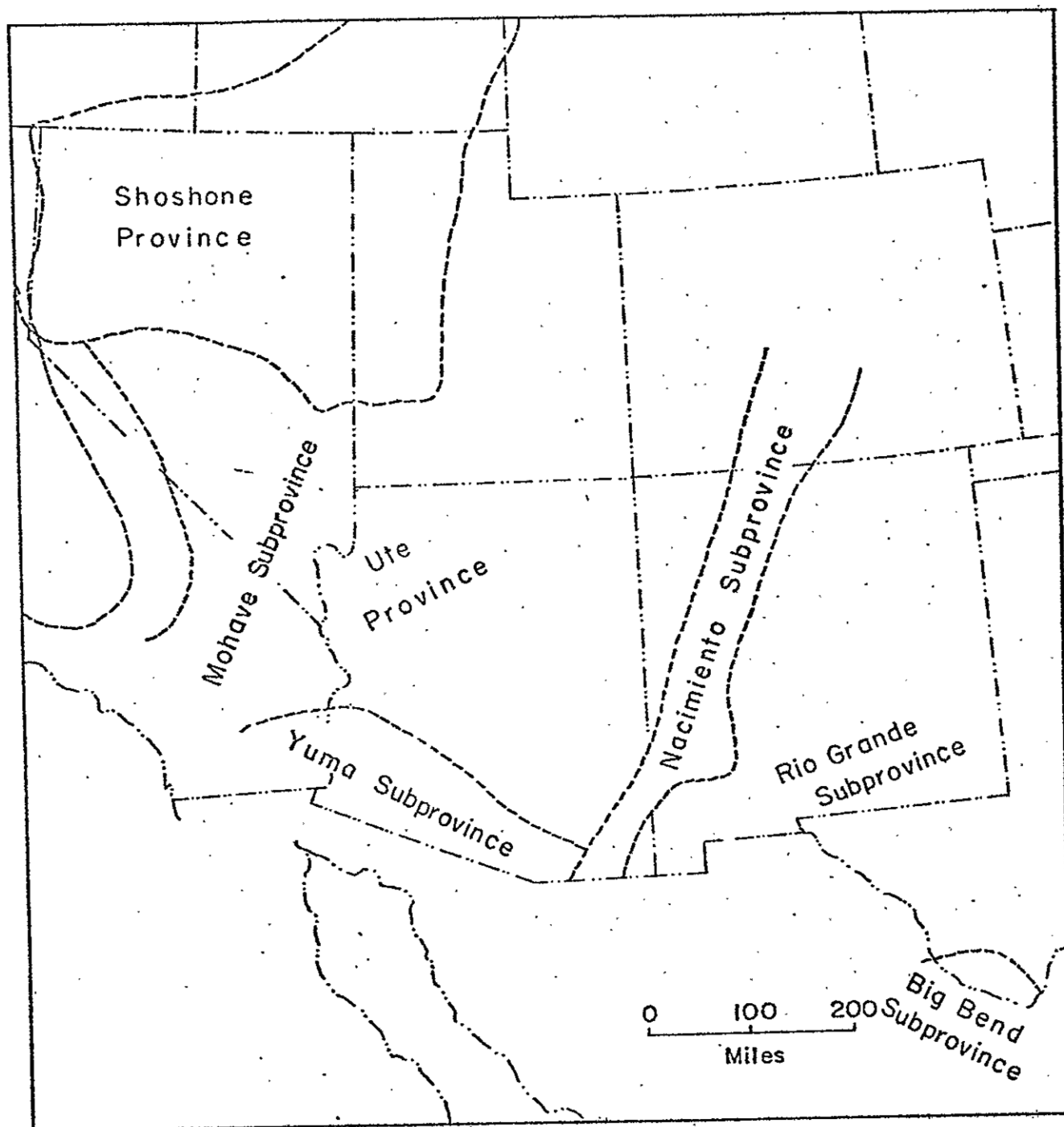


Fig. 42. Volcanic provinces of the western United States.  
After Coats and others, 1963.



TABLE VII

Spectrographic analyses for F and Sn in hypohyaline  
Cenozoic silicic volcanic rocks from the southwestern United States.  
Data are from R. R. Coats (1970, pers. comm.).

<u>Nacimiento</u>		<u>Rio Grande</u>		<u>Mohave</u>	
<u>Sn</u>	<u>F</u>	<u>Sn</u>	<u>F</u>	<u>Sn</u>	<u>F</u>
6	650	20	500	20	400
6	1300	10	150	0	420
9	1300	10	500	0	440
10	2100	7	300	0	545
10	3400	7	325	0	560
20	3700	6	200	0	580
20	4000	5	125	0	760
20	4000	5	300	4	230
30	4000	5	1700	4	350
0	1500	0	850	4	700
				5	420
				7	500
				6	560
				8	400

## Nacimiento Subprovince

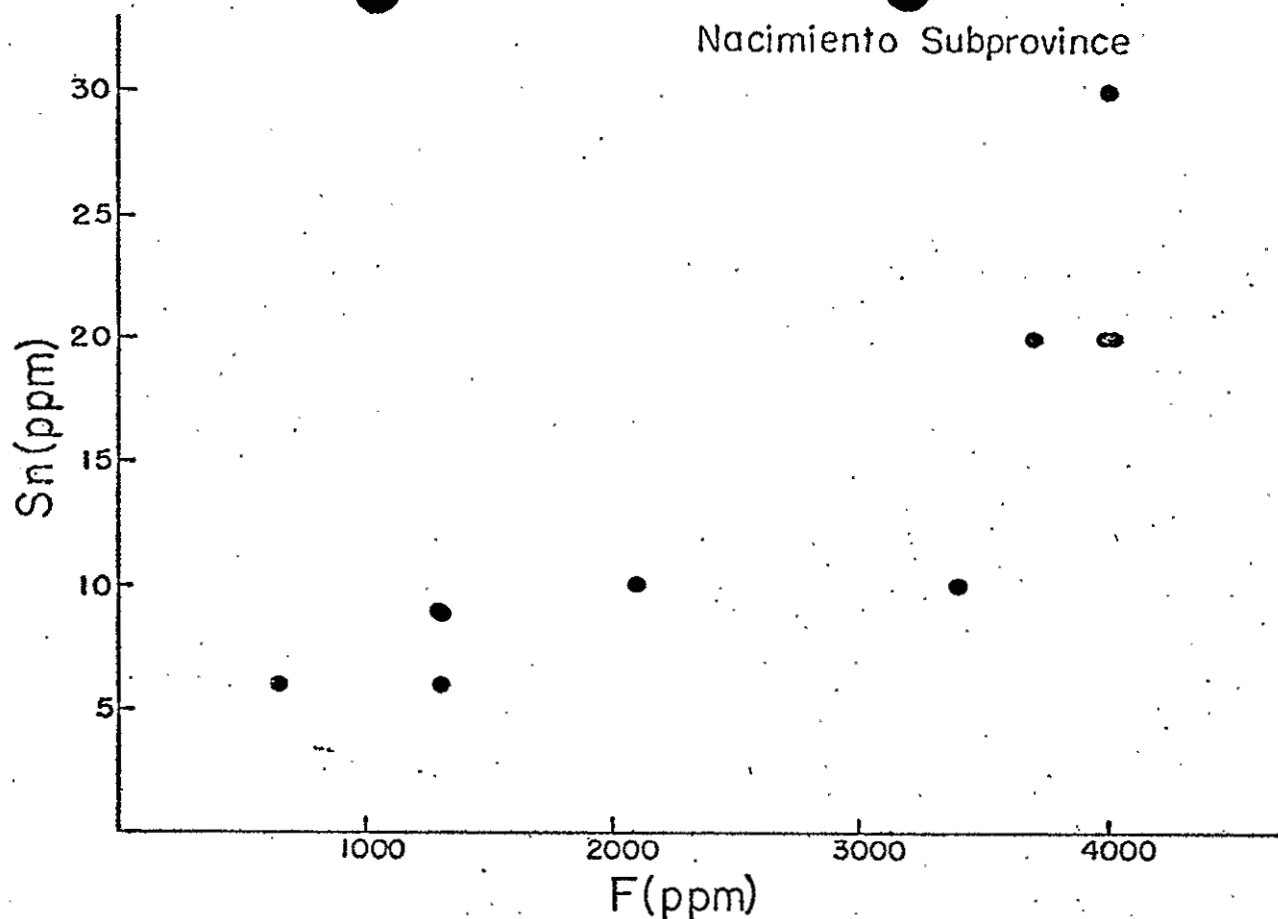


Fig. 43. Plot of Sn versus F for Cenozoic hypohyaline silicic volcanic rocks from the Nacimiento Subprovince. Data from R. R. Coats, 1970, personal communication.

## Rio Grande Subprovince

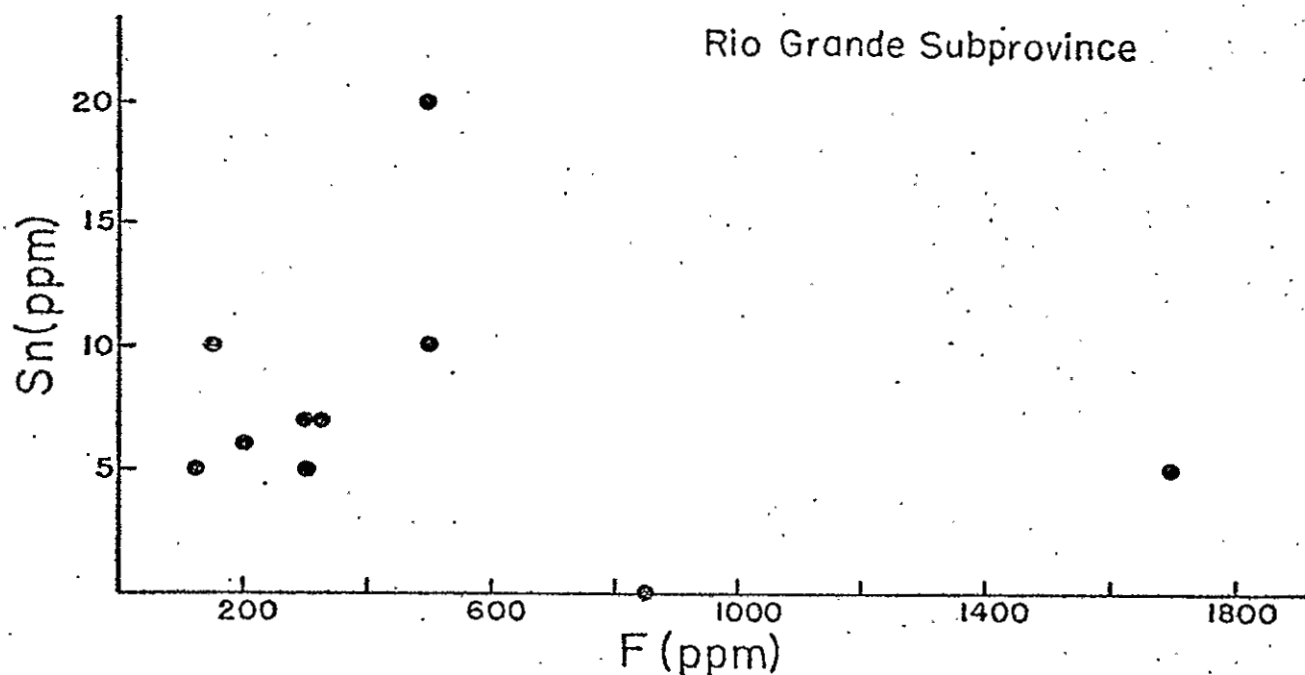


Fig. 44. Plot of Sn versus F for Cenozoic hypohyaline silicic volcanic rocks from the Rio Grande Subprovince. Data from R. R. Coates, 1970, personal communication.

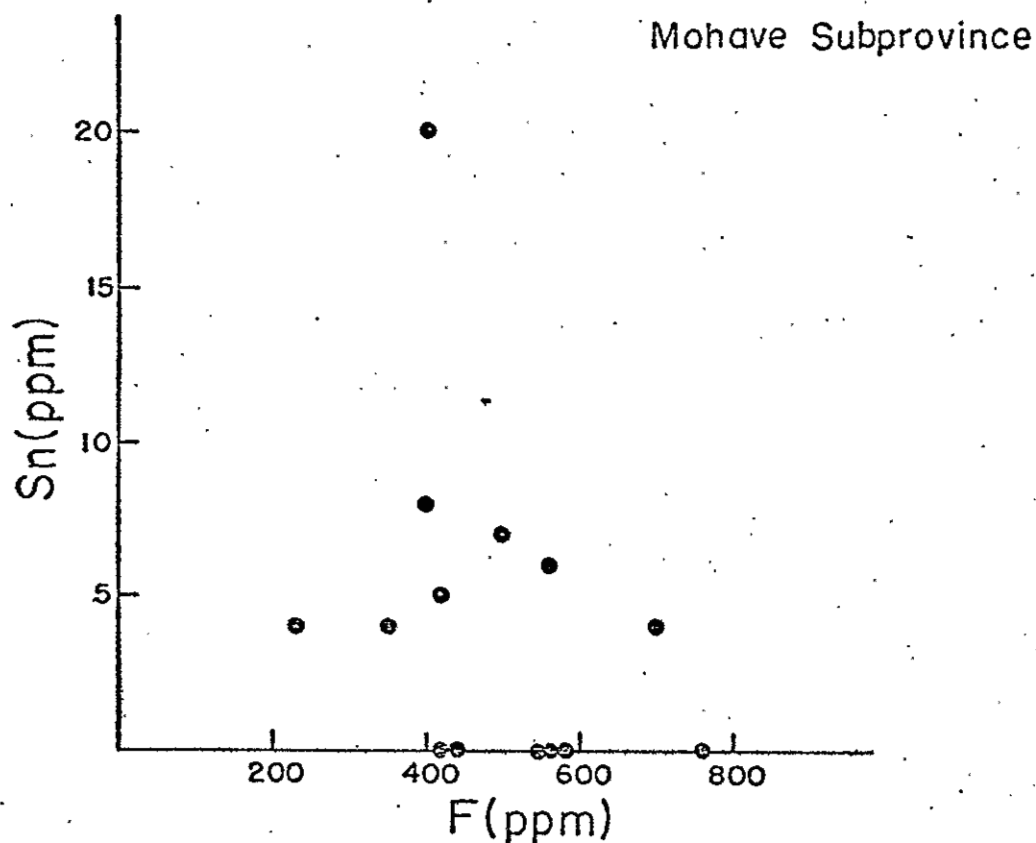


Fig. 45. Plot of Sn versus F for hypohyaline silicic volcanic rocks from the Mohave Subprovince. Data from R. R. Coates, 1970, personal communication.

## APPENDIX

### TIN-BEARING NUGGETS

#### Introduction

During the course of this study, several tin-bearing nuggets were collected from placer deposits and were analyzed for their tin content. Two of them also were analyzed for their contents of trace elements. Data gathered from this satellite study could not be readily integrated with the foregoing report, hence they are presented here as an Appendix.

Wood-tin, the colloform or layered variety of finely crystalline cassiterite, has long been of interest to the miner and mineral collector. Such cassiterite is particularly interesting because of its high specific gravity and the unusual, delicate textures and variety of colors it displays. Few details are known, however, concerning its origin or mode of crystallization, as the material is found chiefly in placer accumulations. Most of the prospecting in the Black Range district has been directed toward recovery of this type of tin.

Tin-bearing nuggets, including fragments of non-colloform cassiterite as well as the wood-tin, were sampled from two localities in the Taylor Creek area. At one of these localities, jig concentrates were obtained from an old tin mill, now dismantled, at the head of Sawmill Canyon south of State Highway 59 (northeast corner

of Plate 2). The other locality is in a bulldozed arroyo adjacent to the Bellamy cabin on Harcastle Creek north of Highway 59.

Most of the nuggets are two centimeters or less in diameter, but some are known to be fist-sized or even larger. Six representative specimens are pictured in Figure 46a for comparison. Nuggets #1, 2, 5, and 6 were obtained from the vicinity of Sawmill Canyon and the others were collected from Harcastle Creek. The external forms of the wood-tin are almost invariably botryoidal, or nodular, which reflects the growth and internal texture of the material. Considerable variations in density, color, texture, and mineralogy characterize these specimens. All are believed to have been derived from cassiterite-hematite veinlets within the Taylor Creek Rhyolite, and to have been concentrated by alluvial and eluvial processes. Typical groundmass rhyolite was found attached to one of the specimens (#1, Fig. 46a). It is noteworthy that the cassiterite-hematite veinlets exposed in the district contain only megascopic crystals of cassiterite and hematite, rather than the colloform varieties typical of the placer accumulations.

#### Mineralogy and Texture

The tin-bearing nuggets exhibit three basic textures, or combinations thereof: a) colloform, or layered, b) non-colloform crystalline, and c) pseudomorphic. Nuggets featuring colloform textures (wood-tin) are the most common. They are varicolored and include two principal mineralogical varieties. One is a layered aggregate of microcrystalline cassiterite and hematite, olive-green to dark brown in color (#4). In polished section and in thin-section

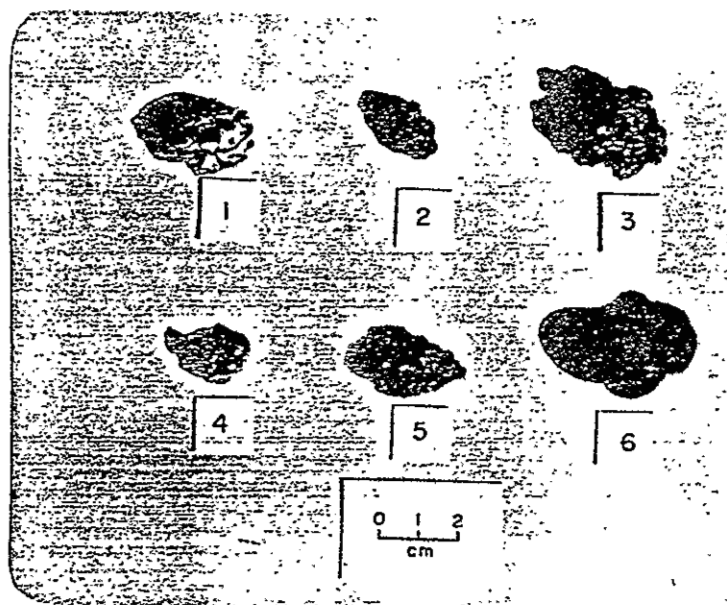


Fig. 46a. Representative specimens of tin-bearing nuggets collected in the Taylor Creek district.



Fig. 46b. Colloform texture in a typical tin nugget. Note radial 'syneresis' cracks. Nugget #4, polished section, 115x.

(Fig. 46b), the colloform texture extends throughout the nugget.

Each concentric layer is distinct from that adjacent to it, both in color and, to a lesser extent, in crystal size. Individual, acicular crystals of cassiterite are arranged normal to the concentric layering, but they generally do not extend through the full width of individual layers. Many nuggets include multiple nucleus-like areas, some of which envelop grains of hematite. Other colloform nuggets have dense, opaque cores of high tin content that are mantled primarily by silica polymorphs. In specimen #1, the nugget core is rimmed by a thin layer of fibrous cristobalite (lussatite?) and minor tridymite, which evidently were deposited against the wall of a fracture in rhyolite; some of this rhyolite remains as a coating on the cristobalite.

In other occurrences, both colloform and non-colloform textures are present in the same nugget. For example, in specimen #2, the core consists of radial plates of hematite that are mantled by colloform cassiterite. The outer rim consists of interlocking crystals of cassiterite; these are relatively large, and in size they resemble those exposed in the cassiterite-hematite veinlets.

A feature characteristic of the wood-tin is the development of radial cracks that are slightly curvilinear. These discontinuities have been referred to as syneresis, or shrinkage cracks in allusion to a colloidal origin. Some cracks intersect the surfaces of nuggets, whereas others begin in the core regions and die out before reaching the surfaces. The crystals within the layers have nowhere been seen to transect these cracks, indicating that the cracks are relatively younger features.

Nuggets that are entirely crystalline but non-colloform are largely hematitic. These hematite nuggets are fine- to coarsely-crystalline aggregates of interlocking specularite plates, with some intermixed silica.

Pseudomorph textures are relatively rare. In one specimen (#5), hematite was found to be pseudomorphic after magnetite, which features intergrown octahedrons, 1 cm or less in maximum dimension. The magnetite has been completely replaced by interlocking blades of hematite.

Some of the characteristic features of the colloform texture, such as the radial growth of cassiterite micro-crystals across color bands, can be explained by recrystallization of a previously laminated fabric that originally might have been cryptocrystalline, or noncrystalline. Following this assumption, the color banding is interpreted as a relict depositional feature, not the result of Liesegang diffusion after crystal growth. The coarser-grained cassiterite layers are nearly colorless, suggesting that the color pigment was removed during recrystallization, a situation commonly observed in the devitrification of volcanic glass to form spherulites. During recrystallization, the formerly cryptocrystalline, or noncrystalline tin oxide would be expected to enlarge outward and cut across the color layers. If the crystals were deposited in successive shells as crystals, the color bands should conform to the crystal layers, and the orientation of these crystals most likely would be irregular, as observed in the lode veinlets.

The fact that the radial cracks do not transect individual micro-crystals suggests that these cracks are relatively younger



features. Such radial cracks have been cited as evidence for shrinkage, or dehydration. It is known, for example, that silica gel produced in the laboratory changes to a chalcedonylike material and that the gel "undergoes a progressive volume reduction caused by the loss of water and develops characteristic shrinkage cracks" (Park and MacDiarmid, 1970, p. 133). Whether or not they are shrinkage phenomena, these cracks most likely formed when the material was nearly solid, and served as boundary surfaces beyond which the crystals could not grow.

The development of multiple nuclei within the colloform texture, but apparently unrelated in some places to the main laminar pattern, is difficult to explain from the standpoint of sequential deposition and/or diffusion phenomena. These growth nuclei are similar in some respects to devitrification spherulites observed in volcanic rocks, such as rhyolite and obsidian.

#### Composition

Chemical analyses made on the above samples range from nearly pure  $\text{Fe}_2\text{O}_3$  to pure  $\text{SnO}_2$ , with no apparent gradation between samples in the range from approximately 0 to 68 weight percent  $\text{SnO}_2$ . Stepped microprobe traverses, spaced 10 to 20 microns apart, were made across several nuggets to analyze for variations in tin. Compositional ranges for these nuggets are recorded in Table VIII. The tin content appears to be uniform from core to rim of the individual nuggets. Where recognizable, sympathetic relations within individual nuggets between the contents of tin and iron are more common than antipathetic.

TABLE VIII

Tin analyses and specific gravities of selected tin-bearing nuggets from the Black Range, New Mexico

Nugget	S.G. <sup>1</sup>	SnO <sub>2</sub> content, in weight percent <sup>2</sup>	
		Range	Mean
1	4.34	58.1- 76.9	68.1
2	6.20	97.7-100	98.9
3	5.68	84.2- 89.9	87.3
4	6.36	83.7- 95.6	88.8
5	4.61	---	---
6	4.81	---	~0.2

<sup>1</sup>Specific gravities were determined by using the Kerr balance at 23°C. Values obtained are believed to be accurate to two decimal places.

<sup>2</sup>Tin analyses were made on an Applied Research Laboratories EMX-SM electron microprobe by Dr. Charles M. Taylor, Stanford University, using high-purity cassiterite as a standard. Instrumental errors were corrected, but no matrix corrections were applied.

As expected, the more coarsely crystalline, red cassiterite (#2, Fig. 46a) is richest in tin content (average ~99 percent SnO<sub>2</sub>), showing little variation from core to rim of the nugget. Of the colloform varieties, specimen #4 has the highest content of tin (~89 percent SnO<sub>2</sub>). The yellow to pale-green layers, present in both the core and the rim areas, appear to be richest in tin. The greatest variation in tin content was noted in the silica-coated nuggets (about 19 percent SnO<sub>2</sub> range for #1). The nuggets of crystalline hematite were found to be almost devoid of tin (about 0.2 percent SnO<sub>2</sub> or less).

A spectral scan was made on a part of nugget #4. The field of view, 260 microns in diameter, included a small nucleus and the outer

part of a larger one. In addition to Sn, the following ten elements were detected: Si, Al, Sb, As, Cl, Fe, Pb, Zn, Ag, and S. Electron photographs were taken to show the distribution of several of these elements (Fig. 47). Except for Ag and S, the detected elements serve to delineate the colloform texture. Silicon and antimony are both concentrated within the nuclei, and also are disseminated outside these areas. Antimony, however, shows a more uniform concentration within the nuclei. As, Pb, Zn, and Cl are concentrated outside the nuclei areas. Their distributions are similar, differing chiefly in intensity. Ag and S are spatially unassociated, and they do not appear to be concentrated in any one area of the nugget.

It is not known whether or not any of these elements, whose concentrations are largely in trace quantities, are chemically combined. The paucity of sulfur and its distribution suggest that the presence of sulfide minerals is negligible. The distribution of Pb, Zn, Cl, and As makes it possible that there may be chemical bonding to form chloride and/or arsenide compounds of Pb and Zn. Antimony, on the other hand, probably is not combined with As, but may be present as an oxide or in native form.

#### Specific Gravity

Specific gravities of the above six nuggets were determined by means of the Kerr balance, and are recorded in Table VIII and in Figure 48. This was done to check an assumption that, since cassiterite (6.8-7.1) is heavier than hematite (5.2-5.25), specific gravity should reflect tin content, if the nuggets are primarily

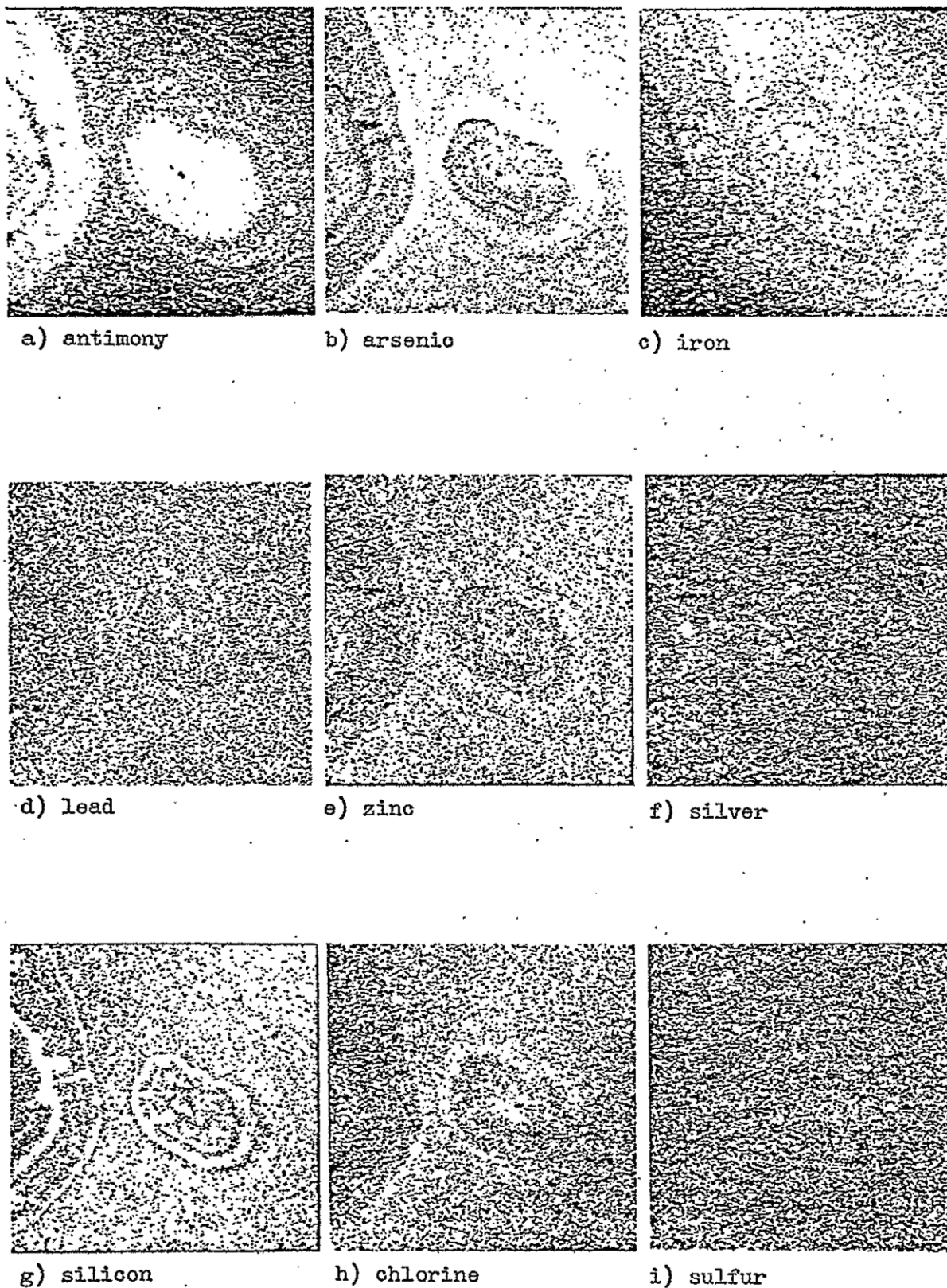
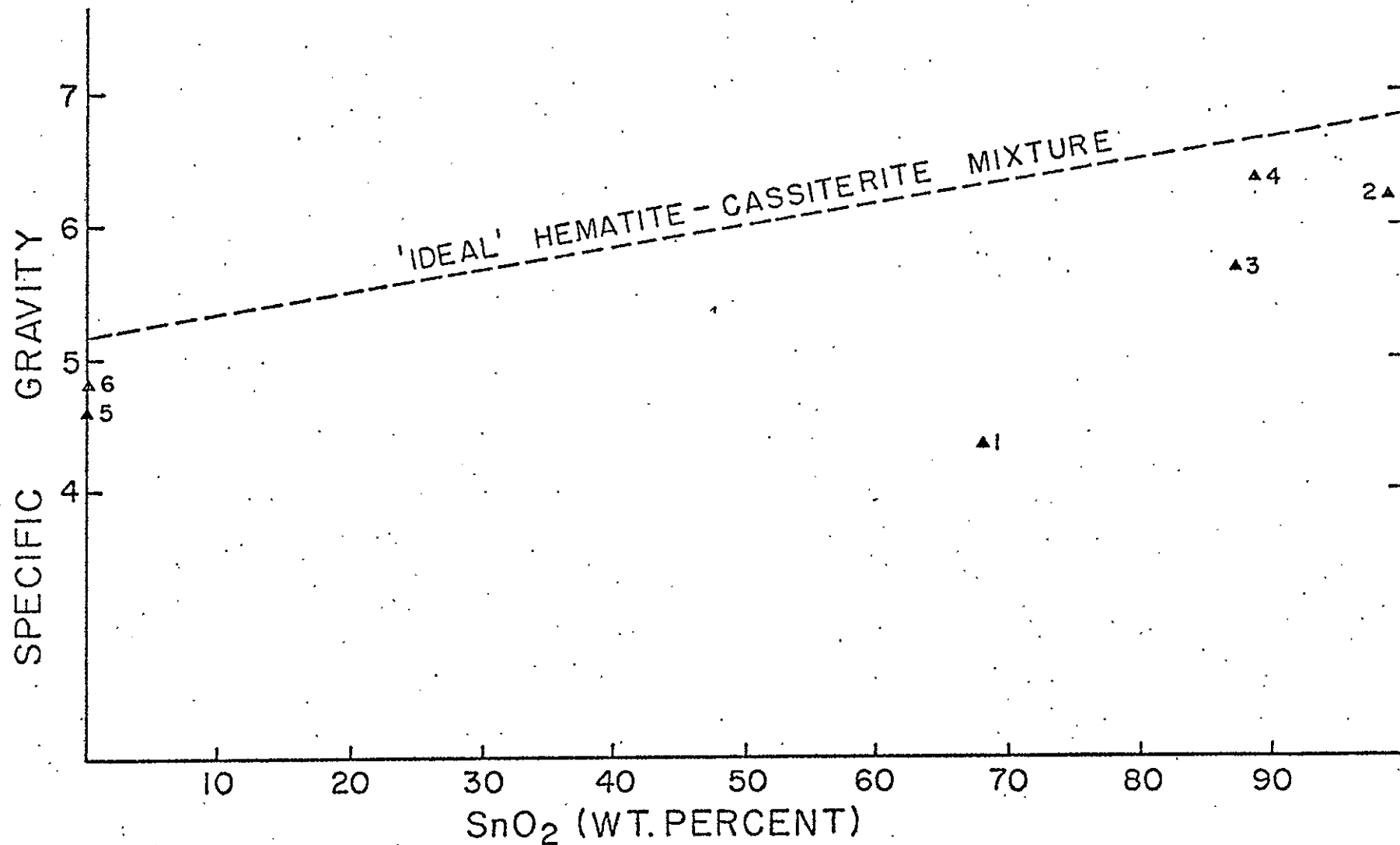


Fig. 47. Electron probe scanning images, showing the distribution of several elements in wood-tin (specimen #4, Fig. 46). Field diameter of each image is 260 microns.

Fig. 48. Plot of specific gravity versus tin content for the tin-bearing nuggets pictured in Fig. 46.



hematite-cassiterite mixtures as indicated under the reflecting and polarizing microscopes.

The nuggets were found to range in S.G. from 4.34 to 6.36, and in tin content from about 0.2 to 99 percent. The specific gravities plotted in Figure 48 clearly do not support the ideal hematite-cassiterite mixture concept, but in a general way, nuggets #2, 3, 5, and 6 conform to the basic assumption. Between nuggets #1 and 6, there is a compositional difference of 68 percent  $\text{SnO}_2$ , but the nugget with the higher tin content has the lower S.G. Departures from the ideal case are best explained by the presence of less dense impurities and differences in internal porosity. Silica and other impurities commonly are present in wood-tin, and these tend to lower the S.G. Further, voids generally are created when specular hematite plates are intergrown, producing a similar effect, particularly within the nugget interiors.

#### Speculations on Mode of Origin

The tin-bearing nuggets are not found in situ, but occur as alluvial and eluvial placer accumulations on top of, and marginal to the rhyolite domes. No tin in the district has been found in rocks younger than the Taylor Creek Rhyolite, including the Gila Conglomerate and the intermediate to mafic volcanic rocks. The distribution of the tin nuggets, as well as the surface coatings of typical rhyolite on some of the nuggets, suggest that the nuggets were derived from the Taylor Creek Rhyolite. The fact that most of the recoverable tin in the placer accumulations is wood-tin, rather than the more coarsely crystalline red cassiterite found in the lode veinlets seems to indi-

cate further that the wood-tin formed in the upper parts of veinlets, which were subsequently removed when the tops of the rhyolite domes were eroded.

The origin of wood-tin nuggets has long been attributed to low-temperature, near-surface phenomena (e.g., Park and MacDiarmid, 1970; Edwards, 1954). The colloform texture is commonly thought to be a result of deposition from colloidal solutions, although "the part played by colloids in ore deposition is poorly understood. . . ." (Park and MacDiarmid, 1970, p. 134). Support for a colloidal origin has been derived, in part, from the study of laboratory gels, which rather faithfully duplicate the banding observed in natural materials. Further, opal and chalcedony, commonly associated with wood-tin, have been produced from synthetic gels at room temperatures. One of the first proponents for the colloidal origin of wood-tin was Knopf (1916, p. 658), who interpreted the "broken ring-like forms" as having "resulted from the bursting of colloidal membranes by osmotic forces."

Recent study (e.g., Roedder, 1968) has largely discredited a colloidal origin for most colloform textures observed in ore samples. Roedder has commented (p. 468) that "the dominant parameter controlling the formation of 'colloform' textures is a relatively high degree of supersaturation, resulting in relatively high rates of nucleation and crystallization." No statement was made, however, regarding the effect of temperature on colloform growth.

Although the colloidal theory has lost much contemporary support, low temperatures for the growth of colloform cassiterite are still advocated. In discussing the tin deposits of Durango, Mexico, Ypma and Simons (1969, p. 12) postulated temperatures of formation of 120°C

and lower: "The extremely delicate banding of the reniform wood-tin and associated chalcedony points to minute adjustments to periodic changes in temperature and chemical composition of the ore-bearing fluid. . . . The colloform textures result from supersaturation; a condition that cannot conceivably be maintained through numerous minor adjustments at high temperatures and (fast reaction rates)." The presence of native bismuth, antimony oxides (?), and lead arsenate were cited as additional evidence for a low-temperature origin. Native bismuth, however, is also found in high-temperature deposits. Mineralogically and texturally, the Black Range wood-tin is similar to that found in Mexico, Nevada, and probably elsewhere, although cristobalite appears to be more common than chalcedony and bismuth has not been detected in the tin-bearing nuggets.

It seems possible that the relatively high rate of nucleation and crystallization necessary to produce colloform textures can also be achieved at higher temperatures, under conditions involving temperature gradients, rather than just low temperatures. Further, the presence of trace amounts of antimony and arsenic (not as sulfides) does not necessarily restrict the temperature range, although antimony sulfides are incompatible with high temperatures. From the published record, it is apparent that the elucidation of variables that control colloform growth is clearly needed, including temperature as an independent variable. Furthermore, if the tin is transported as a colloid at low temperatures, the colloform textures of wood-tin should be reproducible in the laboratory.



# REFERENCES

- Akimoto, S., Nagata, T., and Katsura, T., 1957, The  $\text{TiFe}_2\text{O}_5$ - $\text{Ti}_2\text{FeO}_5$  solid solution series: *Nature*, v. 179, p. 37-38.
- Batley, M. H., 1966, The "Two-magma theory" and the origin of ignimbrites: *Bull. Volcanol.*, v. 29, p. 407-424.
- Buddington, A. F., and Lindsley, D. H., 1964, Oxide minerals and synthetic equivalents: *Jour. Petrol.*, v. 5, p. 310-337.
- Borg, I. Y., and Smith, D. K., 1969, Calculated powder patterns. Part II. Six potassium feldspars and barium feldspar: *Amer. Mineral.*, v. 54, p. 163-181.
- Carmichael, I. S. E., 1963, The crystallization of feldspar in volcanic acid liquids: *Geol. Soc. London Quart. Jour.*, v. 119, p. 95-131.
- 1967, The iron-titanium oxides of salic volcanic rocks and their associated ferromagnesium silicates: *Contr. Mineral. and Petrol.*, v. 14, p. 36-64.
- Chapin, C. E., 1965, Geologic and petrologic features of the Thirty-nine Mile volcanic field, central Colorado: Unpub. D.Sc. Thesis, Colorado School of Mines, 172 p.
- Chesterman, C. W., 1956, Pumice, pumicite, and volcanic cinders in California: *Calif. Div. Mines Bull.* 174, 97 p.
- Christiansen, R. L., and Lipman, P. W., 1966, Emplacement and thermal history of a rhyolite flow near Fortymile Canyon, southern Nevada: *Geol. Soc. Amer. Bull.*, v. 77, p. 671-684.
- Clark, S. P., Jr., (editor), 1966, Handbook of physical constants: *Geol. Soc. Amer. Mem.* 97.
- Coats, R. R., Barnett, P. R., and Conklin, N. M., 1962, Distribution of beryllium in unaltered silicic volcanic rocks of the western conterminous United States: *Econ. Geol.*, v. 57, p. 963-968.
- Coats, R. R., Goss, W. D., and Rader, L. F., 1963, Distribution of fluorine in unaltered silicic volcanic rocks of the western conterminous United States: *Econ. Geol.*, v. 58, p. 941-951.

- Cross, Whitman, 1891, Constitution and origin of spherulites in acid eruptive rocks: Phil. Soc. Wash. Bull., v. 11, p. 411-444.
- Dane, C. H., and Backman, G. O., 1965, Geologic map of New Mexico: U. S. Geol. Survey, 2 sheets.
- Deer, W. A., Howie, R. A., and Zussman, J., 1962, Rock-forming minerals: New York, John Wiley and Sons, Inc., 333 p.
- Edwards, A. B., 1954, Textures of ore minerals and their significance, 2nd ed.: Melbourne, Brown, Prior, Anderson Pty. Ltd., 242 p.
- Elston, W. E., Coney, P. J., and Rhodes, R. C., 1968, A progress report on the Mogollon Plateau volcanic province, southwestern New Mexico: Colorado School Mines Quart., v. 63, p. 261-287.
- , 1969, Progress report on the Mogollon Plateau volcanic province, southwestern New Mexico: No. 2: New Mexico Geol. Soc. Guidebook 21, Tyrone-Big Hatchet Mountains-Florida Mountains Region, p. 75-86.
- Ericksen, G. E., Wedow, Helmut, Jr., Eaton, G. P., and Leland, G. R., 1970, Mineral resources of the Black Range Primitive Area, Grant, Sierra, and Catron Counties, New Mexico: U. S. Geol. Survey Bull. 1319-E, 162 p.
- Evans, H. T., Jr., Appleman, D. E., and Handwerker, D. S., 1963, The least squares refinement of crystal unit cells with powder diffraction data by an automatic computer indexing method (abstract): Program Ann. Meeting, Cryst. Assoc., Mar. 38, 1963, Cambridge, Mass., p. 42-43.
- Fenner, C. N., 1926, The Katmai magmatic province: Jour. Geol., v. 34, p. 740-743.
- Foshag, W. F., and Fries, Carl, Jr., 1943, Tin deposits of Mexico: U. S. Geol. Survey Bull. 935-C, p. 99-176.
- Friedman, I., Long, W., and Smith, R. L., 1963, Viscosity and water content of rhyolite glass: Jour. Geophys. Research, v. 68, p. 6523-6535.
- Fries, Carl, Jr., 1940, Tin deposits of the Black Range, Catron and Sierra Counties, New Mexico, a preliminary report: U. S. Geol. Survey Bull. 922-M, p. 355-370.
- Fries, Carl, Jr., and Butler, A. P., 1943, Geologic map of the Black Range tin district, New Mexico: U. S. Geol. Survey open-file map.

- Fries, Carl, Jr., Schaller, W. T., and Glass, J. J., 1942, Bixbyite and pseudobrookite from the tin-bearing rhyolite of the Black Range, New Mexico: *Amer. Mineral.*, v. 27, p. 305-322.
- Fyfe, W. S., 1970, Some thoughts on granitic magmas, in Newall, G., and Rast, N., (editors), *Mechanism of igneous intrusion*, Gallery P., p. 201-216, Liverpool.
- Haggerty, S. E., and Lindsley, D. H., 1970, Stability of the pseudobrookite ( $\text{Fe}_2\text{TiO}_5$ )-ferropseudobrookite ( $\text{FeTi}_2\text{O}_5$ ) series: *Carnegie Inst. Washington Year Book* 68, p. 247-249.
- Hampton, M. A., 1970, Subaqueous debris flow and generation of turbidity currents: Ph.D. Thesis, Stanford University, 180 p.
- Harris, P. G., Kennedy, W. Q., and Scarfe, C. M., 1969, Volcanism versus plutonism--the effect of chemical composition, in Newall, G., and Rast, N., (editors), *Mechanism of igneous intrusion*, Gallery P., p. 187-200, Liverpool.
- Hemley, J. J., and Jones, W. R., 1964, Chemical aspects of hydrothermal alteration with emphasis on hydrogen metasomatism: *Econ. Geol.*, v. 59, p. 538-569.
- Hill, J. H., 1921, The Taylor Creek tin deposits, New Mexico: U. S. Geol. Survey Bull. 725, p. 347-359.
- Iddings, J. P., 1887, The nature and origin of lithophysae and the lamination of acid lavas: *Amer. Jour. Sci.*, v. 133, p. 36-45.
- 1891, Spherulitic crystallization: *Phil. Soc. Wash. Bull.*, v. 11, p. 445-463.
- Jahns, R. H., 1944a, Beryllium and tungsten deposits of the Iron Mountain district, Sierra and Catron Counties, New Mexico: U. S. Geol. Survey Bull. 945-C, p. 45-79.
- 1944b, "Ribbon rock," an unusual beryllium-bearing tactite: *Econ. Geol.*, v. 39, p. 173-205.
- Johnson, A. M., 1965, A model for debris flow: Ph.D. Thesis, The Penn State University, 232 p.
- Keith, H. D., and Padden, F. J., Jr., 1963, A phenomenological theory of spherulitic crystallization: *Jour. Appl. Physics*, v. 34, p. 2409-2421.
- Knopf, Adolph, 1916, Wood tin in Tertiary rhyolites of northern Lander County, Nevada: *Econ. Geol.*, v. 11, p. 652-661.
- Krauskopf, K. B., 1948, Lava movement at Parícutin Volcano, Mexico: *Geol. Soc. Amer. Bull.*, v. 59, p. 1267-1284.

Krauskopf, K. B., 1957, The heavy metal content of magmatic vapor at 600°C: *Econ. Geol.*, v. 52, p. 786-807.

————— 1964, The possible role of volatile metal compounds in ore genesis: *Econ. Geol.*, v. 59, p. 22-45.

Larsen, E. S., and Cross, Whitman, 1956, *Geology and petrology of the San Juan region, southwestern Colorado*: U. S. Geol. Survey Prof. Paper 258, 303 p.

Lindgren, Waldemar, 1933, *Mineral deposits*, 4th ed.: New York, McGraw-Hill Book Co., Inc., 930 p.

Little, W. M., 1960, Inclusions in cassiterite and associated minerals: *Econ. Geol.*, v. 55, p. 485-509.

Lofgren, G. E., 1968, Experimental devitrification of rhyolite glass: Ph.D. Thesis, Stanford University, 99 p.

Lovering, T. S., 1955, Temperatures in and near intrusions: *Econ. Geol.*, 50th Ann. Vol., Part I, p. 249-281.

Luth, W. C., and Tuttle, O. F., 1966, The alkali feldspar solvus in the system  $\text{Na}_2\text{O}-\text{K}_2\text{O}-\text{Al}_2\text{O}_3-\text{SiO}_2-\text{H}_2\text{O}$ : *Amer. Mineral.*, v. 51, p. 1359-1373.

————— 1969, The hydrous vapor phase in equilibrium with granite and granite magmas: *Geol. Soc. Amer. Mem.* 115, p. 513-548.

Luth, W. C., and Querol-Suñé, F., 1970, An alkali feldspar series: *Contr. Mineral. and Petrol.*, v. 25, p. 25-40.

MacChesney, J. B., and Muan, A., 1959, Studies in the system iron oxide-titanium oxide: *Amer. Mineral.*, v. 44, p. 926-945.

Martin, R. F., 1969, The hydrothermal synthesis of low albite: *Contr. Mineral. and Petrol.*, v. 23, p. 323-339.

Martin, R. F., and Piwinski, A. J., 1969, Experimental data bearing on the movement of iron in an aqueous vapor: *Econ. Geol.*, v. 64, p. 798-803.

Mason, Brian, 1943, Mineralogical aspects of the system  $\text{FeO}-\text{Fe}_2\text{O}_3-\text{MnO}-\text{Mn}_2\text{O}_3$ : *Geol. Foren. Forh.*, v. 65, p. 97-180.

Merwin, H. E., and Hostetter, J. C., 1919, Hematite and rutile formed by the action of chlorine at high temperatures: *Amer. Mineral.*, v. 4, p. 126-127.

Muan, A., and Sōmiya, S., 1962, The system iron oxide-manganese oxide in air: *Amer. Jour. Sci.*, v. 260, p. 230-240.

- Mulligan, R., 1966, Geology of Canadian tin occurrences: Geol. Survey Can. Paper 64-54, 22 p.
- Nemoto, T., Hayakawa, M., Takahashi, K., and Oana, S., 1957, Report on the geological, geophysical, and geochemical studies of Showa-shinzan, Usu Volcano: Geol. Surv. Japan Rept. 170, 149 p. (in Japanese)
- Noble, D. C., 1965, Ground-water leaching of sodium from quickly cooled volcanic rocks (abstract): Amer. Mineral., v. 50, p. 289.
- 1967, Sodium, potassium, and ferrous iron contents of some secondarily hydrated natural silicic glasses: Amer. Mineral., v. 52, p. 280-286.
- Noble, D. C., Smith, V. C., and Peck, L. C., 1967, Loss of halogens from crystallized and glassy silicic volcanic rocks: Geochim. et Cosmochim. Acta., v. 31, p. 215-223.
- Nockolds, S. R., 1954, Average chemical composition of some igneous rocks: Geol. Soc. Amer. Bull., v. 65, p. 1007-1032.
- Orville, P. M., 1963, Alkali ion exchange between vapor and feldspar phases: Amer. Jour. Sci., v. 261, p. 201-237.
- 1967, Unit-cell parameters of the microcline-low albite and the sanidine-high albite solid solution series: Amer. Mineral., v. 52, p. 55-86.
- Ottemann, J., and Frenzel, G., 1965, Der Chemismus der Pseudobrookite von Vulkaniten: Schweiz. Mineralogische u. Petrographische Mitteilungen, Band 45, Heft 2, p. 819-836.
- Palache, Charles, 1935, Pseudobrookite: Amer. Mineral., v. 19, p. 16-20; v. 20, p. 660-663.
- Park, C. F., Jr., and MacDiarmid, R. A., 1970, Ore Deposits, 2nd ed.: San Francisco, W. H. Freeman and Co., 522 p.
- Penfield, S. L., and Foote, H. W., 1897, On bixbyite, a new mineral, and notes on the associated topaz: Amer. Jour. Sci., v. 4, p. 105-110.
- Petrova, Z. I., and Legeydo, V. A., 1965, Geochemistry of tin in the magmatic process: Geochem. Intern., v. 2, p. 301-307.
- Pirsson, L. V., 1910, On an artificial lava flow and its spherulitic crystallization: Amer. Jour. Sci., v. 180, p. 97-114.
- Pollard, D. D., and Johnson, A. M., (in press), Mechanics of growth of laccolithic intrusion in the Henry Mountains, Utah.

- Ribbe, P. H., and Gibbs, G. V., 1971, The crystal structure of topaz and its relation to physical properties: *Amer. Mineral.*, v. 56, p. 24-30.
- Roedder, Edwin, 1968, The non-colloidal origin of colloform textures in sphalerite ores: *Econ. Geol.*, v. 63, p. 451-471.
- Rosenberg, P. E., 1965, The stability of topaz: a preliminary report (abstract): *Trans. Amer. Geophys. Union*, v. 46, p. 180.
- 1967, Variations in the unit-cell dimensions of topaz and their significance: *Amer. Mineral.*, v. 52, p. 1890-1895.
- Ross, C. S., 1964, Volatiles in volcanic glasses and their stability relations: *Amer. Mineral.*, v. 49, p. 258-271.
- Roy, Rustum, and Osborn, E. F., 1954, The system  $\text{Al}_2\text{O}_3\text{-SiO}_2\text{-H}_2\text{O}$ : *Amer. Mineral.*, v. 39, p. 853-885.
- Sainsbury, C. L., 1960, Metallization and post-mineral hypogene argillization, Lost River tin mine, Alaska: *Econ. Geol.*, v. 55, p. 1478-1506.
- Sand, L. B., Roy, Rustum, and Osborn, E. F., 1954, The stability relations of some minerals in the system  $\text{Na}_2\text{O-Al}_2\text{O}_3\text{-SiO}_2\text{-H}_2\text{O}$  (abstract): *Amer. Mineral.*, v. 39, p. 341.
- Schneiderhöhn, H., 1955, *Erzlagertätten*, 3rd ed.: Stuttgart, Fischer Verlag, 375 p.
- Shaw, H. R., 1965, Comments on viscosity, crystal settling, and convection in granitic magmas: *Amer. Jour. Sci.*, v. 263, p. 120-152.
- Shaw, H. R., Wright, T. L., Peck, D. L., and Odamura, R., 1968, The viscosity of basaltic magma: an analysis of field measurements in Makaopuhi Lava Lake, Hawaii: *Amer. Jour. Sci.*, v. 266, p. 225-264.
- Staatz, M. H., and Carr, W. J., 1964, Geology and mineral deposits of the Thomas and Dugway Ranges, Juab and Tooele Counties, Utah: *U. S. Geol. Survey Prof. Paper* 415.
- Stearns, C. E., 1962, Geology of the north half of the Pelona Quadrangle, Catron County, New Mexico: *New Mexico Inst. Min. and Tech., State Bur. Mines and Mineral Res. Bull.* 78, 45 p.
- Taylor, S. R., 1964, Abundance of chemical elements in the continental crust: *Geochim. et Cosmochim. Acta*, v. 28, p. 1280-1281.
- Tilley, C. E., 1922, Density, refractivity, and composition relations of some natural glasses: *Mineral. Mag.*, v. 19, p. 275-294.

- Tuttle, O. F., and Bowen, N. L., 1958, Origin of granite in the light of experimental studies: Geol. Soc. Amer. Mem. 74.
- Valle, F. Bracho, 1960, Yacimientos de Estano en la Siorra de Chapultepec, Zac., La Ochoa, Dgo. y Cosio, Acs. Consejo de Recursos Naturales no Renovables, Bolotin 48, p. 117.
- Volin, M. E., Russell, P. L., Prive, F. L. C., and Mullen, D. H., 1947, Catron and Sierra Counties tin deposits, New Mexico: U. S. Bur. Mines Rept. Inv. 4068, 60 p.
- Warner, L. A., Holser, W. T., Wilmarth, V. R., and Cameron, E. N., 1959, Occurrence of nonpegmatite beryllium in the United States: U. S. Geol. Survey Prof. Paper 318, 198 p.
- Weber, R. H., and Willard, M. E., 1959a, Reconnaissance geologic map of Mogollon thirty minute quadrangle, New Mexico Inst. Min. and Tech., State Bur. Mines and Mineral Res., Geol. Map 10.
- 1959b, Reconnaissance geologic map of Reserve thirty minute quadrangle, New Mexico Inst. Min. and Tech., State Bur. Mines and Mineral Res., Geol. Map 12.
- White, D. E., and Waring, G. A., 1963, Data of geochemistry, 6th ed., Chap. K; Volcanic emanations: U. S. Geol. Survey Prof. Paper 440-K, p. 1-29.
- Willard, M. E., 1957a, Reconnaissance geologic map of Leura Spring thirty minute quadrangle, New Mexico Inst. Min. and Tech., State Bur. Mines and Mineral Res., Geol. Map 2.
- 1957b, Reconnaissance geologic map of Piñonville thirty minute quadrangle, New Mexico Inst. Min. and Tech., State Bur. Mines and Mineral Res., Geol. Map 3.
- Willard, M. E., and Givens, D. B., 1958, Reconnaissance geologic map of Datil thirty minute quadrangle, New Mexico Inst. Min. and Tech., State Bur. Mines and Mineral Res., Geol. Map 5.
- Williams, Howel, 1932, The history and character of volcanic domes: Univ. Calif. Publ. Bull., Dept. Geol. Sci., v. 21, p. 51-146.
- Wright, T. L., and Stewart, D. B., 1968, X-ray and optical study of alkali feldspar. I. Determination of composition and structural state from refined unit-cell parameters and 2V: Amer. Mineral., v. 54, p. 38-87.
- Ypma, P. J. M., and Simons, J. H., 1969, Genetical aspects of the tin mineralization in Durango, Mexico: Intern. Tin Council, London, and Dept. Mineral Res., Bangkok, 14 p.

Zies, E. G., 1924, The fumarolic incrustations in the Valley of Ten Thousand Smokes: Nat. Geog. Soc. Washington, Contr. Tech. Papers, Katmai ser., v. 1, no. 3, p. 157-179.

---

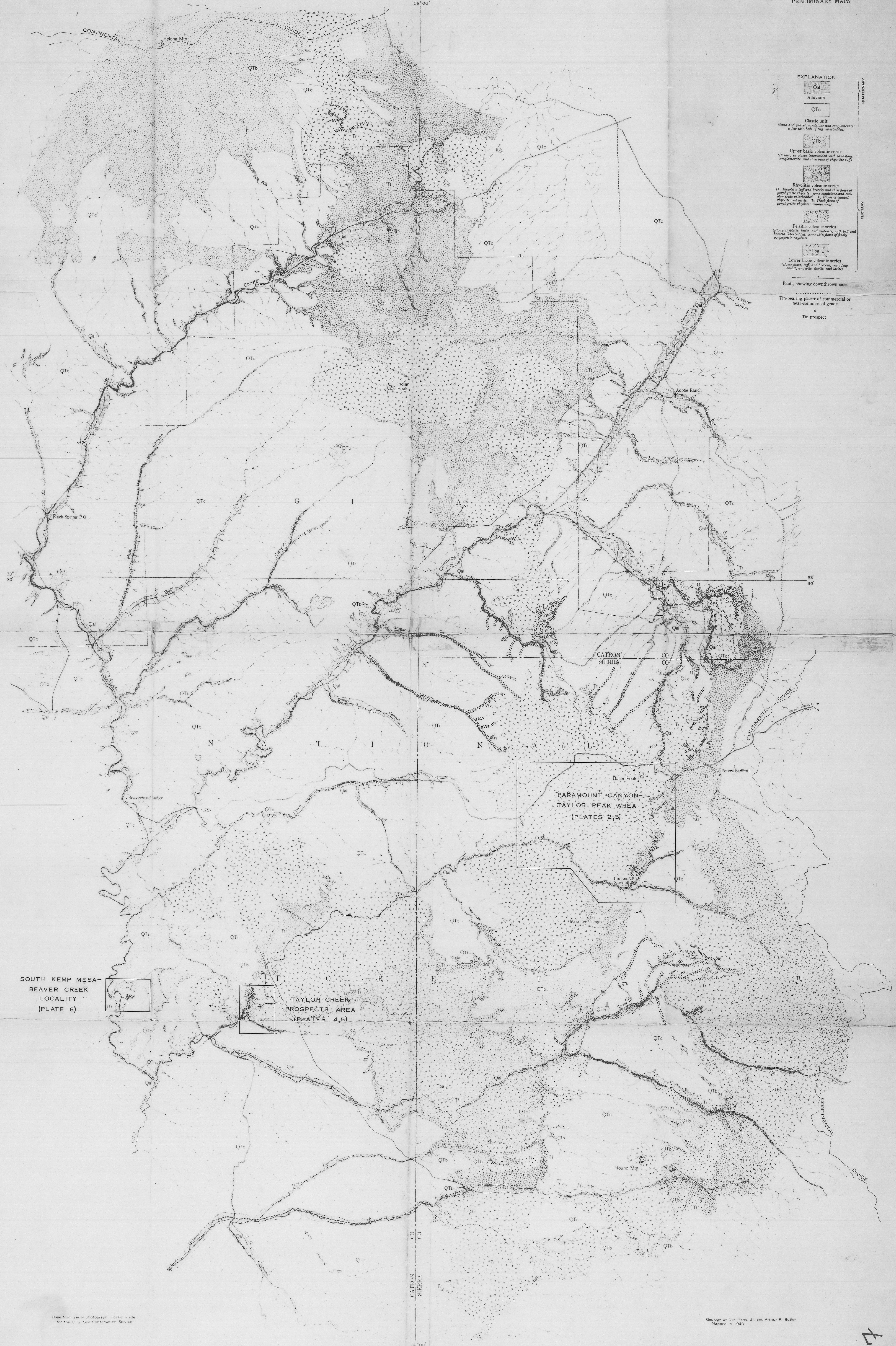
1929, The Valley of Ten Thousand Smokes: Nat. Geog. Soc. Washington, Contr. Tech. Papers, Katmai ser., v. 1, no. 4, 79 p.



OF 57

OF 57

106°00'



**EXPLANATION**

**QUATERNARY**

Qal Alluvium

QTc Clastic unit  
(Sand and gravel, sandstone and conglomerate, a few thin beds of tuff interbedded)

QTb Upper basic volcanic series  
(Basalt, in places interbedded with sandstone, conglomerate, and thin beds of rhyolitic tuff)

**TERTIARY**

Tr Rhyolitic volcanic series  
(Tr. Rhyolitic tuff and breccia and thin flows of porphyritic rhyolite, some sandstone and conglomerate interbedded. T. Flows of banded rhyolite and tuff. T. Thick flows of porphyritic rhyolite, no-burrowing)

Ti Pelitic volcanic series  
(Flows of plate, tuff, and sandstone, with tuff and breccia interbedded, some thin flows of finely porphyritic rhyolite)

Lower basic volcanic series  
(Basalt flows, tuff, and breccia, including basalt, andesite, dacite, and tuff)

Fault, showing downthrown side

..... Tin-bearing placer of commercial or near-commercial grade

x Tin prospect

SOUTH KEMP MESA-  
BEAVER CREEK  
LOCALITY  
(PLATE 6)

TAYLOR CREEK  
PROSPECTS' AREA  
(PLATES 4,5)

PARAMOUNT CANYON-  
TAYLOR PEAK AREA  
(PLATES 2,3)

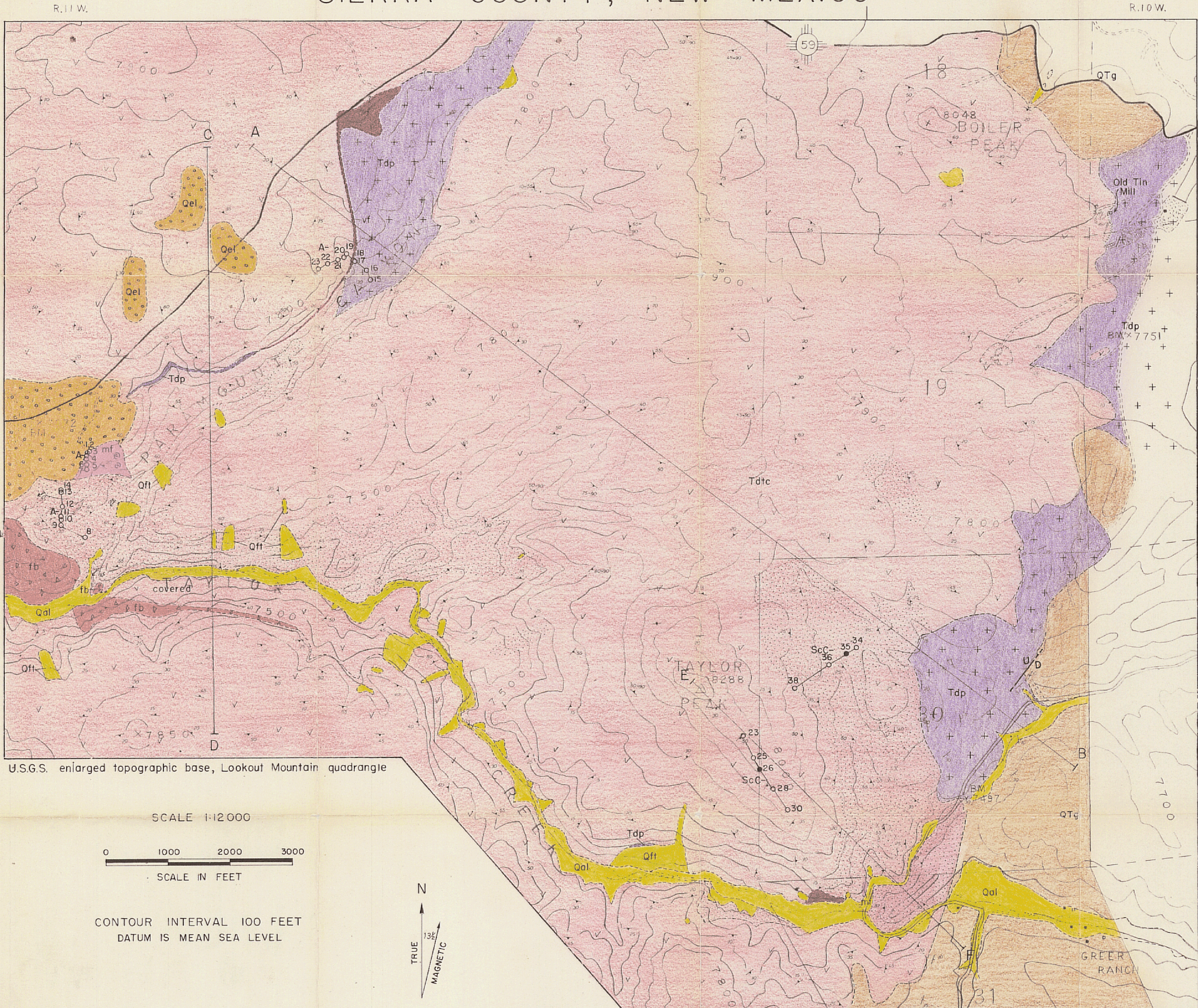
Base from aerial photograph mosaic made  
for the U. S. Soil Conservation Service

Geology by J. H. Fries, Jr. and Arthur P. Butler  
Mapped in 1940

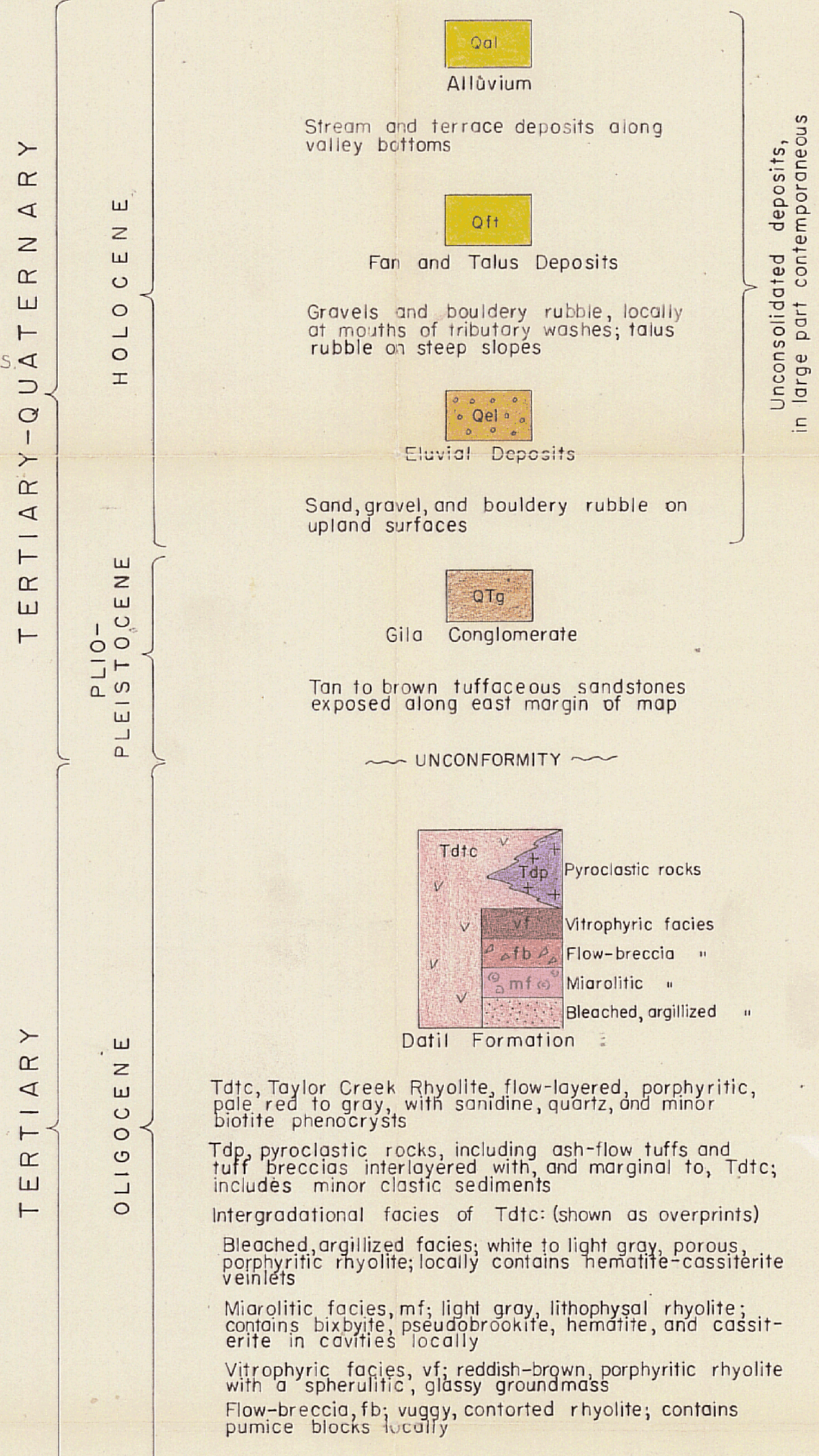
OF 57



# GEOLOGIC MAP OF PARAMOUNT CANYON - TAYLOR PEAK AREA, SIERRA COUNTY, NEW MEXICO



## EXPLANATION



U.S.G.S. enlarged topographic base, Lookout Mountain quadrangle

SCALE 1:12000

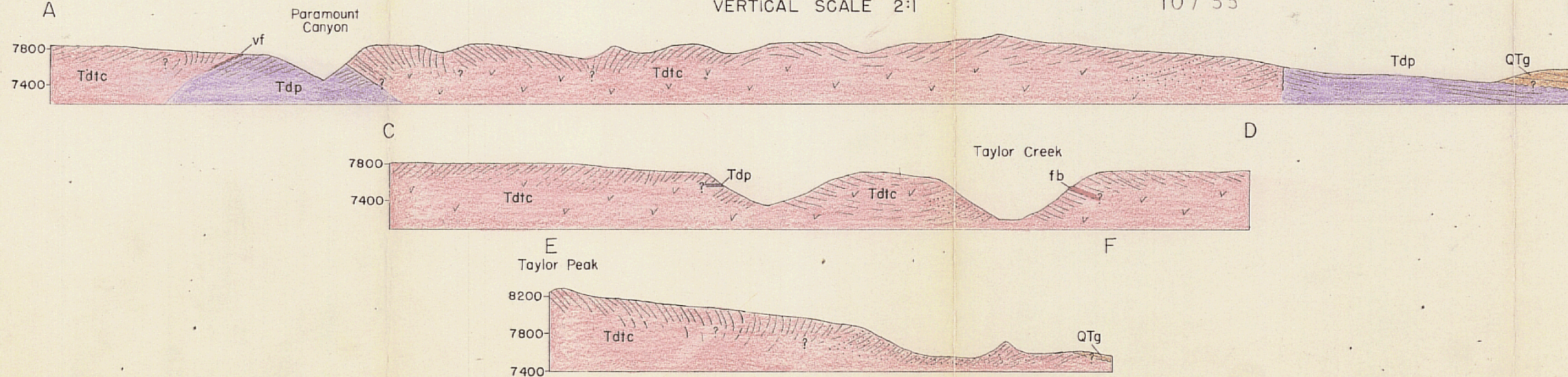
0 1000 2000 3000  
SCALE IN FEET

CONTOUR INTERVAL 100 FEET  
DATUM IS MEAN SEA LEVEL

TRUE  
MAGNETIC

GEOLOGIC SECTIONS  
VERTICAL SCALE 2:1

Geology by John L. Lufkin, 1969-70





0F-57-10

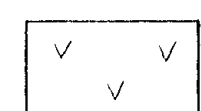
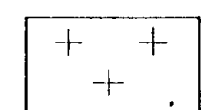
# GENERALIZED FLOW DIRECTIONS IN PART OF THE BOILER PEAK DOME

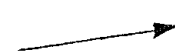
PLATE 3.

OPEN FILE REPORT 57  
PLATE 3



## EXPLANATION

-  Taylor Creek Rhyolite
-  Pyroclastics

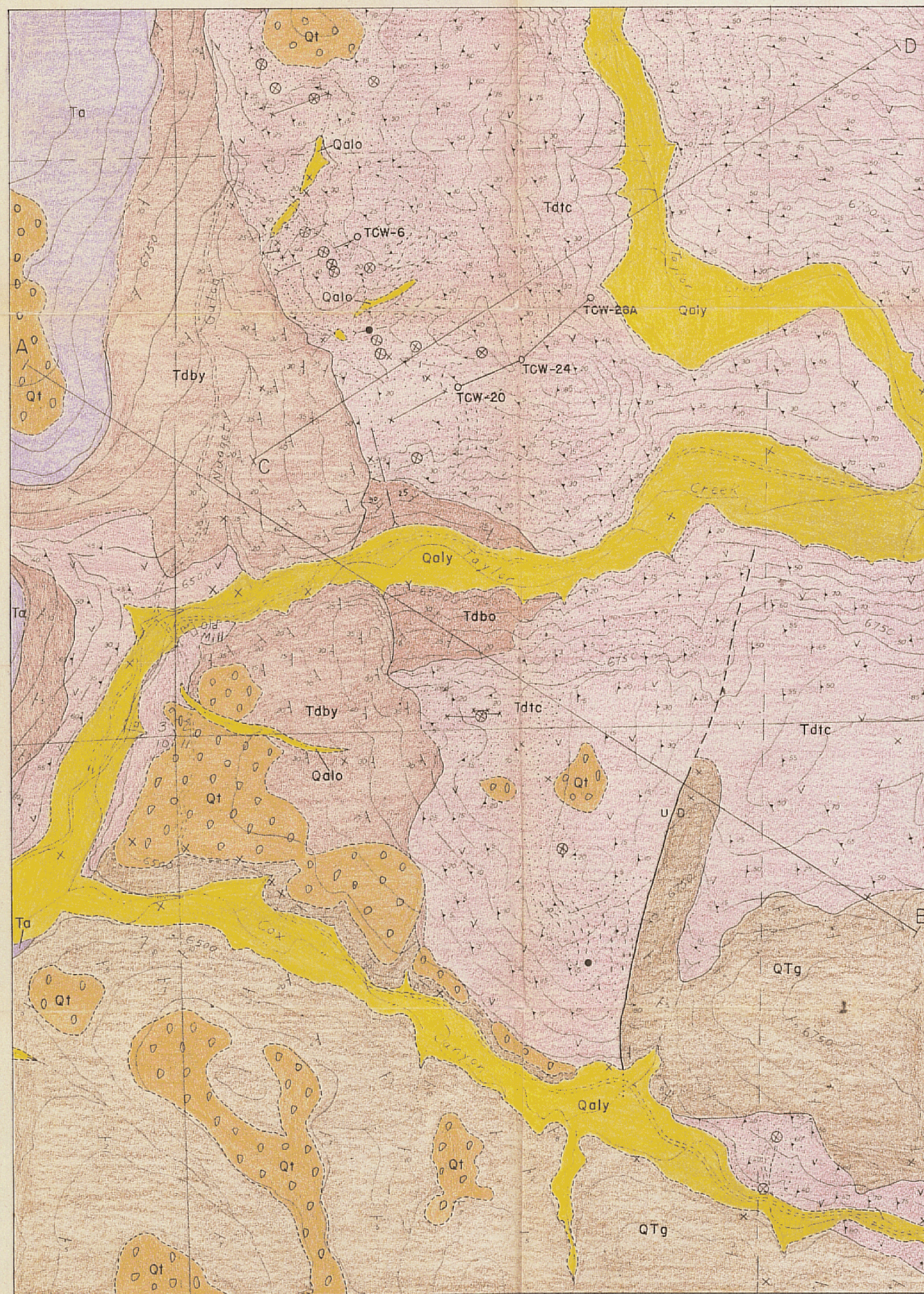
 Horizontal component of flow direction

0F-57-10

0F-57-10

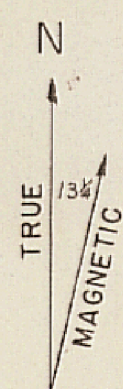


# GEOLOGIC MAP OF THE TAYLOR CREEK PROSPECTS AREA, CATRON COUNTY, NEW MEXICO



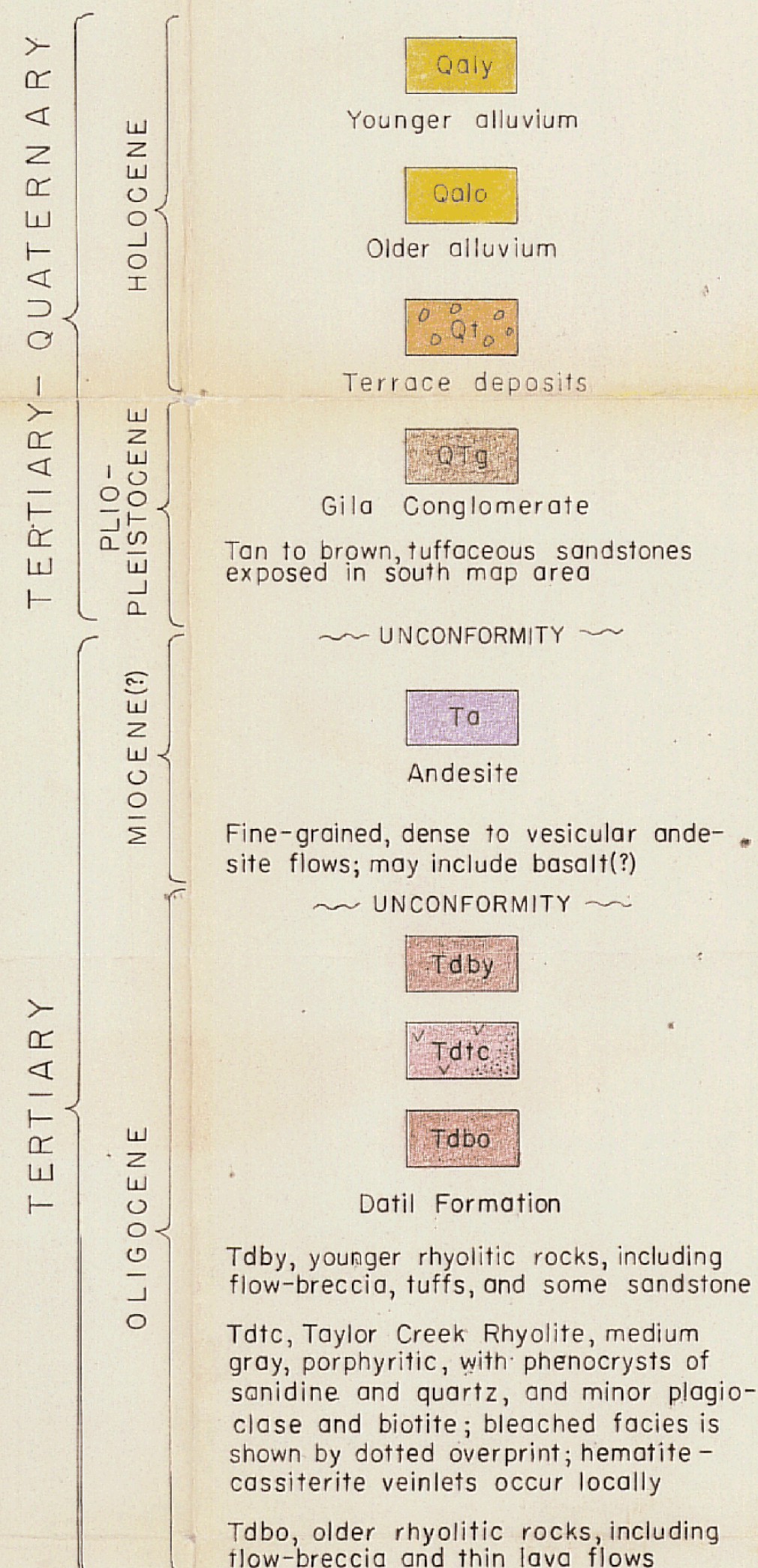
0 400 800 1200  
SCALE IN FEET

CONTOUR INTERVAL 50 FEET  
DATUM IS MEAN SEA LEVEL

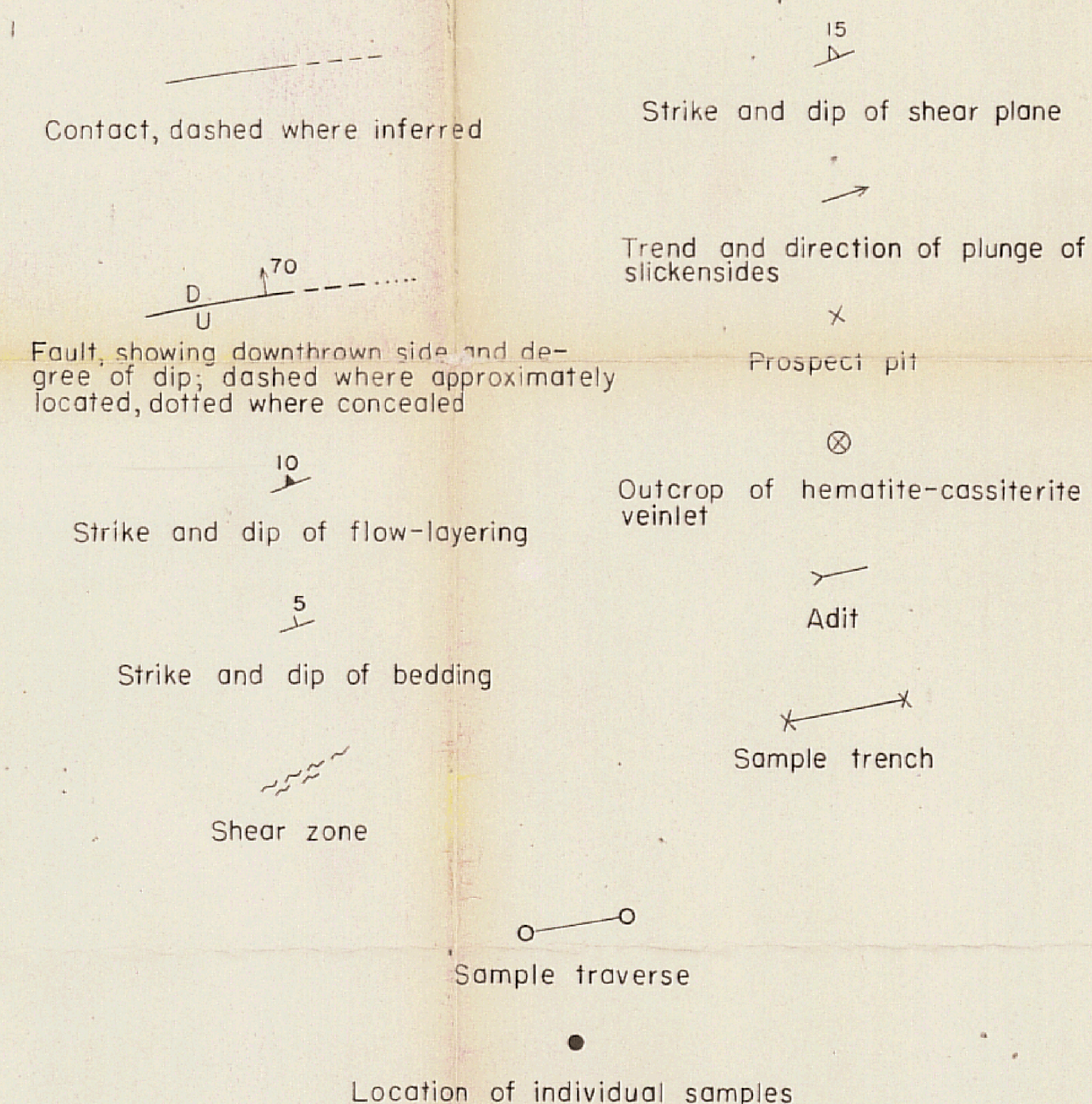


Geology compiled from the work of Fries(1940) and Johns(1957-62, unpublished).

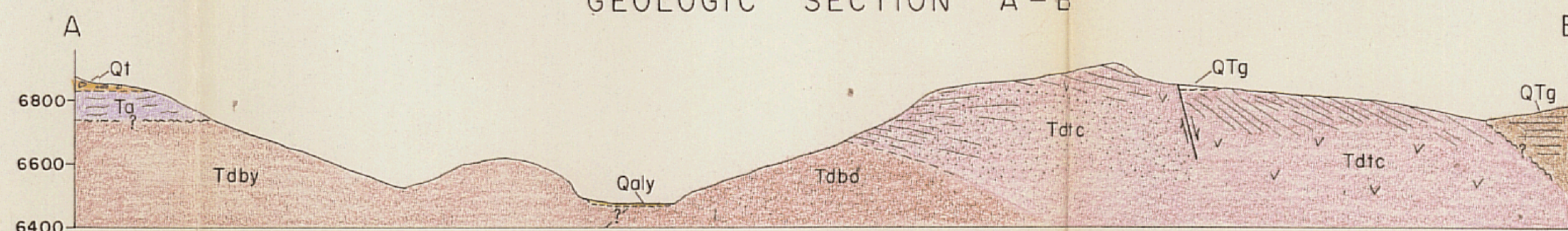
## EXPLANATION



## SYMBOLS



## GEOLOGIC SECTION A-E

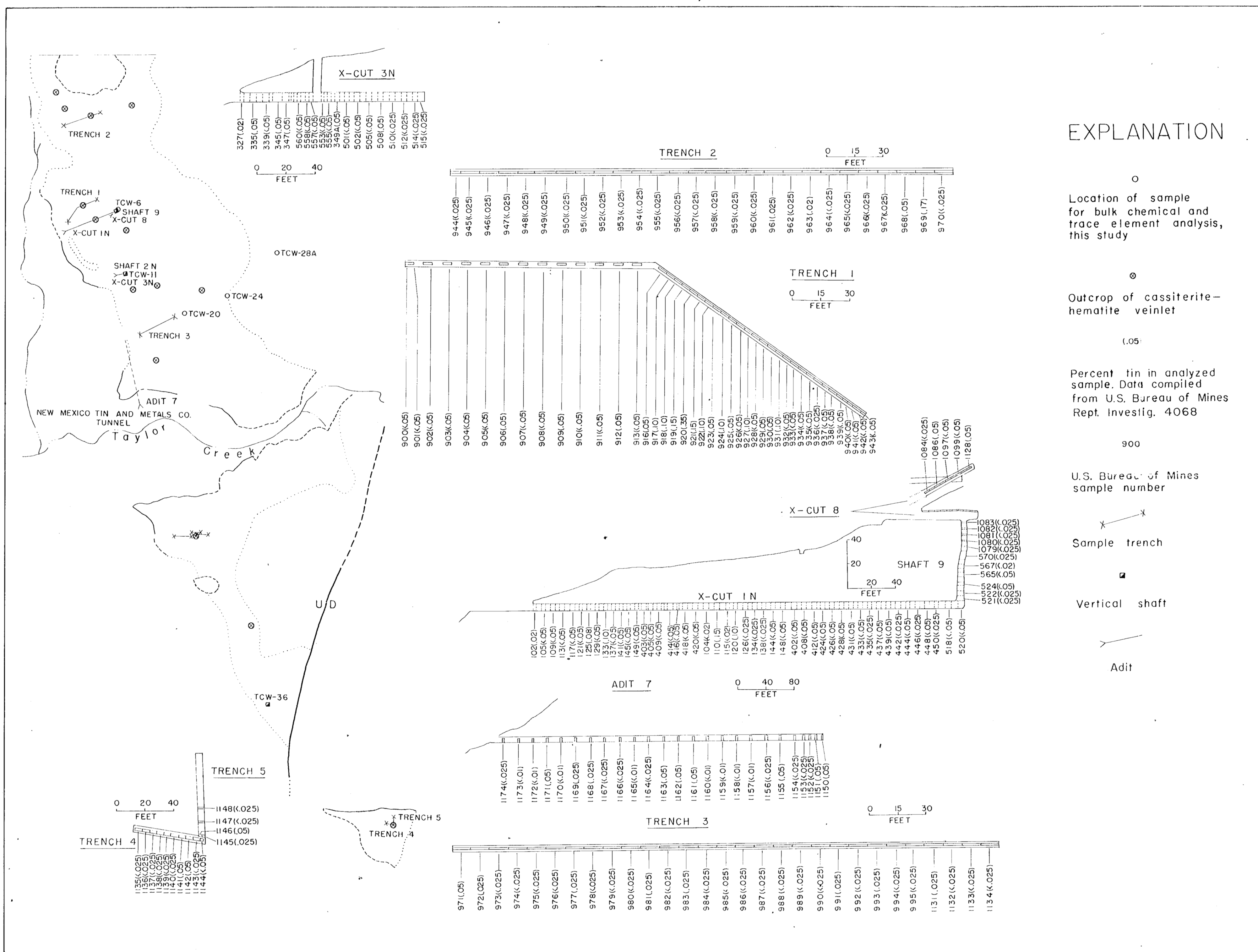


## GEOLOGIC SECTION C-D



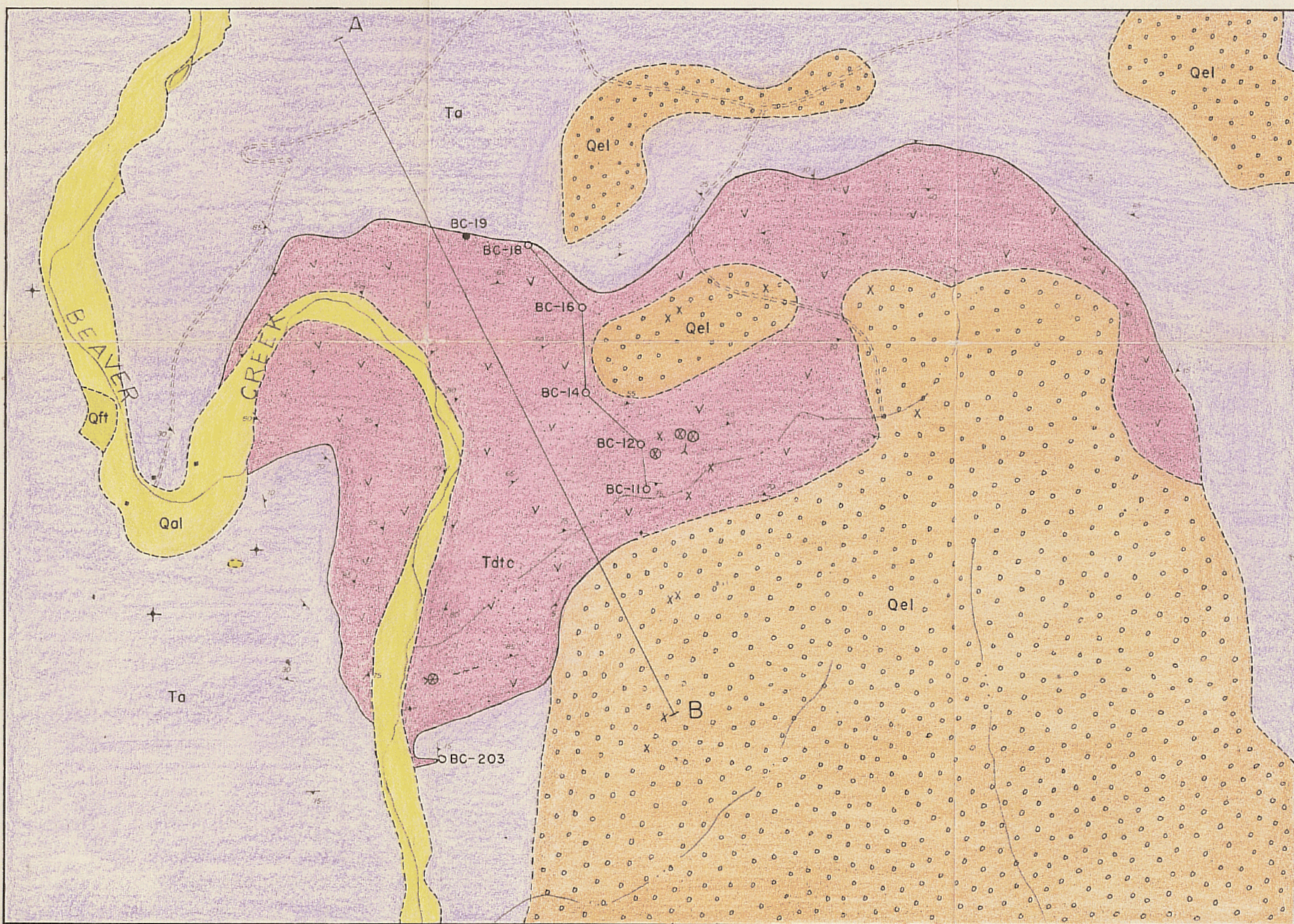


TIN ASSAYS OF TAYLOR CREEK RHYOLITE, TAYLOR CREEK PROSPECTS AREA

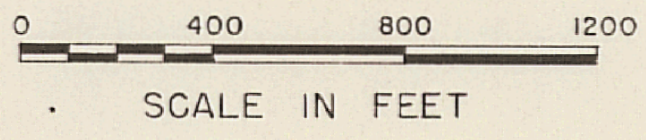




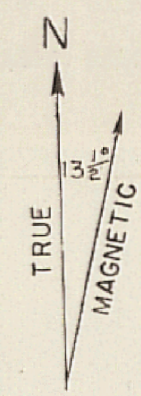
# GEOLOGIC MAP OF SOUTH KEMP MESA - BEAVER CREEK AREA, CATRON COUNTY, NEW MEXICO



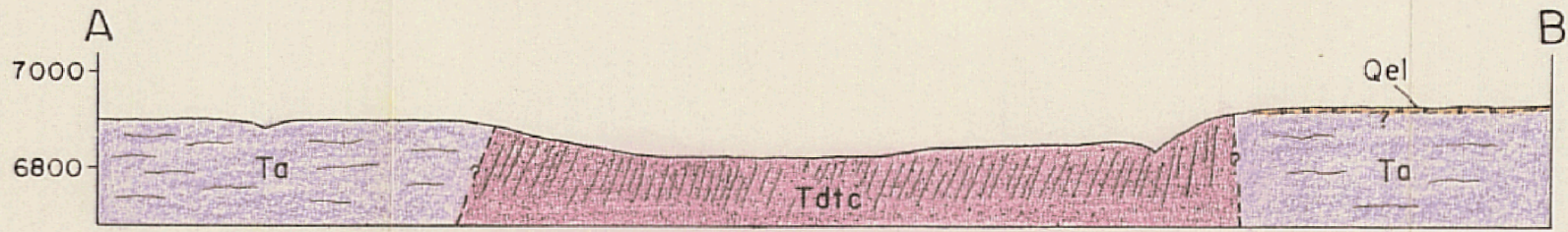
U.S. Forest Service enlarged aerial photograph base



Geology by John L. Lufkin, 1969-70



## GEOLOGIC SECTION A-B



## EXPLANATION

QUATERNARY	HOLOCENE		Qal
		Alluvium	
		Stream and terrace deposits along valley bottoms	
QUATERNARY	HOLOCENE		Qft
		Fan and Talus Deposits	
		Gravels and bouldery rubble, locally at mouths of tributary washes; talus rubble on steep slopes	
QUATERNARY	HOLOCENE		Qel
		Eluvial Deposits	
		Sand, gravel, and bouldery rubble on upland surfaces; overlie rhyolite and andesite to the north and Gila Conglomerate in the south map area	
TERTIARY	MIOCENE(?)		Ta
		Andesite	
		Fine-grained, dense to vesicular andesite in flows. May include basaltic rocks(?)	
TERTIARY	MIOCENE(?)		UNCONFORMITY
			Tdtc
		Datil Formation	
TERTIARY	MIOCENE(?)	Taylor Creek Rhyolite, flow-layered, porphyritic, argillized facies, white to light gray; locally contains hematite-cassiterite veinlets	

Unconsolidated deposits, in large part contemporaneous

## SYMBOLS

	Contact, dashed where approximately located
	Strike and dip of flow-layering
	Horizontal flows
	Shear zone
	Prospect pit
	Outcrop of hematite-cassiterite veinlet
	Adit
	Unimproved dirt road
	Sample traverse
	Location of individual samples